Polimery w Medycynie

Polymers in Medicine

BIANNUAL ISSN: 0370-0747 e-ISSN: 2451-2699 polimery.umw.edu.pl

2024, Vol. 54, No. 2 (July–December)

Ministry of Science and Higher Education – 70 pts.
Index Copernicus (ICV) – 121.14 pts.

Wroclaw Medical University

Polimery w Medycynie

Polymers in Medicine

Polimery w Medycynie
Polymers in Medicine

ISSN 0370-0747 (PRINT) ISSN 2451-2699 (ONLINE) polimery.umw.edu.pl

BIANNUAL
2024, Vol. 54, No. 2
(July–December)

"Polymers in Medicine" is an independent, multidisciplinary forum to exchange scientific and clinical information, which publishes original papers (technical, analytical, experimental, clinical), preliminary reports and reviews regarding the use of polymers (natural and synthetic) and biomaterials in different specialties of medicine (biochemistry, clinical medicine, pharmacology, dentistry, implantology), biotechnology and veterinary science.

Address of Editorial Office
Marcinkowskiego 2–6
50-368 Wrocław, Poland
Tel.: +48 71 784 11 33
E-mail: redakcja@umw.edu.pl

Publisher
Wroclaw Medical University
Wybrzeże L. Pasteura 1
50-367 Wrocław, Poland

Online edition is the original version of the journal

Editorial Policy

During the review process, the Editorial Board conforms to the "Uniform Requirements for Manuscripts Submitted to Biomedical Journals: Writing and Editing for Biomedical Publication" approved by the International Committee of Medical Journal Editors (http://www.icmje.org/). Experimental studies must include a statement that the experimental protocol and informed consent procedure were in compliance with the Helsinki Convention and were approved by the ethics committee.

For more information visit the following page: https://polimery.umw.edu.pl

Polimery w Medycynie – Polymers in Medicine has received financial support from the resources of Ministry of Science and Higher Education within the "Social Responsibility of Science – Support for Academic Publishing" project based on agreement No. RCN/SP/0504/2021.

Ministry of Education and Science
Republic of Poland

Czasopismo Polimery w Medycynie – Polymers in Medicine korzysta ze wsparcia finansowego ze środków Ministerstwa Edukacji i Nauki w ramach programu „Społeczna Odpowiedzialność Nauki – Rozwój Czasopism Naukowych" na podstawie umowy nr RCN/SP/0504/2021.

Ministerstwo
Edukacji i Nauki

Indexed in: OCLC, WorldCat, PBL, EBSCO, MEDLINE, Index Copernicus

Typographic design: Monika Kolęda, Piotr Gil
Cover: Monika Kolęda
DTP: Wroclaw Medical University Press
Printing and binding: Drukarnia I-BiS Bierońscy Sp.k.

Circulation: 11 copies

Polimery w Medycynie
Polymers in Medicine

BIANNUAL 2024, Vol. 54, No. 2 (July–December)

ISSN 0370-0747 (PRINT)
ISSN 2451-2699 (ONLINE)
polimery.umw.edu.pl

Contents

PREFACE

Dear Readers,

The winter issue of our periodical contains as many as 10 articles on the production, research or use of polymers in medicines, therapeutic procedures, or in scientific research related to medicine.

Three works on polymers that can be used as implants constitute a distinct group. Two of them focus on mixtures of biodegradable polymers with apatite, while the 3rd one, from an Upper Silesian center, describes the use of biodegradable polymers in 3D printing to regenerate the spinal cord. Interesting applications of polymers as carriers of medicinal substances in potential pharmaceutical preparations are presented in the next triad of articles. The 1st of them, a review, prepared in collaboration by researchers from the Wroclaw Medical University and from the Wrocław University of Environmental and Life Sciences, describes classic and innovative methods of producing microcapsules using physical methods, such as coacervation, spray methods, agglomeration, cross-linking in suspension and extrusion, and chemical methods, such as interfacial polymerization, in situ polymerization or encapsulation in microcylinders obtained from a 3D printer.

The next 2 original articles, also from Wrocław, raise the extremely interesting issue of the influence of hydrophilic polymers on the physicochemical properties of preparations intended for use in dermatology and laryngology. The remaining works focus on application studies of drugs in the context of their interaction with polymers and biopolymers, with 2 works from a Poznań center being fine examples. The 1st one delves into the problems of durability of tuberculostatics interacting, among others, with macromolecular structures of the cell wall and the interior of the pathogen cell. The 2nd one introduces the design of analytical procedures using neural networks. Some of the presented works are the result of the 2nd edition of the scientific conference entitled "Physical chemistry and biophysics for pharmacy 2024", organized at the Wroclaw Medical University, and our editorial team would like to thank the conference participants for submitting valuable experimental and review manuscripts to our journal.

I encourage you to read the latest issue of *Polimery w Medycynie – Polymers in Medicine*, and I wish our readers, authors, reviewers and editorial team a peaceful Christmas and all the best in the coming New Year 2025. All the best!

Prof. Witold Musiał
Editor-in-Chief

WSTĘP

Drodzy Czytelnicy,

zimowe wydanie naszego periodyku zawiera aż 10 artykułów na temat wytwarzania, badania lub zastosowania polimerów w lekach, postępowaniu leczniczym, albo w badaniach naukowych związanych z medycyną.

Trzy prace nt. polimerów, które mogą znaleźć zastosowanie jako implanty, stanowią wyróżniającą się grupę. Dwie z nich skupiają się na mieszaninach polimerów biodegradowalnych z apatytem, natomiast w trzeciej, z ośrodka górnośląskiego, opisano wykorzystanie polimerów biodegradowalnych w druku 3D, w celu regeneracji rdzenia kręgowego. Kolejna triada artykułów prezentuje ciekawe zastosowania polimerów jako nośników substancji leczniczych w potencjalnych preparatach farmaceutycznych. Pierwsza z tych prac, przeglądowa, powstała we współpracy badaczy z Uniwersytetu Medycznego we Wrocławiu i Uniwersytety Przyrodniczego we Wrocławiu, opisuje klasyczne i innowacyjne metody wytwarzania mikrokapsułek metodami fizycznymi, takimi jak koacerwacja, metody rozpyłowe, aglomeracja, sieciowanie w zawiesinie czy ekstruzja, oraz metodami chemicznymi, takimi jak polimeryzacja międzyfazowa, polimeryzacja in situ lub enkapsulacja w mikrocylindrach otrzymanych z drukarki 3D.

Kolejne dwa artykuły oryginalne, także z Wrocławia, poruszają niezwykle ciekawe zagadnienie wpływu polimerów hydrofilowych na właściwości fizykochemiczne preparatów przeznaczonych do stosowania w dermatologii i laryngologii. Pozostałe prace koncentrują się na badaniach aplikacyjnych leków w kontekście ich oddziaływania z polimerami i biopolimerami. Przykładem są dwie prace z ośrodka poznańskiego. Pierwsza z nich pozwala zagłębić się w problemy trwałości tuberkulostatyków oddziałujących m.in. z wielkocząsteczkowymi strukturami ściany komórkowej i wnętrza komórki patogenu. Druga przybliża projektowanie procedur analitycznych za pomocą sieci neuronowych. Część z prezentowanych artykułów stanowi pokłosie drugiej edycji konferencji naukowej pt. „Chemia fizyczna i biofizyka dla farmacji 2024", zorganizowanej w Uniwersytecie Medycznym we Wrocławiu, i niniejszym nasz zespół redakcyjny pragnie serdecznie podziękować uczestnikom konferencji za nadesłanie do naszego czasopisma wartościowych prac eksperymentalnych i przeglądowych.

Zachęcam Państwa do lektury najnowszego wydania *Polimerów w Medycynie – Polymers in Medicine*, i życzę spokojnych świąt Bożego Narodzenia oraz wszelkiej pomyślności w nadchodzącym nowym roku 2025 naszym czytelnikom, autorom, recenzentom oraz zespołowi redakcyjnemu. Wszystkiego dobrego!

Prof. Witold Musiał
Redaktor Naczelny

Behavior of PGS/apatite foam scaffolds during incubation in SBF, PBS, Ringer's solution, artificial saliva, and distilled water

Badanie inkubacyjne pianek PGS/hydroksyapatyt w SBF, PBS, płynie Ringera, sztucznej ślinie i wodzie destylowanej

Paweł J. Piszko[1,A–E], Dagmara Słota[2,A,B,D], Agnieszka Sobczak-Kupiec[2,E,F], Agnieszka Tomala[2,A,B], Karina Niziołek[2,A,B], Wioletta Florkiewicz[2,A], Konrad Szustakiewicz[1,E,F]

[1] Department of Polymer Engineering and Technology, Faculty of Chemistry, Wroclaw University of Science and Technology, Poland
[2] Department of Materials Science, Faculty of Materials Science and Physics, Cracow University of Technology, Poland

A – research concept and design; B – collection and/or assembly of data; C – data analysis and interpretation; D – writing the article; E – critical revision of the article; F – final approval of the article

Polymers in Medicine, ISSN 0370-0747 (print), ISSN 2451-2699 (online) *Polim Med*. 2024;54(2):91–104

Address for correspondence
Paweł J. Piszko
E-mail: pawel.piszko@pwr.edu.pl

Funding sources
The "Multifunctional biologically active composites for applications in bone regenerative medicine" project is carried out within the TEAM-NET program of the Foundation for Polish Science financed by the European Union under the European Regional Development Fund (POIR.04.04.00-00-16D7/18).

Conflict of interest
None declared

Received on December 15, 2023
Reviewed on November 20, 2024
Accepted on November 26, 2024

Published online on December 3, 2024

Cite as
Piszko PJ, Słota D, Sobczak-Kupiec A, et al. Behavior of PGS/apatite foam scaffolds during incubation in SBF, PBS, Ringer's solution, artificial saliva, and distilled water. *Polim Med*. 2024;54(2):91–104. doi:10.17219/pim/196496

DOI
10.17219/pim/196496

Abstract

Background. Poly(glycerol sebacate) is a polymeric material with potential biomedical application in the field of tissue engineering. In order to act as a biodegradable scaffold, its incubation study is vital to simulate its behavior.

Objectives. This study explores the degradation of porous poly(glycerol sebacate)/hydroxyapatite scaffolds subjected to incubation in various physiological solutions.

Materials and methods. The research involved monitoring pH and conductivity values over a 14-day period, as well as analyzing the swelling capacity and mass alterations of the scaffolds.

Results. In simulated body fluid (SBF) and phosphate-buffered saline (PBS), the pH levels remained relatively stable, whereas Ringer's solution caused a pH decrease. Conversely, artificial saliva demonstrated an increase in pH, and distilled water caused a slight decrease. The conductivity values remained stable in SBF and Ringer's solution, slightly decreased in PBS, increased in artificial saliva, and significantly increased in distilled water. The swelling capacity of the scaffolds varied depending on the solution used, with the lowest equilibrium swelling observed in SBF and PBS. The effect of the presence of ceramics on this parameter was also observed. The mass changes of the scaffolds indicated deposition of particles or salts from the incubation solutions, and subsequent rinsing in distilled water led to a decrease in mass. Scanning electron microscopy (SEM) imaging and elemental analysis confirmed the presence of crystallized salts on the scaffold surfaces after incubation in SBF. Surface roughness measurements revealed changes in roughness depending on the solution, with deposition of additional layers in SBF and degradation in artificial saliva.

Conclusions. In summary, the scaffolds exhibited biodegradation in physiological solutions, with variations in pH, conductivity, swelling capacity, mass changes, and surface morphology depending on the specific solution and scaffold composition.

Key words: hydroxyapatite, incubation, poly(glycerol sebacate), scaffolds

Streszczenie

Wprowadzenie. Poli(sebacynian gliceryny) to materiał polimerowy o potencjalnym zastosowaniu biomedycznym w dziedzinie inżynierii tkankowej. Aby efektywnie pełnił rolę biodegradowalnego rusztowania komórkowego, niezbędne jest przeprowadzenie badania inkubacyjnego w celu symulacji jego zachowania.

Cel pracy. Prezentowane badanie przedstawia zachowanie pianek z poli(sebacynianu gliceryny) oraz hydroksyapatytu podczas inkubacji w różnych roztworach fizjologicznych.

Materiał i metody. Badania obejmowały monitorowanie wartości pH i przewodności przez okres 14 dni, a także analizę pęcznienia i zmian masy materiałów.

Wyniki. W buforze SBF (ang. simulated body fluid) oraz PBS (ang. phosphate-buffered saline) wartość pH pozostawała na stałym poziomie, podczas gdy w płynie Ringera wartość pH ulegała obniżeniu. Podczas inkubacji w sztucznej ślinie wartości pH wrastały, a w wodzie destylowanej ulegały niewielkiemu obniżeniu. Wartości przewodności pozostawały stabilne w SBF i płynie Ringera. Uległy natomiast niewielkiemu spadkowi w PBS, wzrosły w sztucznej ślinie, a znacznie wzrosły w wodzie destylowanej. Pęcznienie pianek ma bazie PGS zależało od użytego roztworu. Najniższe wartości pęcznienia równowagowego zaobserwowano w SBF i PBS. Zmiany masy rusztowań wskazywały na osadzanie się cząstek lub soli z roztworów inkubacyjnych. Przepłukanie materiałów wodą destylowaną powodowało obniżenie masy. Obrazowanie techniką skaningowej mikroskopii elektronowej (SEM) oraz analiza elementarna potwierdziły obecność soli wykrystalizowanych na powierzchniach materiałów po inkubacji w SBF. Pomiar chropowatości wykazał zmiany w wartościach współczynnika Sa w zależności od rodzaju wykorzystanego roztworu. W SBF dochodziło do depozycji dodatkowych warstw apatytowych oraz do zwiększonej degradacji w sztucznej ślinie.

Wnioski. Rusztowania wykazywały biodegradację w roztworach fizjologicznych. Różnice w przebiegu inkubacji były ilustrowane pomiarami wartości pH, przewodności, zdolności do pęcznienia, zmianie mas oraz morfologii powierzchni. Różnice wynikały z wykorzystanego roztworu oraz składu pianki.

Słowa kluczowe: hydroksyapatyt, inkubacja, poli(sebacynian glieryny), scaffoldy

Introduction

Poly(glycerol sebacate) (PGS) is an emerging biodegradable polyester for biomedical application, foremost in tissue engineering.[1–4] This polymeric material is considered biodegradable,[5,6] which is a desired trait for modern biomedical application. However, a biomaterial can behave diversely in various physiological fluids. In this study, PGS was combined with bioactive hydroxyapatite (HAp) in order to obtain porous scaffolds for bone tissue regeneration. This ceramics was selected considering its impressive properties in terms of its impact on osseointegration processes. Hydroxyapatite is widely applied in dentistry as well as orthopedics for its similarity in chemical composition to the inorganic phase of bone.[7–9] For this reason, as well as because of its osteoconductive properties, HAp is used in tissue engineering, with both in vitro and in vivo applications widely reported in the literature.[10] A material exhibiting osteoconductivity ensures the appropriate environment for the ingrowth of bone-forming elements from the surrounding area. Furthermore, by stimulating osteoblasts to proliferate, the growth of new apatite layers occurs.[11,12] Therefore, PGS is a great addition to biomaterials for bone regeneration, especially polymers, which often display significantly lower mechanical strength.[13,14]

In order to simulate the behavior of biomaterials in living organisms, different types of artificial biological fluids are used, of which the most common are simulated body fluid (SBF), artificial saliva, Ringer's fluid (which corresponds to the composition of extracellular fluid), or phosphate-buffered saline (PBS), whose composition corresponds to body fluids.[15–17] Different pH values as well as the composition of various artificial biological fluids affect the behavior of biomaterials in their presence, and in the case of in vitro tests, they can quickly provide the first information.[18,19] Such incubation studies are particularly important in the context of materials that are assumed to degrade in the body environment. Detailed potentiometric as well as conductometric monitoring helps to determine whether, during the process of degradation of the material into finer elements, there is precipitation and/or release of other components that could negatively affect the cellular balance. Strong acidification, i.e., a spike in pH values to highly alkaline, is a cause for concern, as under such conditions, cells in the area of the implant are unable to proliferate.[20,21] Therefore, in vitro studies are advisable before proceeding to cellular or in vivo studies on animal models.

As the physico-chemical and mechanical properties as well as cytocompatibility with L929 fibroblast cells of the very same materials was reported previously,[22] this study puts an emphasis on the behavior of the PGS and PGS/HAp scaffold materials during incubation. It is crucial to investigate the behavior of the biomaterial in various conditions and incubation fluids in order to consider further clinical application. Graphical scheme of the study is presented in Fig. 1.

Materials and methods

All of the chemical compounds utilized for synthesis of HAp and obtaining buffers were obtained from Chempur (Piekary Śląskie, Poland), except ammonia solution, which was obtained from Stanlab (Lublin, Poland).

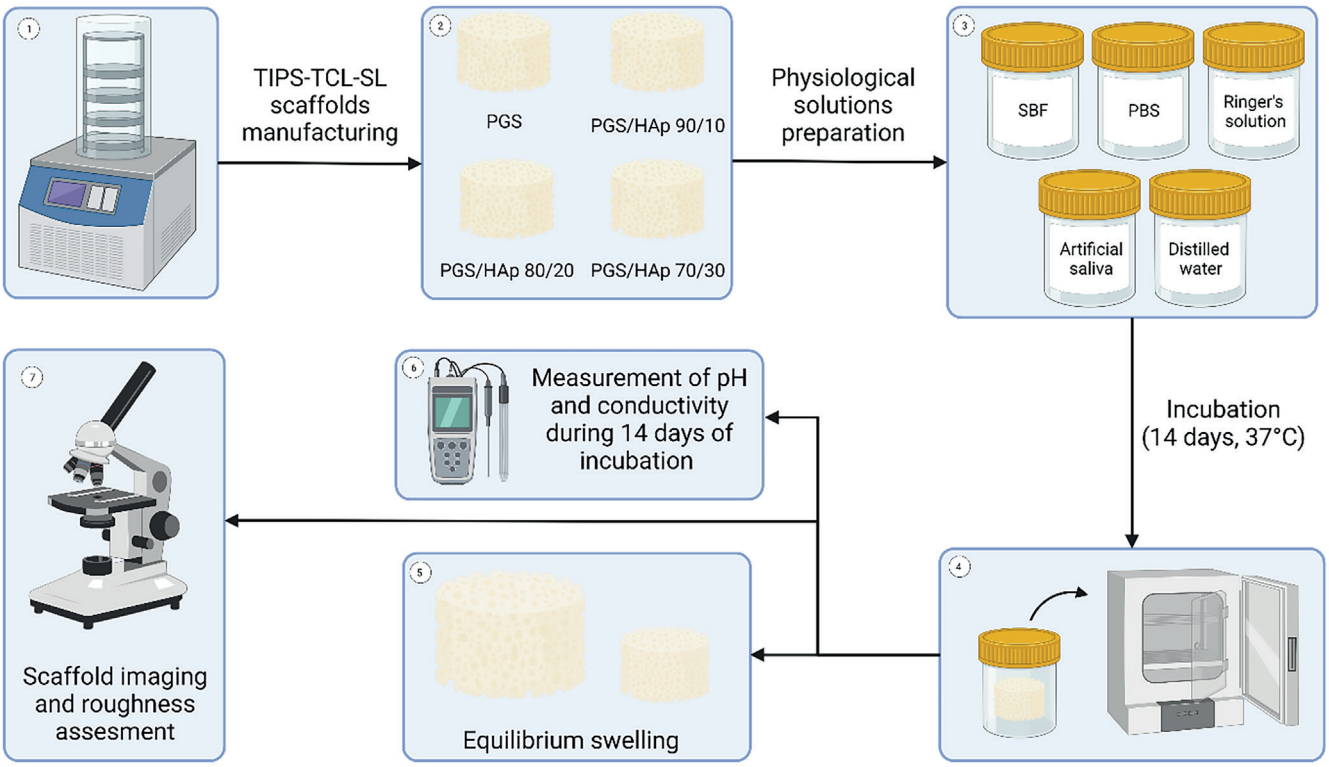

Fig. 1. Graphical scheme of the conducted study, created with BioRender.com

Synthesis of HAp

The synthesis process followed a previously reported wet precipitation method protocol.[23,24] First, 3.63 g of Na_2HPO_4 was dissolved in 80 mL of distilled water. The solution was transferred to the 3-necked, round-bottomed flask equipped with condenser and a thermocouple. Subsequently an additional 520 mL of water was added to dilute the solution. To achieve a pH of 11, a few drops of 25% ammonia solution were carefully added. After boiling the water, a solution of $Ca(CH_3COO)_2$ (created by dissolving 4.51 g of salt in 200 mL of water) was added dropwise with rate of 1 drop/s. After the solution was added, the reaction mixture was cooled to the ambient temperature and transferred to the beaker for sedimentation in the course of 24 h. The precipitate was subsequently washed with water until it reached a neutral pH. After centrifuging, the supernatant was decanted and obtained HAp was submitted to freeze-drying (–50°C, $p < 10$ Pa) after subsequent freezing (–15°C).

pPGS prepolymer synthesis and TIPS-TCL-SL scaffold manufacturing

The synthesis of poly(glycerol sebacate) prepolymer (pPGS) followed a previously established procedure by the authors.[22,25] Briefly, sebacic acid and glycerol were combined in an equimolar ratio with glycerol in 130°C. Reaction was allowed to proceed for 24 h and was halted by reducing the temperature to 25°C. Porous PGS scaffolds containing 0, 10, 20, and 30 wt% of HAp were manufactured using thermally induced phase separation followed by thermal cross-linking and salt leaching (TIPS-TCL-SL) technique described previously.[22,23] In brief, pPGS was dissolved in 1,4-dioxane at a concentration of 20 wt% and the corresponding amount of HAp was added to the mixture (with respect to the prepolymer mass) and stirred for 24 h. Solution was poured onto the porogen (400–500 µm NaCl particles) in a multi-well plates and frozen overnight. Afterwards, the specimens were freeze-dried and cured at 130°C for 7 days. After cross-linking, the porogen was leached out with water and samples were dried before subjecting for further experiments.

The authors had previously conducted physicochemical and structural characterization of the prepolymer[22,23,25] which included identification of characteristic structural bands on Fourier-transform infrared spectroscopy (FT-IR) spectrum, structural characterization with nuclear magnetic resonance (MRI) technique and contact angle measurement. Furthermore, the porous scaffolds manufactured in the same conditions were also characterized with respect to their thermal and mechanical properties.[22]

Buffer preparation and scaffold incubation

The scaffolds underwent a 14-day incubation period in 5 different physiological solutions: SBF, PBS, Ringer's solution, artificial saliva, and distilled water. A detailed

Table 1. Composition of buffers utilized for the study

Solution	Ingredient	Quantity
PBS	NaCl	8.00 g/L
	KCl	0.20 g/L
	Na_2HPO_4	1.15 g/L
	KH_2PO_4	0.20 g/L
SBF	NaCl	8.04 g/L
	$NaHCO_3$	0.36 g/L
	KCl	0.23 g/L
	$K_2HPO_4{\cdot}3H_2O$	0.23 g/L
	$MgCl_2{\cdot}6H_2O$	0.31 g/L
	1M HCl	40 mL
	$CaCl_2$	0.29 g/L
	Na_2SO_4	0.07 g/L
	Tris	6.12 g/L
	1M HCl (for adjusting pH)	0–5 mL
Ringer's solution	NaCl	8.60 g/L
	KCl	0.30 g/L
	$CaCl_2{\cdot}2H_2O$	0.48 g/L
Artificial saliva	NaCl	0.40 g/L
	KCl	0.40 g/L
	$CaCl_2{\cdot}2H_2O$	0.80 g/L
	$Na_2HPO_4{\cdot}H_2O$	0.78 g/L
	$Na_2S{\cdot}7H_2O$	0.01 g/L
	urea	1.00 g/L

PBS – phosphate-buffered saline; SBF – simulated body fluid.

breakdown of the composition of the utilized buffers can be found in Table 1. Solutions were obtained by dissolving the appropriate ingredients in distilled water except for the PBS solution, which was prepared by dissolving in water a ready-made commercial product in the form of tablet (Oxoid; Thermo Fisher Scientific, Waltham, USA). The SBF solution was prepared in the sequence presented in the Table 1 in 36.5°C. After all ingredients were dissolved, 1M HCl was added until pH was in the range of 7.5–8.0. The rest of the solutions were prepared in the room temperature. Four scaffolds of each type were placed in separate sterile 100 mL containers and poured over with 75 mL of each buffer. The incubation was performed in ST 5 SMART incubator (POL-EKO, Wodzisław Śląski, Poland) in 37°C for 14 days.

Buffer preparation and scaffold incubation

Throughout the incubation period, the solutions containing the scaffolds were regularly analyzed for pH and conductivity to investigate interactions between the samples and the incubation fluids. Conductivity and pH were assessed using a CX-701 pH-meter (Elmetron, Zabrze, Poland). These assessments were conducted at specific time intervals, namely, on the 1st, 3rd, 7th, 9th, and 14th day of the incubation process.

Equilibrium swelling

The swelling capacity of the tested scaffolds was assessed in all 5 incubation fluids over a 14-day period, with measurements taken at specific time intervals: 15 min, 30 min, 1 h, 2 h, 4 h, 1 day, 2 days, 7 days, 9 days, and 14 days. Samples with an initial mass ranging from 0.14 g to 0.22 g were placed in sterile 100 mL containers and submerged with 75 mL of the corresponding buffer solution. The swelling ratio (S_w) was calculated using Equation 1,[24,26,27] where *Wt* is the mass of swollen sample after given time and *W0* is the initial mass of the scaffold.

$$S_w = \frac{W_t - W_0}{W_0} \times 100\% \quad (1)$$

The swelling kinetics of the scaffolds was investigated using Voigt-based viscoelastic model using Equation 2,[28,29] where *St* is swelling ratio at given time (t), *Se* is equilibrium swelling and τ is a swelling rate parameter (time required to reach 0.63 of maximum swelling value).[30,31]

$$S_t = S_e \times \left(1 - e^{-\frac{t}{\tau}}\right) \quad (2)$$

The exponential fitting was performed in Origin software v. 2021b (OriginLab Corporation, Northampton, USA). The R^2 Pearson's correlation parameter was higher or equal to 0.92 within each fitting.

Optical imaging, 3D reconstruction and surface roughness measurement

Surface of the scaffolds were imaged using VHX Series Digital Microscope (Keyence, Osaka, Japan). Images were captured in 4k mode, providing a resolution of 4,000 × 3,000 pixels with additional depth of focus analysis. The CMOS VHZ-700 sensor (Keyence) enabled roughness analysis and the creation of 3D reconstructions of the scaffold surfaces. Scanning electron microscopy (SEM) microphotographs and local elemental analysis measured with energy dispersive spectroscopy (EDS) were registered using SEM Jeol 5510LV system (Jeol, Tokyo, Japan). Measurement parameters included threshold angle of 30° and voltage of 10 kV. The SEM microphotographs were registered with ×500 magnification. Before imaging the samples were spray-coated with gold using Cressington 108 sputter coater (Cressington Scientific Instruments, Watford, UK).

Results

Structural, physico-chemical and biological properties of porous PGS-based materials was reported by the authors previously.[22,23] Therefore, this article explores divergent

area which is stability, swelling, mass loss, and imaging during in vitro incubation in 5 different physiological solutions. Furthermore, the parameters of HAp synthesized and utilized in the presented study, including surface specific area, crystallinity and imaging, were published previously.[22,32]

Evolution of pH and conductivity during incubation

During an incubation of scaffolds in the physiological liquids the pH (Fig. 2,3), conductivity values were registered after 1, 3, 7, 9, and 14 days. The reference pH values of the solutions were 7.76 for SBF, 7.27 for PBS, 6.31 for Ringer's solution, 5.07 for artificial saliva, and 6.28 for distilled water. During the process, the pH values remained approximately constant for SBF and PBS. In the Ringer's solution, the pH values lowered after 14 days to 4.90 for PGS, 5.56 for PGS/HAp 90/10, 5.10 for PGS/HAp 80/20, and 5.58 for PGS/HAp 70/30. The decrease was the biggest for PGS and PGS/HAp 80/20 samples. The reverse effect was observed for artificial saliva. The pH values of the solutions increased over the incubation time up to 7.70 for PGS, 7.90 for PGS/HAp 90/10, 8.10 for PGS/HAp 80/20, and 8.70 for PGS/HAp 70/30.

Values of conductivity change with the concentration of the ions during incubation in the environment of solutions imitating physiological conditions.[33] Measured values for the reference solutions were 143.5 mS for SBF, 140.6 mS for PBS, 137.8 mS for Ringer's solution, 29,8 mS for artificial saliva, and 41.2 mS for distilled water. The conductivity remained approximately constant for SBF and Ringer's solution. In PBS, the measurements were also constant. However, they were slightly lower the buffer's reference value. In artificial saliva, a slight increase in measured property was noted (from ~30 mS to ~50 mS for all materials). The highest increase was observed in distilled water (even by 400% for PGS/HAp 80/20).

Equilibrium swelling

The swelling curves for all evaluated scaffolds were fitted using Equation 2 and presented on Fig. 4. The corresponding values of S_e and τ were juxtaposed in Table 2,3. Swelling analysis was performed for all solutions utilized previously. Based on the evolution of pH and conductivity over time, physiological solutions can be divided into groups: 1) those in which neither pH nor conductivity changed statistically significant over time (G1: SBF and PBS); 2) those in which pH level dropped down during incubation while conductivity was not affected (G2: Ringer's solution); and 3) solution in which both conductivity and pH values changed over the course of 14 days (G3: artificial saliva and distilled water). This division is beneficial for analyzing the swelling capacity of the scaffolds.

In G1, the material with lowest equilibrium swelling was PGS/HAp 70/30 with S_e of 166.7% in SBF and 236.7% in PBS. It is worth mentioning that in SBF, except for PGS/HAp 70/30 sample, all other materials possessed

Table 2. Values of equilibrium swelling for the evaluated scaffolds in SBF, PBS, Ringer's solution, artificial saliva, and distilled water

Solution	Se [%]			
	PGS	PGS/HAp 90/10	PGS/HAp 80/20	PGS/HAp 70/30
SBF	488.7 ±3.7	441.0 ±8.0	646.9 ±9.6	166.7 ±4.7
PBS	335.3 ±14.1	465.5 ±15.9	390.4 ±4.7	236.7 ±7.9
Ringer's solution	211.1 ±6.5	160.2 ±7.1	61.5 ±0.9	43.4 ±0.9
Artificial saliva	536.2 ±19.3	319.6 ±15.9	562.7 ±3.5	530.1 ±10.6
Distilled water	253.7 ±8.4	452.1 ±7.8	436.2 ±6.0	351.9 ±7.3

PBS – phosphate-buffered saline; SBF – simulated body fluid; PGS – poly(glycerol sebacate); HAp – hydroxyapatite.

Table 3. Values of τ rate parameter for the evaluated scaffolds in SBF, PBS, Ringer's solution, artificial saliva, and distilled water

Solution	τ [min]			
	PGS	PGS/HAp 90/10	PGS/HAp 80/20	PGS/HAp 70/30
SBF	0.05 ±0.01	0.03 ±0.01	0.03 ±0.01	1.46 ±0.32
PBS	0.94 ±0.38	0.92 ±0.23	0.53 ±0.05	1.17 ±0.24
Ringer's solution	0.66 ±0.23	0.99 ±0.33	0.26 ±0.06	0.73 ±0.27
Artificial saliva	0.63 ±0.21	3.20 ±0.72	2.91 ±0.07	3.39 ±0.25
Distilled water	1.17 ±0.23	0.65 ±0.08	1.98 ±0.13	0.57 ±0.09

PBS – phosphate-buffered saline; SBF – simulated body fluid; PGS – poly(glycerol sebacate); HAp – hydroxyapatite.

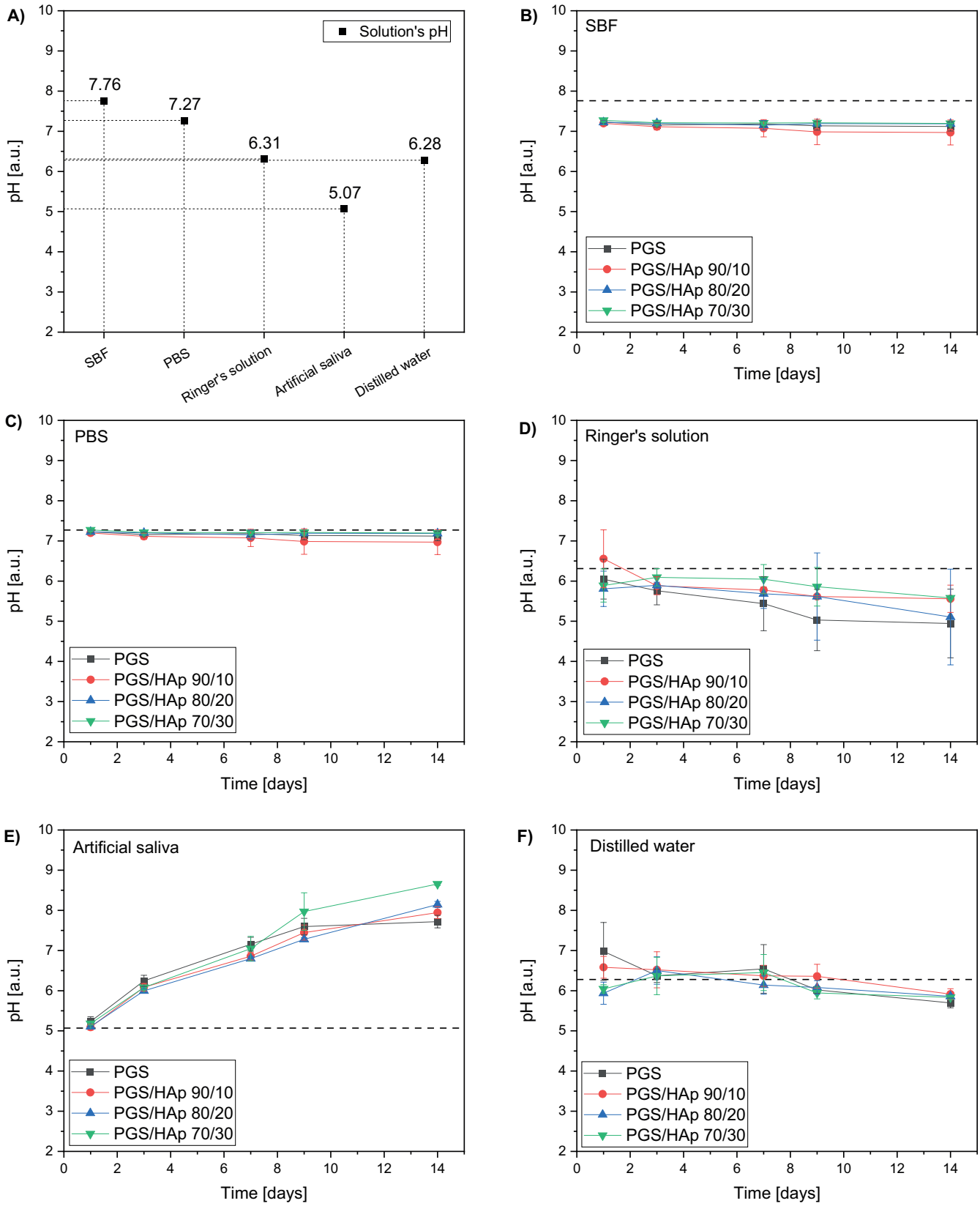

Fig. 2. The pH values of the reference solutions used for incubation of the scaffolds (A) as well its values during 14 days of incubation in simulated body fluid (SBF) (B), phosphate buffered saline (PBS) (C), Ringer's solution (D), artificial saliva (E), and distilled water (F)

the highest τ for all measured samples and therefore their swelling was the swiftest. In Ringer's solution (G3) the S_e swelling was the lowest among all solutions and gradually lowered with the concentration of HAp (from 211% for PGS down to 43% for PGS/HAp 70/30). The highest τ values (except for PGS) were observed in artificial saliva, indicating

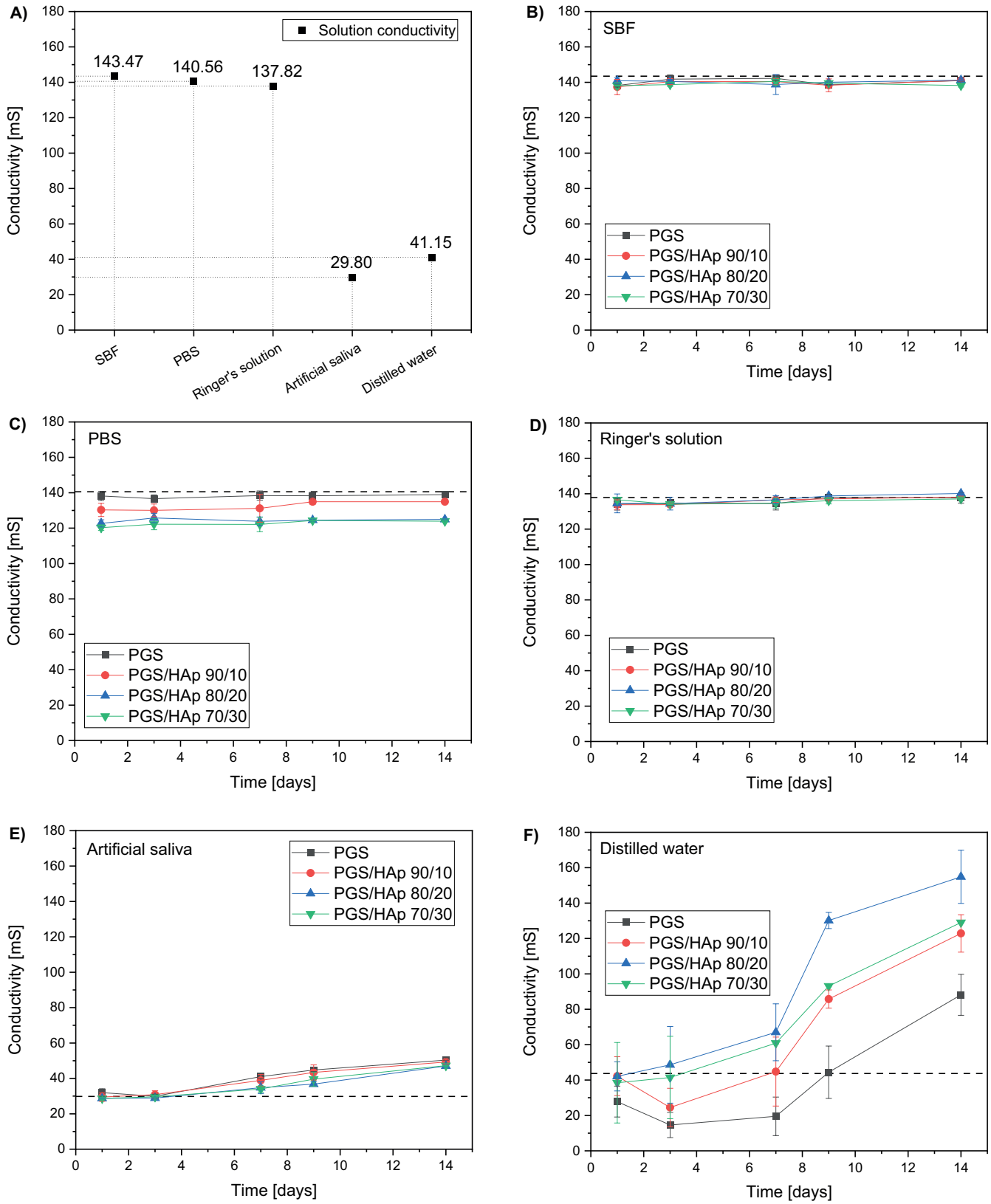

Fig. 3. Conductivity values of the reference solutions used for incubation of the scaffolds (A) as well its values during 14 days of incubation in simulated body fluid (SBF) (B), phosphate buffered saline (PBS) (C), Ringer's solution (D), artificial saliva (E), and distilled water (F).

the highest time required to achieve full swelling capacity (3.20 for PGS/HAp 90/10, 2.91 for PGS/HAp 80/20 and 3.39 for PGS/HAp 70/30). In H_2O, PGS exhibited lowest S_e (211%) and PGS/HAp 90/10 the highest (452%). In G3 no direct correlations between pH, conductivity and S_e is present.

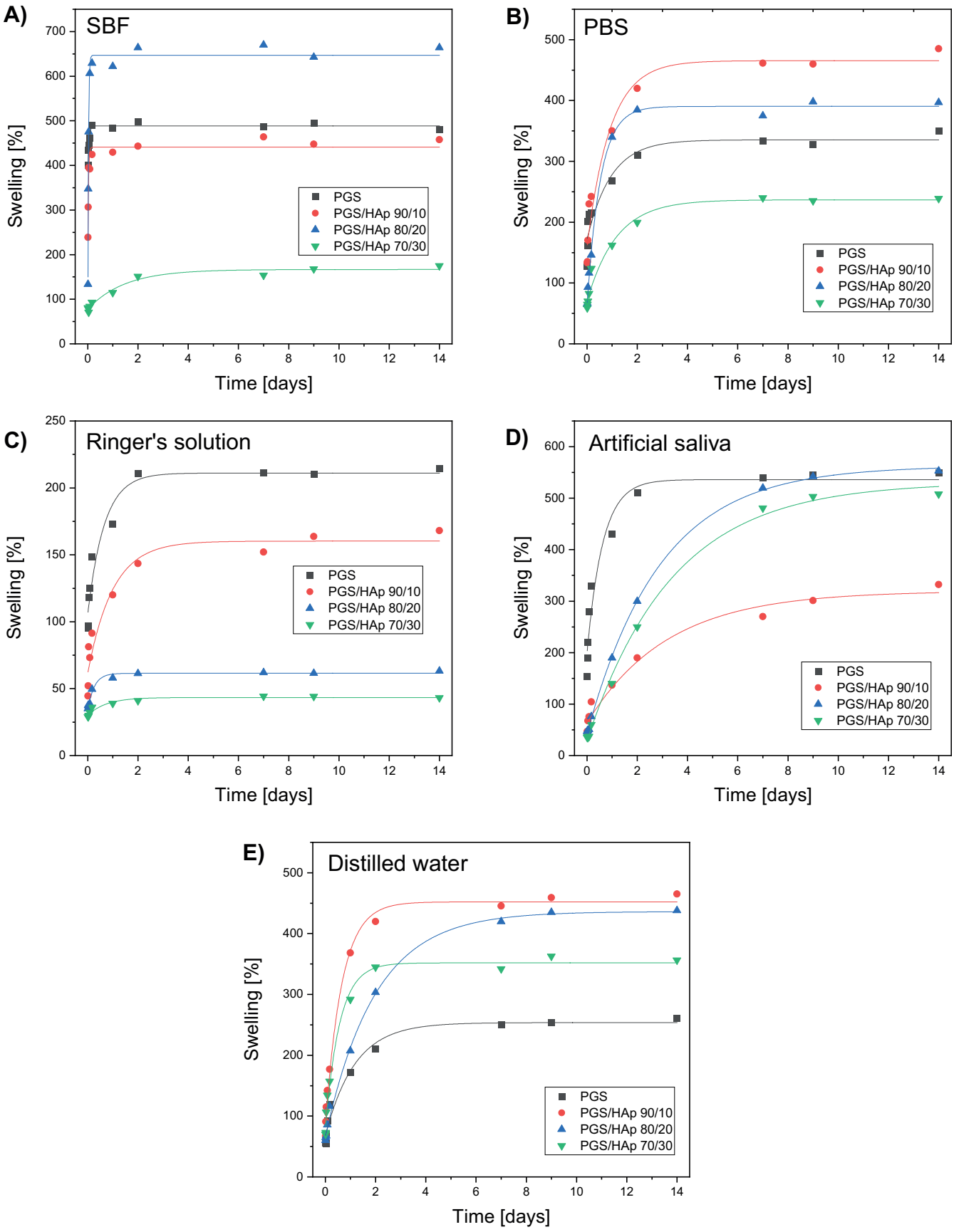

Fig. 4. Swelling of the evaluated scaffolds over 14 days in simulated body fluid (SBF) (A), phosphate buffered saline (PBS) (B), Ringer's solution (C), artificial saliva (D), and distilled water (E).

Scaffolds' imaging and roughness assessment

The change of scaffolds mass after the incubation is presented in Fig. 5. Samples were weighted directly after drying from incubation solutions (Fig. 5A) and after subsequent rinsing overnight in distilled water (Fig. 5B). For all scaffolds incubated in SBF, PBS and Ringer's solution, the change of mass was positive, weighted after drying straight from the incubation solutions.

After subsequent rinsing of the samples in water, the mass decreased in comparison to samples dried directly after incubation in all specimens and solution (Fig. 5B). The change of mass was the most significant in distilled water and dropped to –15% for polymer scaffold.

Moreover, the SEM imaging and EDS measurement revealed that for sample incubated in SBF, crystallized domains of salts present in the buffer composition were observed (Fig. 6). The accurate areas of EDS measurements are indicated as red marks on the SEM image. The detailed elemental composition is presented in Table 4. Most importantly, the majority of abundance consists of Na and Cl elements not present in the initial sample before incubation. The EDS measurement and SEM imaging performed on reference

Table 4. Weight and atomic % of C, O, Na, Mg, P, Cl, K, and Ca elements based on EDS analysis for the evaluated PGS/HAp 70/20 scaffold incubated in SBF. Presented results concern the points on the SEM images designated as 1 and 2

Sample	PGS/HAp 80/20 in SBF	
Point	1	2
C [at%]	45,061	46,317
C [wt%]	25,250	24,363
O [at%]	5,407	8,768
O [wt%]	4,036	6,144
Na [at%]	20,637	2,023
Na [wt%]	22,135	2,037
Mg [at%]	0,094	0,278
Mg [wt%]	0,106	0,296
P [at%]	0,488	1,898
P [wt%]	0,705	2,575
Cl [at%]	27,288	37,577
Cl [wt%]	45,134	58,343
K [at%]	0,196	0,375
K [wt%]	0,358	0,641
Ca [at%]	0,729	2,655
Ca [wt%]	1,364	4,661

PBS – phosphate-buffered saline; SBF – simulated body fluid; PGS – poly(glycerol sebacate); HAp – hydroxyapatite; SEM – scanning electron microscopy; EDS – energy dispersive spectroscopy.

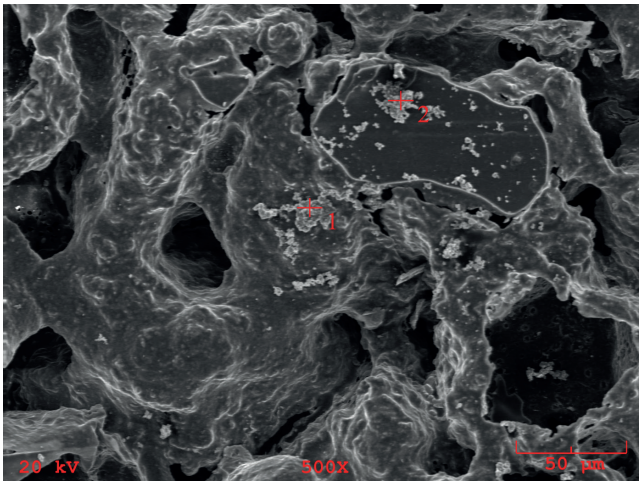

Fig. 6. Scanning electron microscopy (SEM) microphotographs of the PGS/HAp 80/20 scaffold after 14 days of incubation in simulated body fluid (SBF). The positions where energy dispersive spectroscopy (EDS) measurements took place are marked with red marks

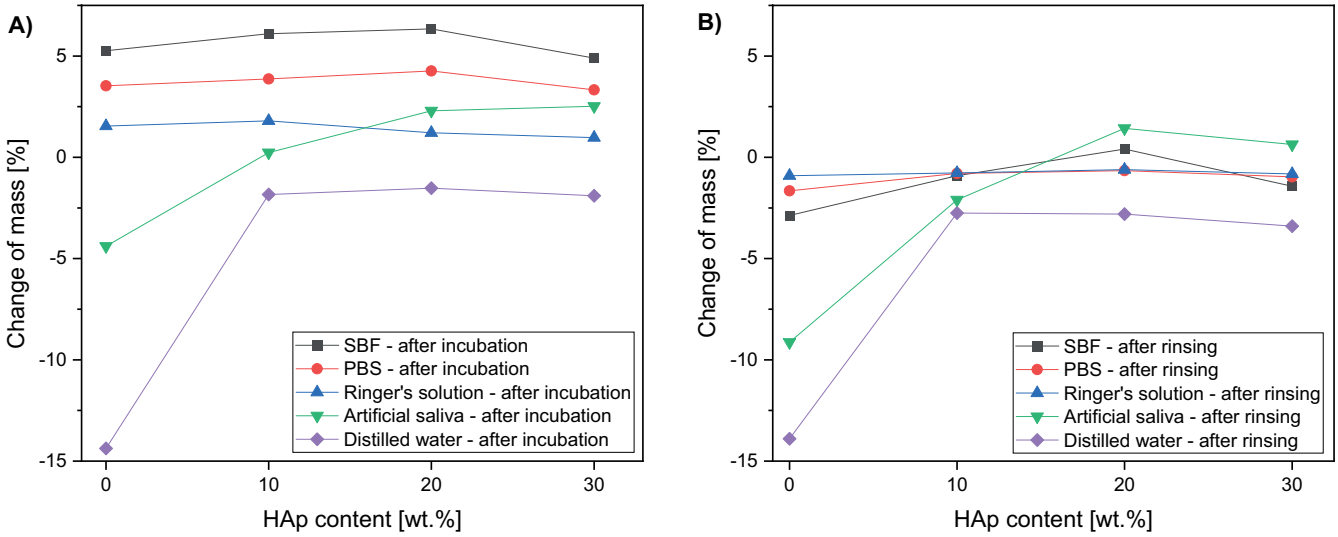

Fig. 5. Change in mass of the reference and composite scaffolds after 14 days incubation in simulated body fluid (SBF), phosphate buffered saline (PBS), Ringer's solution, artificial saliva, and distilled water for specimens dried straight after incubation (A) and samples dried followed by rinsing in distilled water in order to remove crystallized impurities (B)

Table 5. Surface roughness of the reference and composite scaffolds before and after 2 week of incubation in SBF, PBS, Ringer's solution, artificial saliva, and distilled water

Incubation medium	Sa [µm]			
	PGS	PGS/HAp 90/10	PGS/HAp 80/20	PGS/HAp 70/30
Sample before incubation	132.2	116.6	89.0	80.6
SBF	127.7	101.2	74.0	63.6
PBS	113.8	97.7	58.8	42.5
Ringer's solution	127.9	77.5	63.7	18.9
Artificial saliva	177.2	122.3	105.2	63.9
Distilled water	123.4	112.8	91.2	76.2

PBS – phosphate-buffered saline; SBF – simulated body fluid; PGS – poly(glycerol sebacate); HAp – hydroxyapatite; Sa – arithmetical mean height of the area.

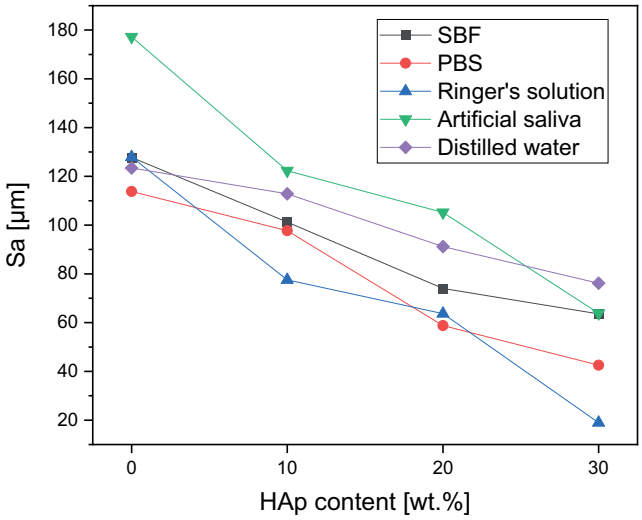

Fig. 7. Surface roughness of the reference and composite scaffolds after 2 week of incubation in simulated body fluid (SBF), phosphate buffered saline (PBS), Ringer's solution, artificial saliva, and distilled water. Roughness data was measured as an arithmetical mean height of the area (Sa) and showcased in the function of filler content

PGS and PGS/HAp scaffolds before incubation showcased the morphology and confirmed presence of apatite filler.[22]

The morphological changes are depicted by the evolution of the surface roughness measurement basing on 3D reconstructions from the optical microscope (VHX Series Digital Microscope; Keyence) (Fig. 7). For the reference samples before the incubation, a decrease in roughness can be observed as the amount of apatite filler increases: 132.2 µm for PGS, 116.6 µm for PGS/HAp 90/10, 89.0 µm for PGS/HAp 80/20, and 80.6 µm for PGS/HAp 90/30. This downward trend with the increasing amount of HAp persisted for all utilized solutions. Surface roughness before and after incubation is also presented in the Table 5.

Surface all of the samples before and after 14 days of incubation in SBF, PBS, Ringer's solution, and distilled water were registered in the form of 2D images, presented in Fig. 8,9. The morphology of the top layer of the scaffolds was visualized using a 3D reconstruction of microscopic images captured on optical microscope (VHX Series Digital Microscope; Keyence). Exemplary photographs of reference samples and samples incubated in SBF and artificial saliva are presented in Fig. 10.

Discussion

In artificial saliva, the greatest increased in pH values were observed among all evaluated buffers. One of the explanations of this effect may lay in the initial slightly acidic pH of the reference solution (5.08) – it may catalyze the degradation process of the scaffolds. Additionally, the ions released during the incubation might have influenced further changes in the pH values. Moreover, during incubation, partial leaching of HAp from the matrix might have occurred.[34] Despite its poor solubility, the solution containing HAp might have gained additional alkaline character.[35] In distilled water, a slight lowering in a pH from the reference value was noted. Changes in the pH value indicate interactions occurring at the fluid–material interface as well as the fact that the foams interact with the medium. In cases of inert (neutral) material, the pH value would remain at a constant level.

Regarding values of conductivity, such steep rise in values in distilled water might be correlated with low ionic force of water, which is disturbed by sudden introduction of new electrostatically charged beings to the solution.[36] Furthermore, in all showcased experiments, using distilled water eliminated the interference of other ions in the solution with evaluated scaffold.

The swelling ability of the material is related to the penetration of the liquid medium into its interior into the free spaces of the polymer chains.[37] In the case of composites, ceramic grains occupy these spaces; hence, a decrease in sorption capacity is observed as the proportion of the ceramic phase increases. However, even a low swelling capacity is a satisfactory result, as such a material can be used as a carrier for an active substance, from which the substance (e.g., a drug, protein or antibiotic) will be able to be slowly released as the liquid medium penetrates into the material.[38–40]

The changes in surface roughness of the scaffolds might indicate either deposition on new HAp particles or salts

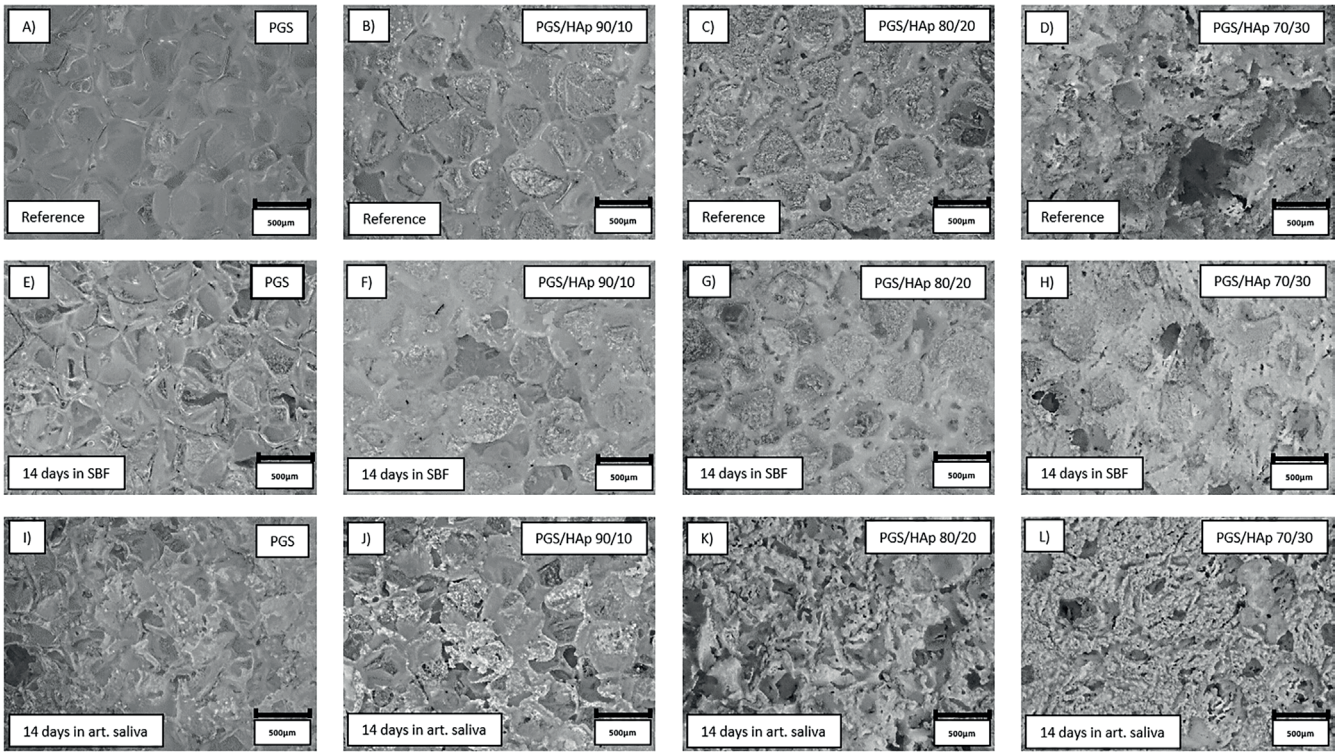

Fig. 8. Optical microscope images depicting surface of reference samples before incubation (A–D) as well as after 14 days of incubation in simulated body fluid (SBF) (E–H) and artificial saliva (I–L). Photographs were taken with ×100 magnification

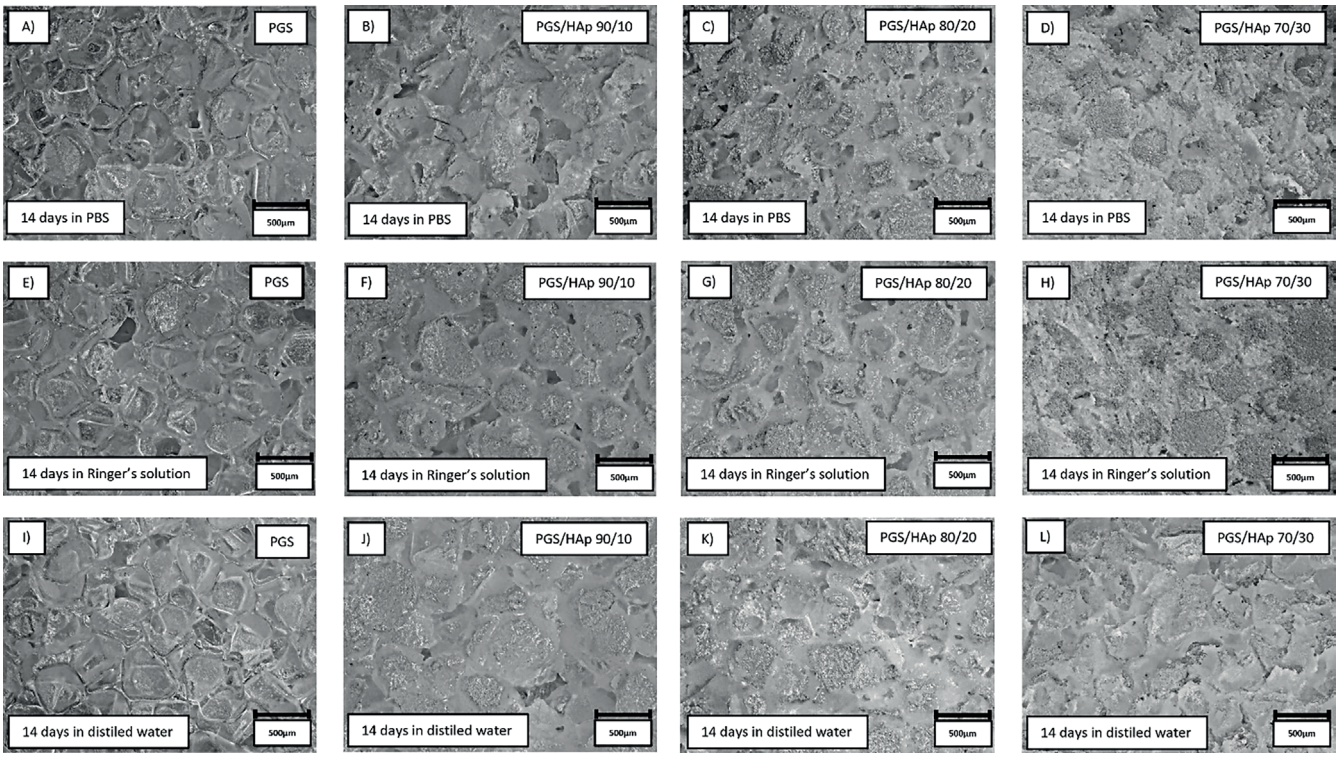

Fig. 9. Optical microscope images depicting surface of samples after 14 days of incubation in phosphate buffered saline (PBS) (A–D), Ringer's solution (E–H) and distilled water (I–L). Photographs were taken with ×100 magnification

present in the solutions. In case of polymer scaffolds, the HAp is not present and thus the gain in mass is due to the plausible crystallization of the salts present in solutions. This hypothesis was confirmed by decrease in mass for all samples incubated in distilled water, which does not contain statistically significant concentrations of ions. The increase of the pH value during incubation in artificial saliva was the greatest among all measured solutions,

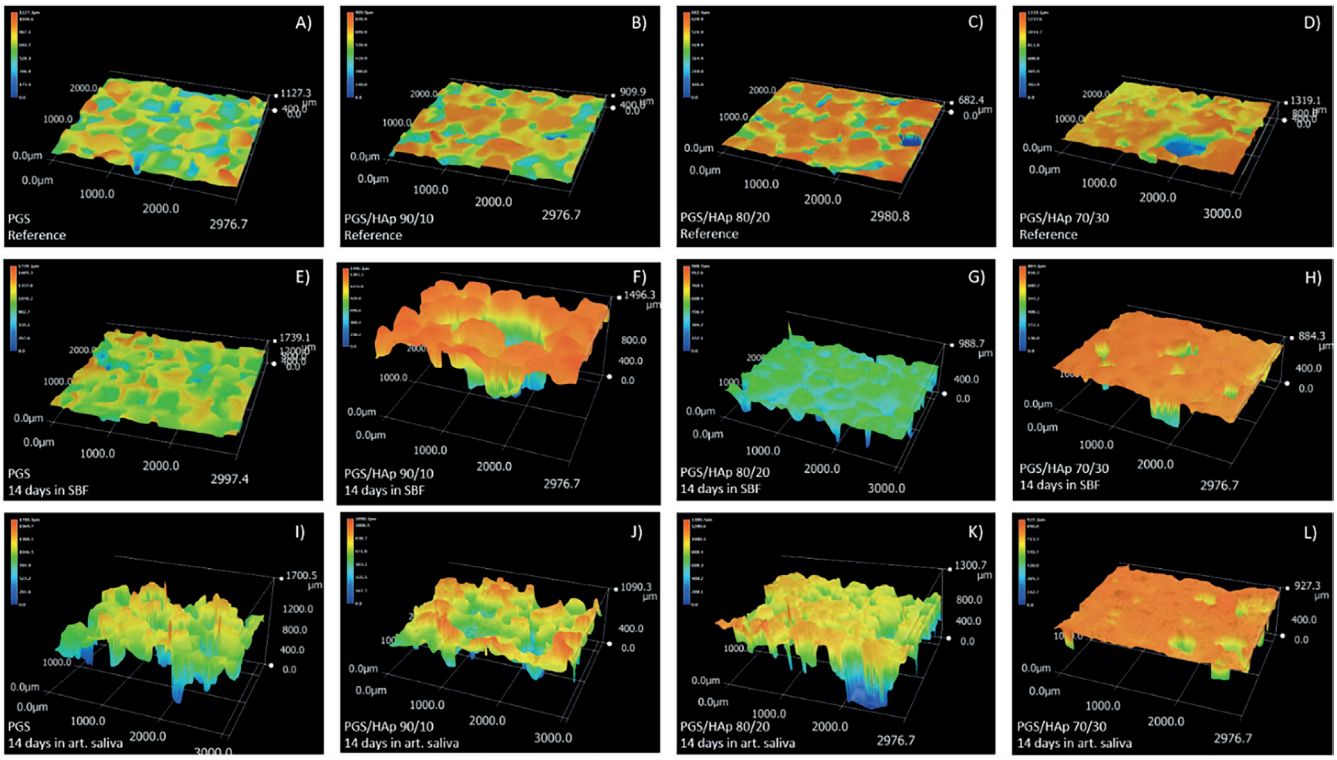

Fig. 10. Three-dimensional reconstructions of the surface of reference samples before incubation (A–D) as well as after 14 days of incubation in simulated body fluid (SBF) (E–H) and artificial saliva (I–L). The topography was obtained using reconstruction mode of optical microscope based on the pictures were taken with ×100 magnification

which might be an indication of degradation process occurring.[41] This was confirmed by loss in mass for PGS sample (approx. –5%). For specimens containing the apatite filler in artificial saliva, the mass change was positive – again most probably due to the salts present in the solution. The initial conclusion regarding crystallization of salts from incubation solutions was supported with changes in mass after subsequent rinsing in water before drying following incubation. Noticeably, the roughness of samples incubated in the distilled water overlapped with the reference values almost ideally. Moreover, the presented data indicate that the artificial saliva was the only solution for which the roughness was greater than for the reference sample. It might be yet another indication of degradation process occurring in this solution. For all other physiological solutions (SBF, PBS and Ringer's solution), the roughness was lowered in comparison with the reference. Therefore, deposition of additional layers on top of the scaffolds might have occurred. As it is clearly visible after incubation in SBF, deposition of additional layers on the surface was observed, while in saliva, the structure appear more frayed and degraded, except for PGS/HAp 70/30 sample.

Conclusions

We investigated the initial (14 days) degradation stage of PGS scaffolds, as well as PGS doped with HAp in 5 different liquids – distilled water, SBF, PBS, Ringer's fluid, and artificial saliva. The results obtained in SBF, PBS, Ringer's solution, and artificial saliva provide a biologically relevant context for potential biomedical applications, as these media simulate the environment of body fluids. Water serves as a reference medium to assess baseline degradation properties. The study showed that scaffold of neat PGS showed the lowest stability, understood as weight loss during degradation (–15% after 14 days of incubation), while doped PGS showed significantly higher stability (–2% after 14 days of incubation). The effect obtained does not depend significantly on the ceramic content (similar values were obtained for systems containing 10, 20 and 30 wt% of ceramics). The greatest loss of PGS scaffold masses is particularly related to degradation in distilled water and artificial saliva. Electrical conductivity tests carried out during incubation showed no significant differences for samples incubated in SBF, PBS and Ringer's fluid, while in the case of artificial saliva, an increase in conductivity was observed from a level of approx. 30 μS at the start of incubation to more than 40 μS after 14 days of incubation in all samples tested. Incubation conducted in distilled water led to an increase in conductivity from a level of approx. 30 μS to 80 μS for the reference sample and from approx. 40 μS to 120–150 μS for the composite scaffolds. This effect is related to the degradation of the PGS and the ingress of mineral matter from the composite into solution. The observed degradation is a beneficial process, as it will eventually be combined with the regeneration of autologous tissue, which aligns with the goals of biomedical applications where scaffold resorption supports tissue regeneration.

The conclusions for future research highlight the necessity for further investigation of long-term degradation beyond the initial 14 days, as well as the exploration of the effects of additional ceramic additives and bioactive compounds on scaffold performance. Furthermore, in vivo validations are required to confirm the behavior of the scaffold in physiological conditions and its integration with tissue. A limitation of this study is that it focuses exclusively on in vitro conditions, which may not fully capture the complexities of the in vivo environment.

ORCID iDs

Paweł J. Piszko https://orcid.org/0000-0002-7577-8509
Dagmara Słota https://orcid.org/0000-0002-8570-3594
Agnieszka Sobczak-Kupiec https://orcid.org/0000-0003-0005-6146
Agnieszka Tomala https://orcid.org/0000-0002-2327-3947
Karina Niziołek https://orcid.org/0000-0001-7970-3478
Wioletta Florkiewicz https://orcid.org/0000-0002-9392-4362
Konrad Szustakiewicz https://orcid.org/0000-0002-2855-852X

References

1. Piszko P, Kryszak B, Piszko A, Szustakiewicz K. Brief review on poly (glycerol sebacate) as an emerging polyester in biomedical application: Structure, properties and modifications. *Polim Med*. 2021;51(1): 43–50. doi:10.17219/pim/139585
2. Vogt L, Ruther F, Salehi S, Boccaccini AR. Poly(glycerol sebacate) in biomedical applications: A review of the recent literature. *Adv Healthcare Mater.* 2021;10(9):2002026. doi:10.1002/adhm.202002026
3. Rai R, Tallawi M, Grigore A, Boccaccini AR. Synthesis, properties and biomedical applications of poly(glycerol sebacate) (PGS): A review. *Prog Polym Sci*. 2012;37(8):1051–1078. doi:10.1016/j.progpolymsci.2012.02.001
4. Loh XJ, Abdul Karim A, Owh C. Poly(glycerol sebacate) biomaterial: Synthesis and biomedical applications. *J Mater Chem B*. 2015; 3(39):7641–7652. doi:10.1039/C5TB01048A
5. Pomerantseva I, Krebs N, Hart A, Neville CM, Huang AY, Sundback CA. Degradation behavior of poly(glycerol sebacate). *J Biomed Mater Res A*. 2009;91A(4):1038–1047. doi:10.1002/jbm.a.32327
6. Wang Y, Kim YM, Langer R. In vivo degradation characteristics of poly(glycerol sebacate). *J Biomed Mater Res A*. 2003;66A(1):192–197. doi:10.1002/jbm.a.10534
7. Wei Y, Chen M, Li M, et al. Aptamer/hydroxyapatite-functionalized titanium substrate promotes implant osseointegration via recruiting mesenchymal stem cells. *ACS Appl Mater Interfaces*. 2022;14(38): 42915–42930. doi:10.1021/acsami.2c10809
8. Kim J, Kang IG, Cheon KH, et al. Stable sol–gel hydroxyapatite coating on zirconia dental implant for improved osseointegration. *J Mater Sci Mater Med*. 2021;32(7):81. doi:10.1007/s10856-021-06550-6
9. Szwed-Georgiou A, Płociński P, Kupikowska-Stobba B, et al. Bioactive materials for bone regeneration: Biomolecules and delivery systems. *ACS Biomater Sci Eng*. 2023;9(9):5222–5254. doi:10.1021/acsbiomaterials.3c00609
10. Brogini S, Sartori M, Giavaresi G, et al. Osseointegration of additive manufacturing Ti–6Al–4V and Co–Cr–Mo alloys, with and without surface functionalization with hydroxyapatite and type I collagen. *J Mech Behav Biomed Mater.* 2021;115:104262. doi:10.1016/j.jmbbm.2020.104262
11. Chang BS, Lee CK, Hong KS, et al. Osteoconduction at porous hydroxyapatite with various pore configurations. *Biomaterials*. 2000;21(12): 1291–1298. doi:10.1016/S0142-9612(00)00030-2
12. Kumar D, Gittings JP, Turner IG, Bowen CR, Bastida-Hidalgo A, Cartmell SH. Polarization of hydroxyapatite: Influence on osteoblast cell proliferation. *Acta Biomater.* 2010;6(4):1549–1554. doi:10.1016/j.actbio.2009.11.008
13. Ramesh N, Moratti SC, Dias GJ. Hydroxyapatite–polymer biocomposites for bone regeneration: A review of current trends. *J Biomed Mater Res B Appl Biomater.* 2018;106(5):2046–2057. doi:10.1002/jbm.b.33950
14. Mahanty A, Shikha D. Changes in the morphology, mechanical strength and biocompatibility of polymer and metal/polymer fabricated hydroxyapatite for orthopaedic implants: A review. *J Polym Eng*. 2022; 42(4):298–322. doi:10.1515/polyeng-2021-0171
15. Yilmaz B, Pazarceviren AE, Tezcaner A, Evis Z. Historical development of simulated body fluids used in biomedical applications: A review. *Microchem J*. 2020;155:104713. doi:10.1016/j.microc.2020.104713
16. Baino F, Yamaguchi S. The use of simulated body fluid (SBF) for assessing materials bioactivity in the context of tissue engineering: Review and challenges. *Biomimetics*. 2020;5(4):57. doi:10.3390/biomimetics5040057
17. Leung VWH, Darvell BW. Artificial salivas for in vitro studies of dental materials. *J Dent*. 1997;25(6):475–484. doi:10.1016/S0300-5712(96)00068-1
18. Schille Ch, Braun M, Wendel HP, et al. Corrosion of experimental magnesium alloys in blood and PBS: A gravimetric and microscopic evaluation. *Mater Sci Eng B*. 2011;176(20):1797–1801. doi:10.1016/j.mseb.2011.04.007
19. Pandey AK, Kumar A, Kumar R, Gautam RK, Behera CK. Tribological performance of SS 316L, commercially pure Titanium, and Ti6Al4V in different solutions for biomedical applications. *Mater Today Proc*. 2023;78(Pt 4):A1–A8. doi:10.1016/j.matpr.2023.03.736
20. Vlădescu A, Pârâu A, Pană I, et al. In vitro activity assays of sputtered HAp coatings with SiC addition in various simulated biological fluids. *Coatings*. 2019;9(6):389. doi:10.3390/coatings9060389
21. Ruan C, Hu N, Ma Y, et al. The interfacial pH of acidic degradable polymeric biomaterials and its effects on osteoblast behavior. *Sci Rep*. 2017;7(1):6794. doi:10.1038/s41598-017-06354-1
22. Piszko P, Kryszak B, Gazińska M, et al. The effect of filler content on mechanical properties and cell response of elastomeric PGS/apatite foam scaffolds. *Ceram Int*. 2023;49(15):25353–25363. doi:10.1016/j.ceramint.2023.05.071
23. Piszko P, Włodarczyk M, Zielińska S, et al. PGS/HAp microporous composite scaffold obtained in the TIPS-TCL-SL method: An innovation for bone tissue engineering. *Int J Mol Sci*. 2021;22(16):8587. doi:10.3390/ijms22168587
24. Słota D, Florkiewicz W, Piętak K, et al. Preparation, characterization, and biocompatibility assessment of polymer-ceramic composites loaded with *Salvia officinalis* extract. *Materials (Basel)*. 2021;14(20):6000. doi:10.3390/ma14206000
25. Piszko P, Kryszak B, Szustakiewicz K. Influence of cross-linking time on physico-chemical and mechanical properties of bulk poly(glycerol sebacate). *Acta Bioeng Biomech*. 2022;24(4):85–93. doi:10.37190/ABB-02208-2023-04
26. Zhang X, Jia C, Qiao X, Liu T, Sun K. Porous poly(glycerol sebacate) (PGS) elastomer scaffolds for skin tissue engineering. *Polym Testing*. 2016;54:118–125. doi:10.1016/j.polymertesting.2016.07.006
27. Chen QZ, Bismarck A, Hansen U, et al. Characterisation of a soft elastomer poly(glycerol sebacate) designed to match the mechanical properties of myocardial tissue. *Biomaterials*. 2008;29(1):47–57. doi:10.1016/j.biomaterials.2007.09.010
28. Omidian H, Hashemi SA, Sammes PG, Meldrum I. A model for the swelling of superabsorbent polymers. *Polymer (Guildf)*. 1998;39(26): 6697–6704. doi:10.1016/S0032-3861(98)00095-0
29. Moini N, Kabiri K. Effective parameters in surface cross-linking of acrylic-based water absorbent polymer particles using bisphenol A diethylene glycidyl ether and cycloaliphatic diepoxide. *Iran Polym J*. 2015;24(11):977–987. doi:10.1007/s13726-015-0386-4
30. Kabiri K, Omidian H, Hashemi SA, Zohuriaan-Mehr MJ. Synthesis of fast-swelling superabsorbent hydrogels: Effect of crosslinker type and concentration on porosity and absorption rate. *Eur Polym J*. 2003;39(7): 1341–1348. doi:10.1016/S0014-3057(02)00391-9
31. Pluta K, Florkiewicz W, Malina D, et al. Measurement methods for the mechanical testing and biocompatibility assessment of polymer-ceramic connective tissue replacements. *Measurement*. 2021; 171:108733. doi:10.1016/j.measurement.2020.108733
32. Słota D, Piętak K, Florkiewicz W, et al. Clindamycin-loaded nanosized calcium phosphates powders as a carrier of active substances. *Nanomaterials*. 2023;13(9):1469. doi:10.3390/nano13091469
33. Słota D, Głąb M, Tyliszczak B, et al. Composites based on hydroxyapatite and whey protein isolate for applications in bone regeneration. *Materials (Basel)*. 2021;14(9):2317. doi:10.3390/ma14092317

34. Heimann RB, Graßmann O, Jennissen HP, Zumbrink T. Biomimetic processes duringin vitro leaching of plasma-sprayed hydroxyapatite coatings for endoprosthetic applications. *Materialwissenschaft und Werkstofftechnik*. 2001;32(12):913–921. doi:10.1002/1521-4052(200112)32:12<913::AID-MAWE913>3.0.CO;2-H
35. Sobczak-Kupiec A, Pluta K, Drabczyk A, Włoś M, Tyliszczak B. Synthesis and characterization of ceramic–polymer composites containing bioactive synthetic hydroxyapatite for biomedical applications. *Ceram Int*. 2018;44(12):13630–13638. doi:10.1016/j.ceramint.2018.04.199
36. Smedley SI. *The Interpretation of Ionic Conductivity in Liquids*. Boston, USA: Springer US; 1980. doi:10.1007/978-1-4684-3818-5
37. Karadag E, Saraydin D, Çetinkaya S, Güven O. In vitro swelling studies and preliminary biocompatibility evaluation of acrylamide-based hydrogels. *Biomaterials*. 1996;17(1):67–70. doi:10.1016/0142-9612(96)80757-5
38. Pietrzyńska M, Tomczak R, Jezierska K, Voelkel A, Jampílek J. Polymer-ceramic monolithic in-needle extraction (MINE) device: Preparation and examination of drug affinity. *Mater Sci Eng C Mater Biol Appl*. 2016;68:70–77. doi:10.1016/j.msec.2016.05.097
39. Carreño G, Marican A, Vijayakumar S, et al. Sustained release of linezolid from prepared hydrogels with polyvinyl alcohol and aliphatic dicarboxylic acids of variable chain lengths. *Pharmaceutics*. 2020;12(10):982. doi:10.3390/pharmaceutics12100982
40. Słota D, Florkiewicz W, Piętak K, et al. Preparation of PVP and betaine biomaterials enriched with hydroxyapatite and its evaluation as a drug carrier for controlled release of clindamycin. *Ceram Int*. 2022;48(23):35467–35473. doi:10.1016/j.ceramint.2022.08.151
41. Woodard LN, Grunlan MA. Hydrolytic degradation and erosion of polyester biomaterials. *ACS Macro Lett*. 2018;7(8):976–982. doi:10.1021/acsmacrolett.8b00424

Efficacy of sulforaphane in skin cancer animal models: A systematic review

Md Masoom[A–D], Mohd Ashif Khan[A–C,E,F]

Department of Translational and Clinical Research, School of Chemical and Life Sciences, Jamia Hamdard University, New Delhi, India

A – research concept and design; B – collection and/or assembly of data; C – data analysis and interpretation;
D – writing the article; E – critical revision of the article; F – final approval of the article

Polymers in Medicine, ISSN 0370-0747 (print), ISSN 2451-2699 (online) *Polim Med*. 2024;54(2):105–111

Address for correspondence
Mohd Ashif Khan
E-mail: makhan@jamiahamdard.ac.in

Funding sources
We would like to acknowledge the funding support provided by the Indian Council of Medical Research (ICMR), which is a national research organization under the Department of Health Research, Ministry of Health and Family Welfare, Government of India. We are grateful for the financial assistance received from ICMR that helped make this possible.

Conflict of interest
None declared

Received on February 22, 2024
Reviewed on May 27, 2024
Accepted on May 28, 2024

Published online on November 18, 2024

Abstract

Globally, skin cancer is the predominant form of cancer, with melanoma identified as its most deadly variant. Projections suggest a surge exceeding 50% in melanoma occurrences by 2040, underscoring the urgency for preventive interventions. Sulforaphane (SFN), a compound found in cruciferous vegetables, is recognized for its cancer-preventive capabilities, particularly against skin cancer. This study employed a rigorous systematic review of various databases, adhering to predefined inclusion criteria for study selection. Data extraction was conducted using a uniform template, and the quality of the included studies was evaluated through the Systematic Review Centre for Laboratory Animal Experimentation (SYRCLE) risk of bias tool, specifically designed for animal research. The review encompasses studies published in English from 2000 to 2023, culminating in the inclusion of 9 pertinent studies. The findings highlight SFN's capacity to act as a protective agent in preventing skin cancer in animal models. It demonstrated efficacy in curbing skin tumorigenesis triggered by assorted carcinogens, reducing the onset of skin tumors and impeding the growth and spread of skin cancer cells. Furthermore, SFN showed preventive effects against UVB-induced skin carcinogenesis by obstructing the activator protein 1 signaling pathway. Based on evidence from animal-based research, SFN emerges as a promising chemopreventive substance against skin cancer. Nevertheless, determining its optimal dosage, application duration and method of administration for human subjects remains pending. If its effectiveness is substantiated, SFN could complement or offer an alternative to existing preventive measures against skin cancer.

Key words: sulforaphane, skin cancer, animal models, chemoprevention

Cite as
Masoom Md, Khan MA. Efficacy of sulforaphane in skin cancer animal models: A systematic review. *Polim Med*. 2024;54(2):105–111. doi:10.17219/pim/189406

DOI
10.17219/pim/189406

Introduction

In 2020, the global incidence of melanoma was estimated at approx. 325,000 cases, resulting in about 57,000 fatalities. The International Agency for Research on Cancer (IARC) forecasts a significant surge in the incidence of cutaneous melanoma by over 50%, reaching more than 500,000 annual cases by 2040, with fatalities anticipated to increase by over 2/3 to nearly 100,000 per annum.[1] Despite the preventable nature of many instances, cutaneous melanoma represents the most lethal form of skin cancer, comprising approx. 20% of all skin cancer diagnoses. Skin cancer is the most frequently diagnosed cancer globally, with an estimated 1.5 million new cases reported in 2020.[1]

The predominant forms of skin cancer include basal cell carcinoma, squamous cell carcinoma and melanoma.[2] A primary risk factor for skin cancer development is ultraviolet (UV) radiation exposure from the sun, with the risk increasing cumulatively over time.[2] While most skin cancer cases are treatable through surgical or alternative therapeutic interventions, prevention plays a pivotal role in reducing the disease's burden.[3] Among the preventative strategies, the use of sunscreen and protective clothing has proven effective in reducing the risk of skin cancer onset. Nevertheless, there is an urgent need for additional preventative measures, particularly for individuals at high risk of the disease.

A variety of promising phytochemicals, such as epigallocatechin-3-gallate, resveratrol, curcumin, pro-anthocyanidins, silymarin, apigenin, capsaicin, genistein, indole-3-carbinol, and luteolin, derived from various fresh fruits, vegetables, roots, and herbs, have been identified to enhance cancer chemoprevention and treatment through diverse mechanisms.[4] Sulforaphane (SFN), an isothiocyanate naturally occurring in cruciferous vegetables such as broccoli, Brussels sprouts and cabbage, has demonstrated chemopreventive properties against various cancers, including skin cancer.[5] Sulforaphane is known for activating the nuclear factor erythroid 2–related factor 2 (Nrf2) pathway, implicated in cellular defense against oxidative stress and inflammation.[6] Activation of the Nrf2 pathway facilitates the induction of phase 2 detoxifying enzymes, aiding in the prevention of carcinogen formation and promoting their elimination from the organism.[7]

Preclinical investigations have explored SFN's efficacy against skin cancer in animal models. For instance, SFN has been shown to inhibit skin tumor growth in mice exposed to the carcinogen 7,12-dimethylbenz(a)anthracene (DMBA).[8] Furthermore, it has provided protection against UV radiation-induced skin carcinogenesis in SKH-1 high-risk mice[9] and has been shown to prevent the development of skin tumors in mice by inhibiting the promotion stage of skin carcinogenesis.[10]

Topical photodynamic therapy (PDT) with 5-aminolevulinic acid (ALA) is commonly used to treat non-melanoma skin cancers, actinic keratoses and various dermatoses. However, it may cause adverse effects, such as pruritus, erythema, edema, and pain. The compound (R)-L-SFN has been found to reduce erythema while inducing DNA fragmentation, leading to apoptotic cell death.[11] Another investigation assessed SFN's impact on protoporphyrin IX (PpIX) production and PDT efficacy, revealing that SFN did not affect PpIX photodegradation and increased PpIX synthesis in human skin, although not in A431 cells. The findings suggest that (R)-L-SFN pre-treatment prior to topical ALA-PDT could enhance ALA penetration through the stratum corneum, thereby increasing PpIX synthesis.[11] Although preclinical studies have shown promising results, more research is needed to understand the potential benefits of SFN for the prevention and treatment of skin cancer in humans. This systematic review aims to collate and analyze the existing evidence regarding the application of SFN in skin cancer across preclinical and clinical studies.

Methodology

This study was meticulously designed following the PROSPERO guidelines, which establish the gold standards for conducting systematic reviews. Registration with PROSPERO, under the No. CRD42023417867, ensured transparency and compliance with the established protocol. The primary aim of this systematic review was to examine the existing scientific literature on the effectiveness of SFN in preventing and treating skin cancer in animal models. To conduct a comprehensive literature survey, searches were conducted across multiple databases, including PubMed, Science Direct, Embase, and Google Scholar. The search strings included combinations of keywords such as "sulforaphane", "skin cancer", "nonmelanoma skin cancer", "squamous cell carcinoma", "basal cell carcinoma", "melanoma", "animal models", and "preclinical studies". Boolean operators (AND, OR) were used to refine the search results. For instance, the PubMed search string was "sulforaphane AND (skin cancer OR melanoma OR squamous cell carcinoma OR basal cell carcinoma) AND (animal model OR preclinical study)". Discrepancies in study inclusion were resolved through discussions between the 2 authors. The search parameters were limited to studies published in English from 2000 to 2023, initiating the search in April 2022 and updating it in March 2023.

The inclusion criteria for this review were rigorously defined. We primarily selected studies that examined the impact of SFN on skin cancer using animal models. Studies were required to provide detailed descriptions of the methodologies used, and they needed to include at least 1 measure evaluating the chemopreventive effects of SFN. Only peer-reviewed scientific journal publications were included in our analysis.

A standardized form was utilized for data extraction from the selected studies, capturing vital information such

as study design, animal models used, sample sizes, intervention types, assessed outcomes, and resulting conclusions.

Risk of bias assessment

In this systematic review, the internal validity of preclinical animal studies was evaluated using the Systematic Review Centre for Laboratory Animal Experimentation (SYRCLE) risk of bias tool, as outlined by Hooijmans et al. in 2014.[12] This comprehensive tool scrutinizes 10 critical domains to assess the risk of bias, namely sequence generation, baseline characteristics, allocation concealment, random housing, blinding, random outcome assessment, incomplete outcome data, selective outcome reporting, other sources of bias, and overall risk of bias.

The assessment revealed a spectrum of bias risks across the included studies. For instance, the studies by Abel et al. and Shibata et al.[13,14] were characterized by low-risk ratings in all domains, indicating methodological rigor and reliability. In contrast, studies by Alyoussef and Taha,[15] Dinkova-Kostova et al.[9] and Gills et al.[10] exhibited higher or indeterminate risks of bias in certain areas. Notably, blinding emerged as a recurring concern, with many studies receiving high or ambiguous ratings for this domain, suggesting potential vulnerabilities in their designs. The bias assessment revealed variability in methodological quality across studies, particularly in sequence generation and allocation concealment, indicating a need for improved randomization processes. Additionally, blinding of outcome assessment was another area with a high risk of bias, particularly in studies by Alyoussef and Taha[15] and Gills et al.[10] These biases could potentially influence the observed effects of SFN on skin cancer. Detailed findings are summarized in Table 1,[8–10,13–18] with annotations on studies exhibiting high or unclear risk in specific domains. Although the SYRCLE risk of bias tool provides a structured approach for identifying potential biases in preclinical animal studies, it is essential to acknowledge that no evaluative mechanism can entirely eliminate bias or confounding variables. Nonetheless, the application of the SYRCLE risk of bias tool is instrumental in identifying and, where possible, mitigating biases, thereby enhancing the internal validity of the preclinical animal research under review.

Results

Search results

The initial search across 4 databases (PubMed, Science Direct, Embase, and Google Scholar) for studies concerning SFN and skin cancer in animals produced a total of 5,661 records. Among these, 143 duplicate records were removed, and 4,222 records were marked as ineligible by automation tools. Additionally, 894 records were excluded for various reasons, resulting in 402 records remaining for screening. During the screening process, 386 records were excluded for reasons such as failing to meet inclusion/exclusion criteria or being associated with cell line studies or human clinical trials. After the eligibility assessment, 16 reports were identified for retrieval, all of which were retrieved. These 16 reports were then screened in their entirety, leading to the exclusion of 7 reports. Exclusion criteria included 2 reports not meeting the inclusion/exclusion criteria, 3 being related to cell line studies, and 1 being a human clinical trial. Subsequently, a Preferred Reporting Items for Systematic reviews and Meta-Analyses (PRISMA) chart was created to reflect these findings (Fig. 1). Summary of preclinical studies on the effects of SFN in various animal models of skin tumorigenesis is presented in Table 2.[8–10,13–18]

Sulforaphane in skin cancer: Molecular pathways and mechanisms

In the context of skin cancer, SFN exerts its potent anticancer effects by intricately modulating various molecular pathways and targets. These include the Nrf2 pathway,

Table 1. Risk of bias assessment

Reference	Sequence generation	Baseline characteristics	Allocation concealment	Random housing	Performance blinding	Random outcome assessment	Detection blinding	Attrition bias	Selective outcome reporting
8	U	U	U	U	U	U	U	L	L
9	U	L	U	L	H	L	H	L	L
10	U	L	U	L	H	L	H	L	U
13	U	L	U	L	U	L	U	L	L
14	U	L	U	L	U	L	U	L	L
15	L	L	U	U	H	L	H	L	L
16	U	H	U	U	U	U	U	L	L
17	U	L	U	L	H	L	H	L	U
18	U	L	U	U	H	L	H	L	L

L – low risk; H – high risk.

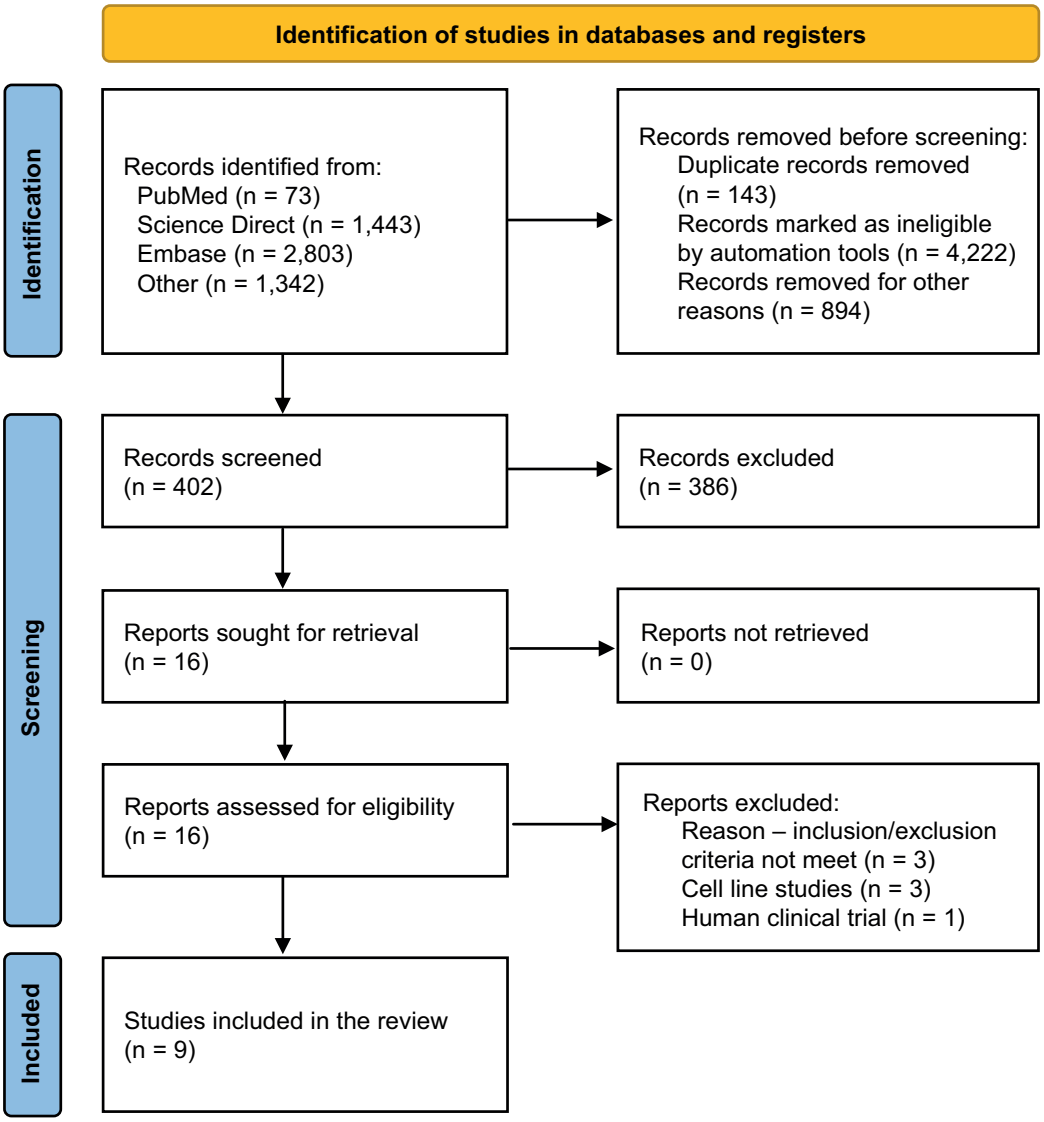

Fig. 1. Preferred Reporting Items for Systematic reviews and Meta-Analyses (PRISMA) flowchart diagram

where SFN acts as a robust activator, facilitating the nuclear translocation of Nrf2 to interact with antioxidant response elements in the DNA. This instigates the transcription of genes encoding antioxidant and detoxification enzymes, thereby shielding cells from oxidative insults. Sulforaphane also activates the p53 pathway, a pivotal tumor suppressor pathway orchestrating cell growth and division through mechanisms involving apoptosis induction, cell cycle arrest and DNA repair. Additionally, SFN exerts an inhibitory influence on the Wnt pathway, responsible for cellular proliferation, differentiation and migration, by suppressing key Wnt signaling proteins. Sulforaphane also intervenes in the transforming growth factor beta (TGF-β) pathway, impeding the activation of TGF-β signaling receptors, thereby affecting various cellular processes, including growth, differentiation and apoptosis. Moreover, SFN regulates the EGFR pathway, which governs cell proliferation, differentiation and survival, by downregulating EGFR and its downstream signaling molecules. Lastly, SFN plays a pivotal role in modulating the PI3K/AKT pathway, associated with cell proliferation, survival and growth, by blocking the activation of PI3K and AKT. These actions collectively underscore the multifaceted and promising potential of SFN as an agent for skin cancer prevention and therapy. The above mechanisms are shown in Fig. 2.

Discussion

This systematic review aimed to assess the effectiveness of SFN in mitigating skin cancer in animal models. It analyzed 10 research studies that explored the impact of SFN on various aspects of skin cancer, including tumor initiation, growth and the underlying molecular processes contributing to cancer advancement. The evidence from these studies collectively indicates a potential protective role of SFN against skin cancer in animal models. Notably, SFN administration was found to mitigate skin tumorigenesis in mouse models exposed to carcinogens such as 7,12-dimethylbenz(a)anthracene (DMBA) and ultraviolet B (UVB) radiation. Xu et al.[8] elucidated that SFN suppresses DMBA-induced skin tumors in C57BL/6

Table 2. Summary of preclinical studies on the effects of sulforaphane (SFN) in various animal models of skin tumorigenesis

Reference	Animal model used	SFN dose	Study duration	Parameters assessed	Conclusions
8	Nrf2(–/–) mice (C57BL/SV129)	100 nmol	14 days	skin tumorigenesis	Sulforaphane demonstrated a significant reduction in skin cancer development in mice with functional Nrf2 (Nrf2(+/+)) but was ineffective in mice without Nrf2 (Nrf2(–/–)).
9	female SKH-1 hairless mice	100 µmol	11 weeks	tumor burden, incidence and multiplicity	Sulforaphane treatment is effective at inhibiting tumorigenesis in this model, especially when using the higher dose of SFN.
10	female CD-1	10 mmol/mouse	5 h	skin tumorigenesis	Sulforaphane inhibited TPA-induced ornithine decarboxylase activity in mouse skin, an obligate step in TPA-induced promotion of carcinogenesis.
13	NSG (NOD/scid/IL-2 receptor gamma knockout) mice	5–10 µM of SFN or cisplatin	5 weeks	impact of SFN and cisplatin on tumor formation	Sulforaphane treatment of cultured cells or tumors increases apoptosis and p21Cip1 level, and both agents increase tumor apoptosis.
14	HR-1 hairless mice	0–25 µM, 1 mg/day (oral)	14 days	effect of oral administration of SF on skin thickening	Sulforaphane has a potential use as a compound for protection against UVB-induced skin inflammation.
15	Swiss albino mice	9 µmol/mouse/day	16 weeks	effect of SFN on skin cell structure, anti-tumor activity	Compared to controls, skin cancer induced a 2.8-fold increase in sulfatase-2 levels after 11 weeks of treatment.
16	NSG mice	10 µmol per treatment	3 weeks	sulforaphane and tumor formation, PRMT5/MEP50 function	By targeting PRMT5/MEP50, SFN suppresses tumor growth, highlighting its essential role in cancer progression.
17	SKH-1 hairless female mice	1 µmol/mouse or 2.5 µmol/mouse	25 weeks	multiplicity and tumor burden	Sulforaphane treatment is effective at inhibiting tumorigenesis in this model, especially when using the higher dose of SFN.
18	NSG (NOD/scid/IL-2 receptor gamma knockout) mice	5–10 µM of SFN or cisplatin	5 weeks	impact of SFN and cisplatin on tumor formation	Sulforaphane treatment of cultured cells or tumors increases apoptosis and p21Cip1 level, and both agents increase tumor apoptosis.

SFN – sulforaphane; Nrf2 – nuclear factor erythroid 2-related factor 2; PRMT5 – protein arginine methyltransferase 5; MEP50 – methionine-tRNA methyltransferase 50; TPA – tetradecanoylphorbol acetate; ODC – ornithine decarboxylase; p21Cip1 – cyclin-dependent kinase inhibitor 1; CEES – chloroacetophenone-induced skin carcinogenesis; UVB – ultraviolet B; HR-1 – hairless.

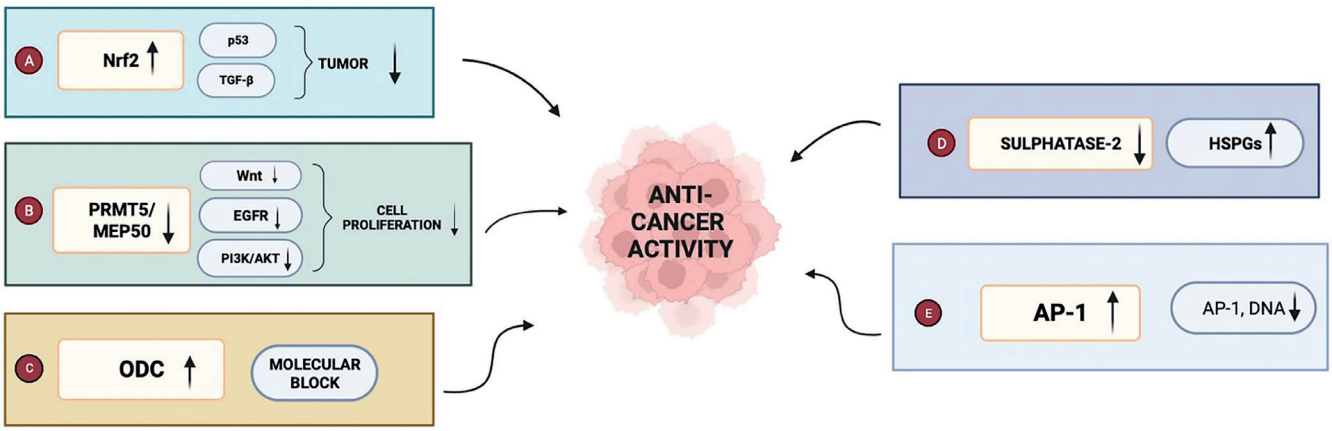

Fig. 2. Molecular pathway of sulforaphane (SFN) in skin cancer

↑ – activation or increase; ↓ – inhibition or decrease; Nrf2 – nuclear factor erythroid 2 related factor 2; PMRT5/MEP50 – protein arginine methyltransferate 5/ methylosome protein 50; ODC – ornithine decarboxylase; AP-1 – activator protein 1; IL-6 – interleukin 6; TNF-α – tumor necrosis factor alpha; HSPGs – heparan sulfate proteoglycans; PGE2 – prostaglandin E2; EGFR – epidermal growth factor receptor; JAK/STAT – Janus kinase/signal transducers and activators of transcription; NF-κB – nuclear factor kappa light-chain-enhancer of activated B cells; MAPK – mitogen-activated protein kinase; PI3K/AKT – phosphoinositide 3-kinase/protein kinase B; TGF-β – transforming growth factor beta.

mice by activating Nrf2. Recent research has highlighted Nrf2's role in modulating antioxidant, detoxifying and drug-metabolizing enzymes, thereby conferring SFN's chemopreventive potential.[19] Similarly, Dinkova-Kostova et al.[9] demonstrated that SFN-enriched broccoli sprout extracts confer protection against UVB-induced skin carcinogenesis in SKH-1 high-risk mice by inducing phase-2 detoxifying enzymes.

The inhibitory effects of SFN on the proliferation and invasion of epidermal squamous cell carcinoma (SCC) cells further underscore its chemopreventive efficacy. Saha et al.[16] reported that SFN curtails SCC tumor formation by downregulating protein arginine methyltransferase 5 and methylosome protein 50, proteins implicated in cancer prognosis and epigenetic regulation.[20] Additionally, SFN's blockade of sulfatase-2, an enzyme with oncogenic properties in human cell lines,[21] significantly reduced melanoma cell growth and metastasis in mouse models.[15] Moreover, SFN exhibits an ability to prevent skin tumorigenesis during the critical tumor promotion stage. Dickinson et al.[17] found that SFN treatment attenuates the expression of proinflammatory cytokines, including interleukin (IL)-1β, IL-6 and tumor necrosis factor alpha (TNF-α), thereby inhibiting tumor promotion. This anti-inflammatory action is complemented by SFN's inhibition of the activator protein 1 pathway, a mechanism proposed to underlie its protective effect against UVB-induced skin cancer.[22]

Emerging clinical evidence suggests the therapeutic potential of SFN in the treatment of skin cancer. A clinical trial conducted by Tahata et al.[18] assessed the safety and efficacy of broccoli sprout extract containing SFN in patients with atypical nevi and a history of melanoma. The study reported dose-dependent increases in SFN levels in plasma and skin, accompanied by reductions in proinflammatory cytokines and an increase in tumor suppression, advocating for further investigation into SFN as a chemopreventive agent for melanoma.

The collective findings from preclinical and preliminary clinical studies underscore SFN's potential as a chemopreventive agent against skin cancer, mediated through multiple mechanisms, including the modulation of carcinogen metabolism, inhibition of cell proliferation and inflammation, and the blockade of oncogenic pathways. Further research, particularly clinical trials, is warranted to fully elucidate SFN's therapeutic efficacy and mechanism of action in skin cancer prevention and treatment.

Limitations

This systematic review was subject to several limitations. First, the inclusion criteria, which only allowed English-language studies, may have introduced language bias. Second, the variability in animal models and SFN dosages across studies complicated direct comparisons and a meta-analysis. Additionally, the predominance of preclinical studies necessitates cautious interpretation when extrapolating to human contexts.

Conclusions

The reviewed studies indicate SFN's potential for skin cancer prevention, but further research is needed to ascertain its optimal dose, duration and administration method. Clinical trials are essential to assess its effectiveness and safety. If successful, SFN could complement existing prevention measures such as skin checks and sunscreen use.

ORCID iDs

Md Masoom https://orcid.org/0000-0003-1065-2857
Mohd Ashif Khan https://orcid.org/0000-0003-1576-8779

References

1. International Agency for Research on Cancer (IARC). Melanoma Awareness Month 2022. Lyon, France: International Agency for Research on Cancer (IARC); May 2, 2022. https://www.iarc.who.int/news-events/melanoma-awareness-month-2022. Accessed March 27, 2023.
2. Armstrong BK, Kricker A. The epidemiology of UV induced skin cancer. *J Photochem Photobiol B*. 2001;63(1–3):8–18. doi:10.1016/S1011-1344(01)00198-1
3. Rogers HW, Weinstock MA, Harris AR, et al. Incidence estimate of nonmelanoma skin cancer in the United States, 2006. *Arch Dermatol*. 2010;146(3):283–287. doi:10.1001/archdermatol.2010.19
4. Ng C, Yen H, Hsiao HY, Su SC. Phytochemicals in skin cancer prevention and treatment: An updated review. *Int J Mol Sci*. 2018;19(4):941. doi:10.3390/ijms19040941
5. Kaiser AE, Baniasadi M, Giansiracusa D, et al. Sulforaphane: A broccoli bioactive phytocompound with cancer preventive potential. *Cancers (Basel)*. 2021;13(19):4796. doi:10.3390/cancers13194796
6. Houghton CA, Fassett RG, Coombes JS. Sulforaphane and other nutrigenomic Nrf2 activators: Can the clinician's expectation be matched by the reality? *Oxid Med Cell Longev*. 2016;2016:7857186. doi:10.1155/2016/7857186
7. Ma Q. Role of Nrf2 in oxidative stress and toxicity. *Annu Rev Pharmacol Toxicol*. 2013;53(1):401–426. doi:10.1146/annurev-pharmtox-011112-140320
8. Xu C, Huang MT, Shen G, et al. Inhibition of 7,12-dimethylbenz(*a*)anthracene-induced skin tumorigenesis in C57BL/6 mice by sulforaphane is mediated by nuclear factor E2–related factor 2. *Cancer Res*. 2006;66(16):8293–8296. doi:10.1158/0008-5472.CAN-06-0300
9. Dinkova-Kostova AT, Jenkins SN, Fahey JW, et al. Protection against UV-light-induced skin carcinogenesis in SKH-1 high-risk mice by sulforaphane-containing broccoli sprout extracts. *Cancer Lett*. 2006;240(2):243–252. doi:10.1016/j.canlet.2005.09.012
10. Gills JJ, Jeffery EH, Matusheski NV, Moon RC, Lantvit DD, Pezzuto JM. Sulforaphane prevents mouse skin tumorigenesis during the stage of promotion. *Cancer Lett*. 2006;236(1):72–79. doi:10.1016/j.canlet.2005.05.007
11. Mikolajewska P, Juzeniene A, Moan J. Effect of (R)L-sulforaphane on 5-aminolevulinic acid-mediated photodynamic therapy. *Transl Res*. 2008;152(3):128–133. doi:10.1016/j.trsl.2008.07.004
12. Hooijmans CR, Rovers MM, De Vries RB, Leenaars M, Ritskes-Hoitinga M, Langendam MW. SYRCLE's risk of bias tool for animal studies. *BMC Med Res Methodol*. 2014;14(1):43. doi:10.1186/1471-2288-14-43
13. Abel EL, Boulware S, Fields T, et al. Sulforaphane induces phase II detoxication enzymes in mouse skin and prevents mutagenesis induced by a mustard gas analog. *Toxicol Appl Pharmacol*. 2013;266(3):439–442. doi:10.1016/j.taap.2012.11.020
14. Shibata A, Nakagawa K, Yamanoi H, et al. Sulforaphane suppresses ultraviolet B-induced inflammation in HaCaT keratinocytes and HR-1 hairless mice. *J Nutr Biochem*. 2010;21(8):702–709. doi:10.1016/j.jnutbio.2009.04.007
15. Alyoussef A, Taha M. Antitumor activity of sulforaphane in mice model of skin cancer via blocking sulfatase-2. *Exp Dermatol*. 2019;28(1):28–34. doi:10.1111/exd.13802
16. Saha K, Fisher ML, Adhikary G, Grun D, Eckert RL. Sulforaphane suppresses PRMT5/MEP50 function in epidermal squamous cell carcinoma leading to reduced tumor formation. *Carcinogenesis*. 2017;38(8):827–836. doi:10.1093/carcin/bgx044
17. Dickinson SE, Melton TF, Olson ER, Zhang J, Saboda K, Bowden GT. Inhibition of activator protein-1 by sulforaphane involves interaction with cysteine in the cFos DNA-binding domain: Implications for chemoprevention of UVB-induced skin cancer. *Cancer Res*. 2009;69(17):7103–7110. doi:10.1158/0008-5472.CAN-09-0770

18. Tahata S, Singh SV, Lin Y, et al. Evaluation of biodistribution of sulforaphane after administration of oral broccoli sprout extract in melanoma patients with multiple atypical nevi. *Cancer Prev Res*. 2018; 11(7):429–438. doi:10.1158/1940-6207.CAPR-17-0268
19. Malakoutikhah Z, Mohajeri Z, Dana N, Haghjooy Javanmard S. The dual role of Nrf2 in melanoma: A systematic review. *BMC Mol Cell Biol*. 2023;24(1):5. doi:10.1186/s12860-023-00466-5
20. Feustel K, Falchook GS. Protein arginine methyltransferase 5 (PRMT5) inhibitors in oncology clinical trials: A review. *J Immunother Precis Oncol*. 2022;5(3):58–67. doi:10.36401/JIPO-22-1
21. Lai JP, Sandhu DS, Yu C, et al. Sulfatase 2 up-regulates glypican 3, promotes fibroblast growth factor signaling, and decreases survival in hepatocellular carcinoma. *Hepatology*. 2008;47(4):1211–1222. doi:10.1002/hep.22202
22. Li S, Yang Y, Sargsyan D, et al. Epigenome, transcriptome, and protection by sulforaphane at different stages of UVB-induced skin carcinogenesis. *Cancer Prev Res*. 2020;13(6):551–562. doi:10.1158/1940-6207.CAPR-19-0522

Design of experiments and artificial neural networks as useful tools in the optimization of analytical procedure

Projektowanie doświadczeń oraz sztuczne sieci neuronowe jako użyteczne narzędzia w optymalizacji procedury analitycznej

Bartosz Sznek[B–D], Aleksandra Stasiak[B,C], Andrzej Czyrski[A–F]

Chair and Department of Physical Pharmacy and Pharmacokinetics, Poznań University of Medical Sciences, Poland

A – research concept and design; B – collection and/or assembly of data; C – data analysis and interpretation;
D – writing the article; E – critical revision of the article; F – final approval of the article

Polymers in Medicine, ISSN 0370-0747 (print), ISSN 2451-2699 (online) *Polim Med*. 2024;54(2):113–116

Address for correspondence
Andrzej Czyrski
E-mail: aczyrski@ump.edu.pl

Funding sources
None declared

Conflict of interest
None declared

Received on November 15, 2024
Reviewed on November 19, 2024
Accepted on November 20, 2024

Published online on November 28, 2024

Abstract

Developing the analytical procedure requires estimating what independent variables will be tested and at what levels. There are statistical models that enable the optimization of the process. They involve statistical analysis, which indicates the crucial factors for the process and the potential interactions between the analyzed variables. Analysis of variance (ANOVA) is applied in the evaluation of the significance of the independent variables and their interactions. The most commonly used chemometric models are Box–Behnken Design, Central Composite Design and Doehlert Design, which are second-order fractional models. The alternative may be the artificial neural networks (ANN), whose structure is based on the connection of neurons in the human brain. They consist of the input, hidden and output layer. In such analysis, the activation functions must be defined. Both approaches might be useful in planning the analytical procedure, as well as in predicting the response prior to performance the measurements. The proposed procedures may be applied for polymeric systems.

Keywords: optimization, artificial intelligence, Box–Behnken Design, Central Composite Design, Doehlert Design

Streszczenie

Opracowanie procedury analitycznej wymaga określenia, jakie zmienne niezależne będą testowane i na jakich poziomach. Istnieją modele statystyczne, które umożliwiają optymalizację procesu. Polegają one na analizie statystycznej, która wskazuje czynniki istotne dla procesu oraz potencjalne interakcje pomiędzy analizowanymi zmiennymi. Analiza wariancji (analysis of variance – ANOVA) stosowana jest do oceny istotności zmiennych niezależnych i ich interakcji. Najczęściej stosowanymi modelami chemometrycznymi są modele Box–Behnken Design, Central Composite Design i Doehlert Design. Są to modele frakcyjne drugiego rzędu. Alternatywą mogą być sztuczne sieci neuronowe (artificial neural networks – ANN), których budowa opiera się na połączeniu neuronów w mózgu człowieka. Składają się one z warstwy wejściowej, ukrytej i wyjściowej. W przypadku tej analizy należy zdefiniować funkcje aktywacji. Obydwa podejścia mogą być przydatne w planowaniu procedury analitycznej, a także w przewidywaniu wyniku przed wykonaniem pomiarów. Zaproponowane procedury mogą być zastosowane w systemach polimerowych.

Słowa kluczowe: optymalizacja, sztuczna inteligencja, Central Composite Design, Box–Behnken Design, Doehlert Design

Cite as
Czyrski A, Sznek B. Design of experiments and artificial neural networks as useful tools in the optimization of analytical procedure. *Polim Med*. 2024;54(2):113–116. doi:10.17219/pim/196209

DOI
10.17219/pim/196209

Background

Sir Ronald Fisher introduced the concept of design of experiments (DoE) in the 1920s. This idea encompassed statistical analysis of the project during the planning of experiments rather than after they were completed. His work was extended to include the 'Quality by Design' (QbD) concept, emphasizing the importance of planning the entire process to ensure the highest quality. The outlined procedure consists of steps such as recognizing the customer, identifying their needs, translating them into product features, developing the process, and implementing the product features. Employing such a perspective in the pharmaceutical sector, which is strongly process-based and focused on high product quality, took place at the beginning of the new millennium.

Nevertheless, the idea of QbD was proposed by regulatory bodies (such as the U.S. Food and Drug Administration (FDA) and European Medicines Agency (EMA)), recognizing that quality cannot be tested in products, i.e., quality should be built into the design. Today, the DoE is a key statistical tool used to introduce the QbD method in both the research and industrial spheres.[1–3] According to QbD principles, adequate product quality can only be ensured if all critical factors affecting product variability are known and properly controlled. The QbD methods do not focus only on the p-values of the input variables but also on their influence on the response.[4]

Objectives

The aim of this review was to present the optimization techniques in a concise way.

The application of DoE

The use of DoE reduces the number of experiments performed while increasing the amount of data obtained. In addition, it makes it possible to analyze the mutual influence of different factors on each other and optimize conditions to increase the efficiency of the process.[4] It expands the knowledge of the process with minimal consumption of raw materials together with identification of interactions between variables and assessment of their significance. With DoE, it is possible to predict the course of the process throughout the project and demonstrate the cause-and-effect relationship between critical parameters and the response. The model identifies abnormal outliers in the matrices, which allows for their possible elimination.[1,5]

The DoE approach has several advantages. It leads to reducing the required resources while maximizing process knowledge. Moreover, DoE efficiently delivers accurate information about the process, the possible interactions between the variables and their impact on the response. Such analysis allows to optimize the quality indicators and makes the process more resilient to changing external conditions.[1] The DoE methods are presently widely applied in applicative aspects of polymeric science, including synthesis of polymers and evaluation of drug forms based on the functional polymers.[6,7]

Pareto principle

The factors affecting the quality characteristics of the final product follow a general pattern known as the Pareto principle, which indicates that only a small number of factors are responsible for a significant portion of the effect. It is also referred to as the 20:80 rule, which means that 20% of the factors cause 80% of the results. These most influential factors are called critical process parameters, which means process parameters whose variability significantly impacts key product quality attributes. In the context of this standard, critical quality attributes are physical, chemical, biological or microbiological properties, or characteristics that must be controlled to ensure the desired quality. The relationship between critical process parameters (denoted as x) and key quality parameters (denoted as y) is defined by the function $y = f(x)$. This enables the identification of critical process parameters, among many possible ones, and determining optimal process parameter values, leading to improved product performance and ensuring critical quality attribute values are at the appropriate level. The analysis also helps to clarify the mutual interactions between independent variables.[1]

The applied models

The second-order models that are used in the optimization are Full Factorial Design, Box–Behnken Design, Central Composite Design, and Doehlert Design.[8] For Full Factorial Design, the variables are analyzed for different levels in all combinations, which might be time- and material-consuming. The fractional analysis is applied for the remaining 3 models. In this case, the variables are tested for different levels but not in all combinations. That results in a lower number of experiments. The most common are the second-order or quadratic models – they are considered to fit in 95% of cases. The second-order models often detect lack-of-fit error or model mismatch, which makes it possible to determine whether a higher-order model is necessary. The second-order model is satisfactory with properly defined factor limits and appropriate tools. Cubic models are rarely used. In fractional analysis, the higher-order interactions between 3 or more variables are irrelevant.[5,9]

Determining the effect of variables on the process under study is possible using analysis of variance (ANOVA), which allows for isolating significant variables and their impact on the response.[4] It is a mathematical method

that gives an idea of what a significant difference is and what the difference is due to errors due to the application of Fisher's test (F-test). This test allows the researcher to determine the independent variable's significance on the dependent response with a well-defined confidence interval (CI) – some authors use CIs of 90%, 95% or 99%.[4,5]

A fitted model is a model that describes the relationships between data in such a way that the predictions within the experimental domain are accurate. A mathematical model can be considered accurate when the regression is statistically significant and the lack-of-fit parameter is not. In addition, the regression coefficients R^2 and $R^2_{adjusted}$ determine the percentage of variation of the dependent variable, which can be explained by their relationship with the independent variables introduced to the model. The closer the value of these coefficients is to 1, the better the regression describes the data statistically. With a statistically significant regression, response surface methodology graph can be used to visualize the optimization of the model.[4] When the optimization process depends on multiple variables, the optimal conditions may conflict with each other – the final result should fall within the optimal area in the experimental domain.[4]

It is recommended that the experiments should be performed in a random order due to the need to obtain a dataset where observed values and errors are independently distributed and randomized. Randomization also helps to average out uncontrolled effects that could be erroneously attributed to one of the analyzed factors.[10] Performing replicates at the central point (a point at which the independent variables are at their intermediate levels) allows for a more accurate estimation of the true value of a given parameter while also providing an estimation of the experimental error (so-called pure error) and stabilizing the variance of the predicted response.[10,11]

Why is DoE necessary?

Applying DoE helps researchers to reduce the time spent developing new processes, improves the reliability and efficiency of existing processes, as well as helps the researchers to assess the susceptibility to change for tested processes. The statistical analysis, an inseparable part of the optimization, also indicates the most significant factors for the process; it also may suggest which variables should not be taken into consideration.

To perform the optimization, it is necessary to define the problem that must be solved, and then to determine the independent variables and their levels. In the latter step, a couple of preliminary experiments are required. Sometimes an experiment conducted for a specific combination of independent variables may fail. The next step is choosing an experimental matrix; Box–Behnken Design, Central Composite Design and Doehlert Design are the most commonly used. Performing the experiments provides the data and allows the researcher to draw the conclusions (Fig. 1).

The choice of the proper experimental matrix is a very important issue. In the study by Czyrski and Jarzębski,[12] the application of different chemometric models was tested for the optimization of recovery of the analyte. The analysis confirmed that Central Composite Design was the most suitable design for optimizing the recovery of the analyte from a matrix. This design was applied in further studies concerning optimization of recovery with cloud point extraction[13] and protein precipitation.[14]

The validity of the model is confirmed not only with the satisfactory results of statistical parameters, but also with the accuracy of dependent variable prediction with the polynomial equation regression. This regression helps the researchers to predict the response value prior to performing the experiments. However, the limitation factor is that the levels of independent variables for the optimized process should be within the experimental domain.

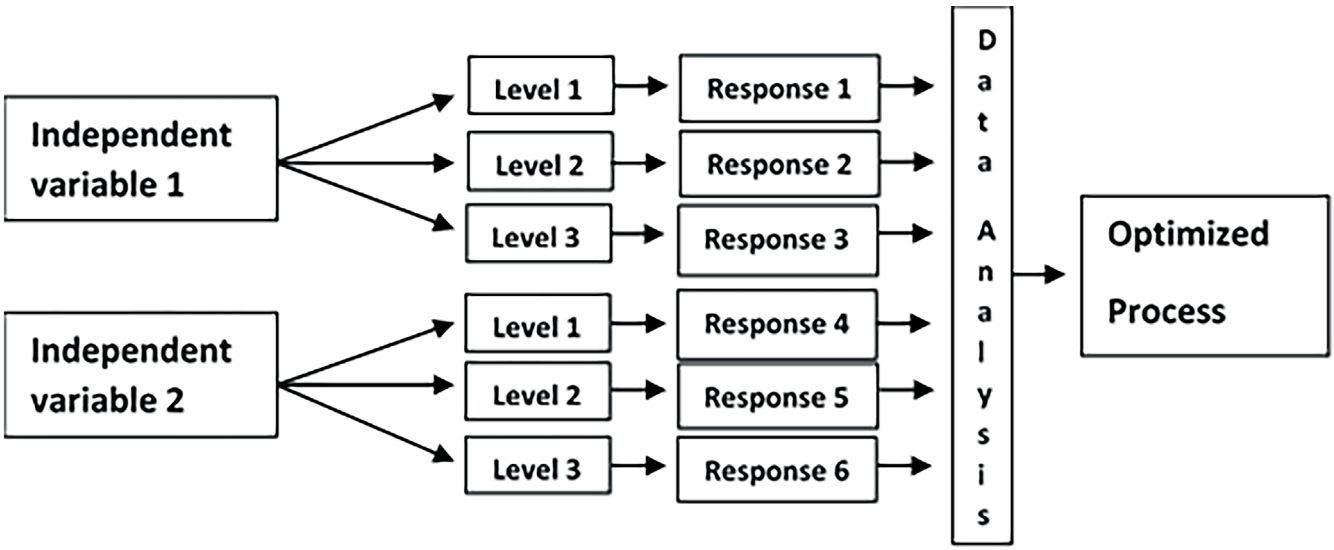

Fig. 1. The steps in the design of experiments (DoE) procedure

Artificial neural networks

Artificial neural networks (ANN), based on the neural structure of the nervous system, can be considered an alternative tool to optimize the analytical procedure.[8] They consist of the 3 following layers: the input, hidden and output (Fig. 2).

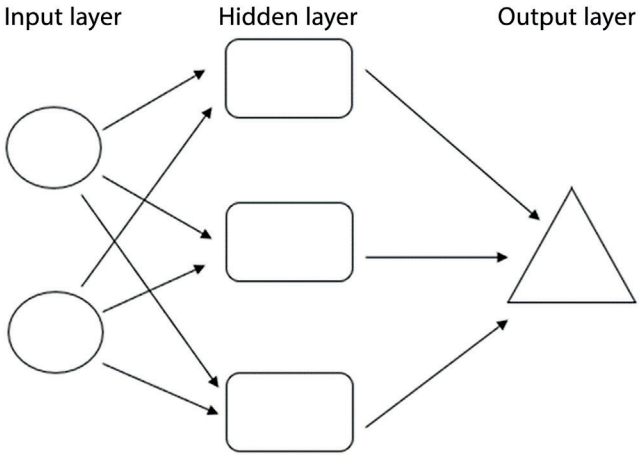

Fig. 2. The scheme of an artificial neural network (ANN)

In the input layer, the independent variables are introduced. For regression analysis, in this layer, the number of neurons equals the number of independent variables. The neurons in this layer transfer the data to the next layer.

In the hidden layer, the number of neurons depends on the operator's needs. The more neurons are in the layer, the higher computation capacity is achieved. On the other hand, too large number of neurons leads to overtraining, which is undesirable. The hidden layer may consist of 1 or more layers of neurons. In the latter case, the process is called deep learning.

The output layer is connected with the hidden layer, and it shows a result as 1 neuron in the case of the regression model or as a number of possibilities in the case of a classification model. The following activation functions for neurons might be used: linear, sigmoidal, logistic, or hiperbolic tangent. The ANN is trained until the error takes the lowest value – the model may predict the response with satisfactory accuracy – and makes optimizing the nonlinear processes possible. It can be useful in optimizing high-performance liquid chromatography (HPLC) methods. Korany et al.[15] applied it in the optimization of the separation of 2 and 3 components in analysis and achieved satisfactory results.

Conclusions

The application of computational techniques makes it possible to evaluate the impact of each variable on the process due to the quantification of the process. Both the DoE and ANN approaches can develop a model that enables the prediction of the result observed for the response of different levels of the independent variables.

ORCID iDs

Bartosz Sznek https://orcid.org/0009-0001-3536-0079
Andrzej Czyrski https://orcid.org/0000-0003-1581-8326

References

1. Politis SN, Colombo P, Colombo G, Rekkas DM. Design of experiments (DoE) in pharmaceutical development. *Drug Dev Ind Pharm*. 2017;43(6):889–901. doi:10.1080/03639045.2017.1291672
2. Box GEP, Wilson KB. On the experimental attainment of optimum conditions. *J Royal Statist Soc B Statist Methodol*. 1951;13(1):1–38. doi:10.1111/j.2517-6161.1951.tb00067.x
3. Khan A, Naquvi KJ, Haider MF, Khan MA. Quality by design: Newer technique for pharmaceutical product development. *Int Pharm*. 2024;2(1):122–129. doi:10.1016/j.ipha.2023.10.004
4. Tavares Luiz M, Santos Rosa Viegas J, Palma Abriata J, et al. Design of experiments (DoE) to develop and to optimize nanoparticles as drug delivery systems. *Eur J Pharm Biopharm*. 2021;165:127–148. doi:10.1016/j.ejpb.2021.05.011
5. Wagner JR, Mount EM, Giles HF. Design of experiments. In: *Extrusion*. Amsterdam, the Netherlands–New York, USA: Elsevier; 2014:291–308. doi:10.1016/B978-1-4377-3481-2.00025-9
6. Gruendling T, Guilhaus M, Barner-Kowollik C. Design of experiment (DoE) as a tool for the optimization of source conditions in SEC-ESI-MS of functional synthetic polymers synthesized via ATRP. *Macromol Rapid Commun*. 2009;30(8):589–597. doi:10.1002/marc.200800738
7. Eckert T, Klein FC, Frieler P, Thunich O, Abetz V. Experimental design in polymer chemistry: A guide towards true optimization of a RAFT polymerization using design of experiments (DoE). *Polymers (Basel)*. 2021;13(18):3147. doi:10.3390/polym13183147
8. Bezerra MA, Santelli RE, Oliveira EP, Villar LS, Escaleira LA. Response surface methodology (RSM) as a tool for optimization in analytical chemistry. *Talanta*. 2008;76(5):965–977. doi:10.1016/j.talanta.2008.05.019
9. Guthrie WF. NIST/SEMATECH e-Handbook of Statistical Methods (NIST Handbook 151). National Institute of Standards and Technology; 2020. doi:10.18434/M32189
10. Gilman J, Walls L, Bandiera L, Menolascina F. Statistical design of experiments for synthetic biology. *ACS Synth Biol*. 2021;10(1):1–18. doi:10.1021/acssynbio.0c00385
11. Ferreira SLC, Bruns RE, Da Silva EGP, et al. Statistical designs and response surface techniques for the optimization of chromatographic systems. *J Chromatogr A*. 2007;1158(1–2):2–14. doi:10.1016/j.chroma.2007.03.051
12. Czyrski A, Jarzębski H. Response surface methodology as a useful tool for evaluation of the recovery of the fluoroquinolones from plasma: The study on applicability of Box–Behnken Design, Central Composite Design and Doehlert Design. *Processes*. 2020;8(4):473. doi:10.3390/pr8040473
13. Michałowska A, Kupczyk O, Czyrski A. The chemometric evaluation of the factors influencing cloud point extraction for fluoroquinolones. *Pharmaceutics*. 2023;15(6):1774. doi:10.3390/pharmaceutics15061774
14. Lewandowski K, Karbownik A, Czyrski A, et al. Bioanalytical method validation for therapeutic drug monitoring of olaparib in patients with ovarian cancer. *Acta Pol Pharm Drug Res*. 2024;81(2):263–278. doi:10.32383/appdr/188521
15. Korany MA, Mahgoub H, Fahmy OT, Maher HM. Application of artificial neural networks for response surface modelling in HPLC method development. *J Adv Res*. 2012;3(1):53–63. doi:10.1016/j.jare.2011.04.001

A review on methods for the production of microcapsules and their application in drug and food technology

Przegląd metod tworzenia mikrokapsułek i ich zastosowania w technologii produktów farmaceutycznych i spożywczych

Tomasz Zięba[1,A–F], Bartosz Raszewski[1,A–D], Małgorzata Kapelko-Żeberska[1,D–F], Justyna Hanna Kobryń[2,B–F]

[1] Department of Food Storage and Technology, Faculty of Biotechnology and Food Science, Wroclaw University of Environmental and Life Sciences, Poland
[2] Department of Physical Chemistry and Biophysics, Faculty of Pharmacy, Wroclaw Medical University, Poland

A – research concept and design; B – collection and/or assembly of data; C – data analysis and interpretation;
D – writing the article; E – critical revision of the article; F – final approval of the article

Polymers in Medicine, ISSN 0370-0747 (print), ISSN 2451-2699 (online) *Polim Med*. 2024;54(2):117–125

Address for correspondence
Justyna Hanna Kobryń
E-mail: justyna.kobryn@umw.edu.pl

Funding sources
None declared

Conflict of interest
None declared

Received on November 15, 2024
Reviewed on November 26, 2024
Accepted on November 27, 2024

Published online on December 3, 2024

Abstract

Microencapsulation is a technology for encapsulating particles in a coating designed to isolate the core substance from external conditions, including oxidation, UV radiation or humidity. Microcapsules reach dimensions of up to 5,000 µm. In the pharmaceutical industry, they are used for the controlled release of active substances, masking their taste, odor or gastrointestinal irritation, and can also reduce the toxicity of some medicinal substances. In the food production industry, the encapsulation process applies to sweeteners, enzymes, microorganisms, vitamins and minerals, flavors, or colors. The production of microcapsules is based on the use of their physical properties such as amphiphilicity, partition coefficient and melting point, while their formation of microcapsules is mainly carried out using physical methods such as coacervation, spray drying, cooling and coating, agglomeration, suspension crosslinking, solvent evaporation, and extrusion, as well as chemical methods: interfacial polymerization and in situ polymerization. Although traditional methods are still used to produce microcapsules, contemporary methods employing the latest technology are also emerging. One such method is encapsulation in microcylinders produced with a 3D printer.

Key words: food products, microcapsules, pharmacy, encapsulation methods

Streszczenie

Mikroenkapsulacja jest technologią polegająca na zamykaniu cząstek w powłoce mającej na celu odizolowanie substancji stanowiącej rdzeń od warunków zewnętrznych, m.in. utlenianiem, promieniowaniem UV czy wilgotnością. Mikrokapsułki osiągają wymiary do 5000 mikrometrów. W przemyśle farmaceutycznym są wykorzystywane do kontrolowanego uwalniania substancji aktywnych, maskując ich smak, zapach czy drażniące działanie na układ pokarmowy; mogą również zmniejszyć toksyczność niektórych substancji leczniczych. W przemyśle produktów spożywczych proces enkapsulacji dotyczy substancji słodzących, enzymów, mikroorganizmów, witamin i minerałów, aromatów oraz barwników. Produkcja mikrokapsułek opiera się na wykorzystaniu ich właściwości fizycznych, takich jak amfifilowość, współczynnik podziału czy temperatura topnienia. Tworzenie mikrokapsułek odbywa się głównie za pomocą metod fizycznych, np. koacerwacji, suszenia, chłodzenia oraz powlekania rozpyłowego, aglomeracji, sieciowania w zawiesinie, odparowania rozpuszczalnika oraz ekstruzji, jak również chemicznych: polimeryzacji międzyfazowej oraz in situ.Tradycyjne metody są ciągle wykorzystywane do produkcji mikrokapsułek, wdrażane są też jednak również najnowsze technologie. Jedną z takich metod jest enkapsulacja w mikrocylindrach wytworzonych za pomocą drukarki 3D.

Słowa kluczowe: produkty spożywcze, mikrokapsułki, farmacja, metody enkapsulacji

Cite as
Zięba T, Raszewski B, Kapelko-Żeberska M, Kobryń JH. A review on methods for the production of microcapsules and their application in drug and food technology. *Polim Med*. 2024;54(2):117–125. doi:10.17219/pim/196538

DOI
10.17219/pim/196538

Introduction

Microencapsulation has its very beginning at the time when the life is born. The emergence of the first cell gives rise to a microcapsule, which is porous in its own specific way. Most eukaryotic cells are excellent examples of capsules that occur naturally in the Universe.[1] Natural shells (coatings) formed in this way are extremely effective in fulfilling their roles.[2] Among the primary functions of such shells are the protection of the internal material (the core) and the regulation of material flow across the cell membrane. Thanks to such an advanced process, bacterial cells, viruses and even plant spores have managed to survive in extreme conditions for up to 1,000 years.[3] An example of this is the black pigment found in fungal cells that protects the core components from sunlight.[3] In turn, lipid bilayer systems, being constituents of cell walls, act as valves that allow various types of substances to pass through. The permeability of these membranes for water can be 1,000 times greater than for ions.[4] Another natural example of a semipermeable membrane is the chicken egg. The egg shell protectst its contents during incubation, allowing free gas exchange between the developing fetus and the external environment.[5] Humans have been trying to replicate mechanisms perfectly functioning in nature for centuries. Researchers have developed microspherical structures capable of selectively isolating their internal environment from the external surroundings. These micro-sized structures, known as microcapsules, exhibit the additional capability of being transported through various biological barriers, such as the skin, bloodstream, or via oral ingestion in the form of food.

The purpose of this review is to present methods for the formation and use of microcapsules in pharmaceutical and food technology as a cross-section through the development of the microencapsulation techniques used starting from the 1930s to the present day.

Encapsulation methods

The first attempts at microencapsulation began in the 1930s at The National Cash Register Company (Dayton, USA).[6] One of the problems investigated at that time was how liquids dispersed in solids would behave. The technological development in those years has triggered new challenges, e.g., how to make paper copies without using carbon paper. The development of a paper printing technique free of CO_2 emissions (thanks to the use of microcapsules) led to a breakthrough also in research on dispersion and coacervation.[7] A concept then emerged to use gelatin as a carrier. In subsequent years, encapsulation processes were improved by implementing new techniques and carriers. As early as in the 1950s, this technique was employed to entrap aromas in order to protect them from oxidation.

Further technological improvement has led to a successful of fortifying orange essential oil in 5-μm coatings, which was undertaken at the Southwest Research Institute (San Antonio, USA) in the 1950s. The resulting product was used in the food industry as a flavor.[8] Techniques were further developed that enabled encapsulating the core, i.e., the center of the capsule, with a stable structure in order to protect it from degradation, stabilize it and extend the shelf-life of various substances. Substances encapsulated in this way have been widely used in the food, cosmetic, chemical, paper, pharmaceutical, and agricultural industries.[2] On a microscopic scale, microcapsules are the capsules not larger than 5,000 μm,[4] whereas the size of nanocapsules should not exceed 100 nm. The sizes of microcapsules have not been explicitly defined in the literature, although some scientific sources indicate that the maximum size of nanocapsules can be up to 5,000 nm due to the formation of agglomerates.

Encapsulation consists in covering materials having micro sizes to protect the encapsulated substance against adverse effects of external factors, like solar radiation, oxygen, humidity, other product components, or effects of the technological process.[8] Microencapsulation is a technology of vital importance in the pharmaceutical industry and medicine.[9–11] Microcapsules consist of the core and a coating (shell). The core can be a solid, liquid (solution, suspension or emulsion) or gas. The mass of the core typically makes up 30–95% of the microcapsule's weight. Microcapsules can be of spherical or irregular shape, depending on core type. Given their structure, they can be divided into monocored, multicored and matrix ones. The monocored microcapsules consist of the core and the coating, whereas the multicored ones are agglomerates of smaller capsules entrapped in one larger capsule. In turn, in the matrix microcapsules, the core is homogenously merged with the coating.[12] The encapsulation technique depends on the physicochemical properties of the core substance,[13] while the properties of coating components enable a desired profile of a therapeutic substance effect.[14,15] The coating may be composed of synthetic polymers (polyvinylpyrrolidone, polyacrylic acid, polymethacrylate, polyamide) or natural polymers (gelatin, gum arabic, starch, cellulose derivatives, wax, paraffin). Natural biopolymers are one of the most common substances used in encapsulation processes. Their main advantage is the presence of a large number of functional groups, which affects capsule core stabilization, while their other advantages include their low production cost, biodegradability and biocompatibility.[16] In addition to its protective effect against external conditions, masking taste and odor, encapsulation also allows for the controlled prolonged release of the drug, thereby reducing its toxicity and alleviating gastrointestinal tract irritation.[17] Microcapsules are administered orally[14] and externally onto the skin.[11,18]

Physical/mechanical methods

Coacervation

Coacervates are nothing more than large micelles that form spontaneously in colloid solutions. First attempts of microencapsulation via phase coacervation were undertaken in 1931 by Bungenburg de Jong and Kass.[19] It was thanks to their research that the first gelatin capsules were created. Coacervates are formed by combining oppositely charged particles, such as polysaccharides, proteins or ions. Another definition states that coacervation is the macromolecular separation of a solution into 2 immiscible phases that are in equilibrium. It is important that the ionic substances contained in the mixture differ in their isoelectric points.[20] Coacervation can be divided into simple coacervation, the simplified model of which is limited to the use of one dispersed colloidal substance (such as gelatin or chitosan), and complex coacervation, in which an aqueous solution of a polymer and an oppositely charged colloid (e.g., gum arabic) are prepared (Fig. 1). It proceeds in 4 stages:

1. dispersion of an active substance in a solution of the active hydrocolloid;
2. addition of the 2nd hydrocolloid in order to induce the polymer–polymer complex (in the case of complex coacervation);
3. colloid precipitation in the form of droplets (by reducing its solubility through external factors, such as temperature or pH changes); and
4. formation and stabilization of capsules by the addition of a crosslinking agent.[2]

The microcapsules formed are separated from the solution by means of filtration or centrifugation, and then rinsed and dried. The resultant capsules may contain 85–90% of the core[21] and be characterized by low porosity and insolubility in cold water. Polymers that can be used in the food industry as core coatings should be suitable for consumption, like, e.g., gelatin, chitosan, shellac, wax, carboxymethylcelluose, gum arabic, or ethylcellulose.[22] In the food industry, coacervation can be applied to flavor cakes, teas or oils.[20]

Spray drying and cooling

The first reports about the use of spray drying for encapsulation appeared in 1927,[2] when A. Bolk-Roberts spray dried flavoring oil in acacia gum. Rapid technological progress observed in the 1950s has led to the use of spray drying of milk, coffee, tea, and dyes on a commercial scale.[8] Further works on the development of the drying industry have paved the way to the production of stable additives with dextrins dissolved in water used as their carriers. Progress in research has enabled the development of carriers that capture volatile substances, constituting an effective barrier against oxidation and degradation. The drying process consists in dispersing a mixture of a core liquid and a coating substance with a particle diameter of 1–300 µm. The liquid in the drying chamber meets the drying medium (warm air) at a temperature of 100–180°C.[23] Despite the high temperatures used, the coating is relatively poorly permeable to volatile compounds. Spray drying occurs in 3 stages:

1. preparation of dispersion or emulsion;
2. homogenization of the material to be dried; and
3. substance spraying in the drying chamber.[24]

Research works on spray drying have aimed to investigate not only the composition and choice of the carrier but also the influence of various factors on core retention in the capsule, such as the size of the emulsion particles, the type of spraying apparatus, the type of solvent, and the inlet and outlet temperatures.[25] Increasing the core concentration can result in greater retention of the component in the capsule. Higher temperature in the chamber also increases its retention but can as well trigger irreversible changes in its chemical structure. The bonds occurring between the core and the coating affect the greater retention of the former.[26] The most common substances used to protect the core include gum arabic, maltodextrins, dextrins, modified starches, whey, and rice starch.

Spray freeze drying

Another modern solution in the encapsulation via drying is the spray freeze drying.[23] Most often, the mixture to be dried is sprayed in liquid nitrogen, which serves as a freezing medium. Then, the frozen capsules are transferred

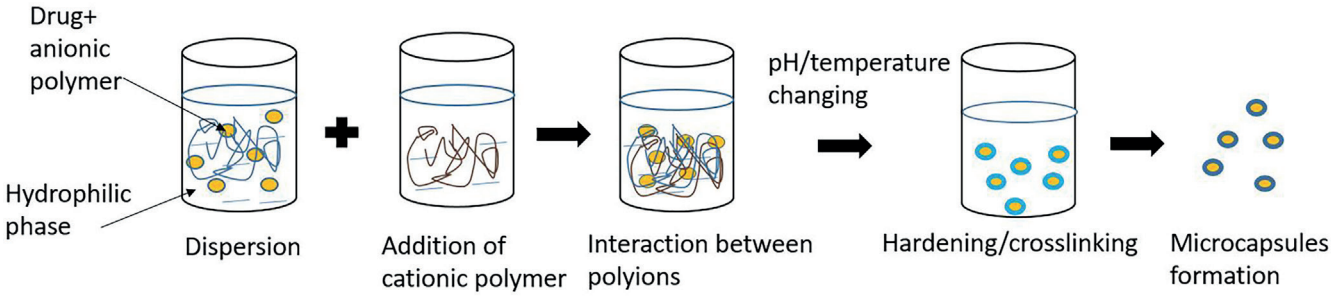

Fig. 1. Scheme for the use of the coacervation method to produce microcapsules

to the freeze drying chamber, where the solvent evaporates by sublimation. In a study conducted by Sonner et al., this method enabled obtaining single spheres with efficiency similar to that achieved upon traditional spray drying.[27] The most common substances used in the spray freezing process as core coating include fats, mixtures of fats, mono- and diglycerides with a melting point of 45–122°C,[28] and hardened oils with lower melting temperatures in the range of 32–42°C. Due to their lower melting point, the lipids mentioned above require special storage conditions. Since the coating is hardened by means of a low temperature treatment and not at the temperature of solvent evaporation as in the case of drying, it may be more easily damaged by various mechanical (friction), thermal (temperature increase) as well as chemical (fat reactions) factors.[29] The core is released when the temperature is higher than the melting point being its main component. In the food industry, capsules with food additives produced by spray freeze drying are used for instant products, cakes and foods with a higher fat content.[30]

Fluidized bed drying and coating

Another modification of spray drying process is fluidized-bed drying, in which agglomeration of the core carrier takes place. This method aims to produce capsule agglomerates, which are formed upon dispersed starch binding with a binding agent, e.g., guar gum or pectin.[31] The rapid drying of such a mixture results in the formation of agglomerates having pores of various sizes, wherein active substances or drugs can be inserted. Excess substance introduced into the capsule is removed from the surface of the agglomerates using ethanol. The fluidized-bed drying enables the use of other protective coatings of microcapsules. The first mentions of the use of agglomerates in this method date back to the 1950s and were made by D.E. Wurster company; hence, the definition of 'Wurster coating' has appeared in the literature.[8] Currently, due to high costs, agglomeration and fluidized-bed drying are used in the pharmaceutical and cosmetic industries. Novel technological solutions allow for producing agglomerates of desired sizes by means of higher pressure, suspension flow rate or regulation of nozzle sizes at the chamber outlet.[32] Wurster coating is based on an additionally designed chamber with a built-in cylindrical nozzle that sprays the coating material, and the agglomerated particles move upwards in the chamber and pass the nozzle there, where they are encapsulated. The material adheres to the surface of the coating by partial evaporation of the solvent. Excess core is washed out with ethanol immediately after leaving the chamber.

Fluidized-bed coating enables the extension of the controlled release, taste masking, and improvement of stability and aesthetics.[33] The main advantages of the agglomeration method include the relatively long stability of the capsules and long release time of the core. The core of capsules produced in the agglomeration process is resistant to oxidation processes, whereas the capsules are highly resistant to external factors. This provides the possibility of encapsulating thermolabile compounds.[32] A characteristic feature of agglomerates is their low porosity, which makes them applicable in many industries. However, their major drawback is the high production cost. In addition, due to the composition of agglomerates (mainly starch), the carbohydrate content increases in the final product. In the food industry, this process is used to release substances such as sweeteners, loosening agents, enzymes, microorganisms, vitamins, minerals, flavors, and colorants.[34]

Suspension crosslinking

Suspension crosslinking is a preferred method for the preparation of protein and polysaccharide microcapsules.[35] It involves dispersing an aqueous solution of the polymer, which contains the core material, in an immiscible organic solvent (suspension/dispersion medium) to form small droplets. The suspension medium typically contains a suitable stabilizer to preserve the integrity of the droplets or microcapsules. The droplets are then hardened with covalent crosslinking, resulting in the formation of the corresponding microcapsules. The crosslinking process can be achieved either thermally (at temperatures above 50°C) or by using a crosslinking agent, such as formaldehyde or terephthaloyl chloride (Fig. 2). Suspension crosslinking is a highly versatile technique, suitable

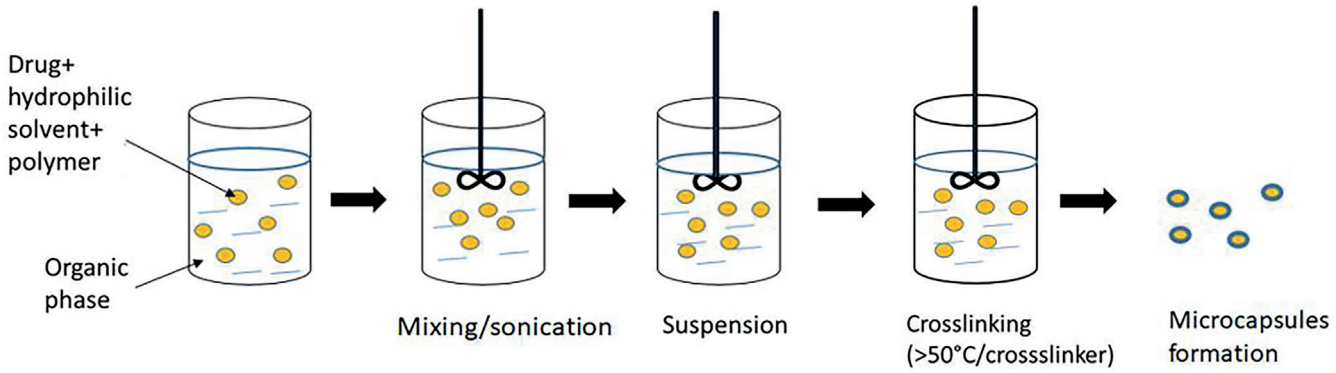

Fig. 2. Scheme for the use of the suspension crosslinking method to produce microcapsules

for microencapsulation of soluble, insoluble, liquid or solid materials, and can be used to produce both microcapsules and nanocapsules. For instance, albumin nanocapsules containing doxorubicin and magnetite particles have been synthesized using this method.[36]

Solvent evaporation

Microcapsule formation by solvent evaporation is similar to suspension crosslinking, but typically involves the use of hydrophobic polymers.[37] In this method, the polymer is dissolved in a water-immiscible volatile organic solvent (dichloromethane or chloroform), into which the core material is also dissolved or dispersed. The resulting solution is then added dropwise to a stirring aqueous solution containing a suitable stabilizer, such as poly(vinyl alcohol) or polyvinylpyrrolidone, to form small polymer droplets that contain the encapsulated material. Over time, the droplets harden, forming the corresponding polymer microcapsules. The hardening process is achieved by removing the solvent from the polymer droplets through solvent evaporation (using heat or reduced pressure) (Fig. 3). The solvent evaporation process is well-suited for the preparation of drug-loaded microcapsules, especially those based on biodegradable polymers. Some of the biodegradable polymers most commonly used as matrices for controlled drug release are poly(lactic acid) (PLA)[38,39] and poly(DL-lactic-co-glycolic acid) (PLGA).[40] Microcapsules are produced by dispersing the drug with the polymer and a hydrophilic solvent, such as water or ethanol, using ultrasound. Direct dispersion to form a suspension can occur, as in the case of doxorubicin and PLA.[38] The drug can also be pre-dispersed with an emulsifier such as dichloromethane to form a solid-in-oil (s/o) emulsion, in order to be subsequently dispersed with a polymer, as is the case of insulin dispersed using PLGA copolymer.[40] In both cases, microcapsules are formed after evaporation of the hydrophilic solvent.

Fortification of substances in the extrusion process

Extrusion is one of the physical methods of encapsulation. It consists in the mechanical extrusion of capsules while mixing the core with the coating agent. Extrusion itself is a mechanical-thermal process, extruding from various bulk materials a plastic mass, which solidifies after some time. This process can be controlled by modifications of temperature, pressure and duration.[41] Modifications of other process parameters enable producing a material with specific physicochemical properties. Such parameters are, e.g., the properties of the raw material used, like moisture content, chemical composition, viscosity, or comminution. Further modifications can be applied to the extrusion process parameters, i.e., the speed of screw rotation, temperature, or the number and type of screws.[42]

The device for microencapsulating substances using the extrusion process differs from typical extruders (Fig. 4). It consists of a droplet generator and a tube with a hardening bath.[28] Droplets with a core encapsulated in the coating fall into a solution of a hardener or a cross-linking agent (ethyl alcohol, isopropyl alcohol, or ethylenediaminetetraacetic acid). The device contains a narrow capillary through which the core is fed, located in a tube with the coating material. Both materials come into contact with each other at the capillary outlet, disintegrating into individual drops within the liquid. Such device has a high throughput, but the uniformity of the capsules is very low.[28]

There are also other modifications of this method which allow improving the efficiency and quality of the produced capsules, like, e.g., a spinning head at the capillary outlet placed on the cylinder. In spinning cylindrical extruders, the coating is pumped through a concentric tube, fed by the internal chamber and then injected to the disc circumference.[43] Similarly to the previous technological solution, the liquid column disintegrates at the capillary outlet in contact with the coating on the disc periphery. This solution offers several significant benefits, i.e., process temperature control, operation in a controlled atmosphere and no losses.[44] It was also noted that the capsule size increases with the increase in the material feeding rate but decreases with the increasing rotational speed of the disc. Both methods can be used to produce capsules that are well soluble in water, with a core content of approx. 10–15%. Their stability can reach up to 5 years, but the simplest solution ensures a stability period of 1–2 years. The encapsulation process by extrusion is carried out at temperatures in the range of 60–120°C.[43]

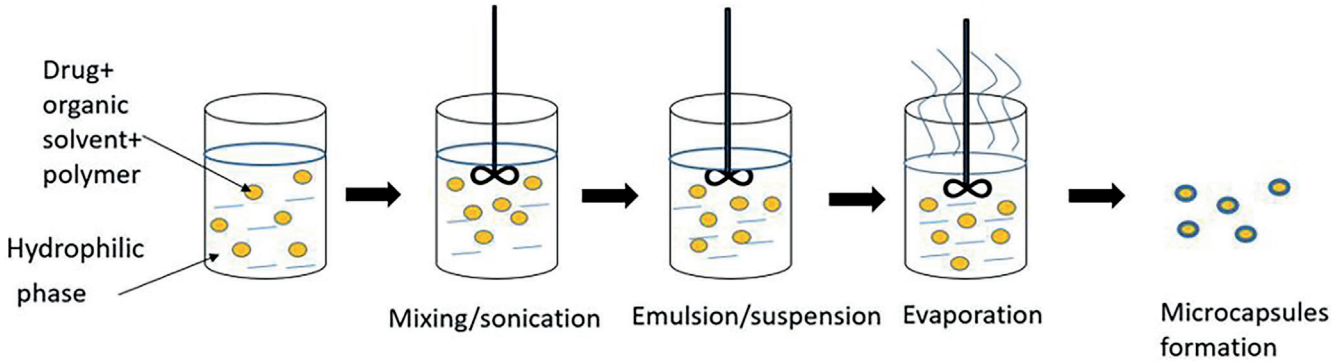

Fig. 3. Scheme for the use of the solvent evaporation method to produce microcapsules

Fig. 4. Example of extruder for food processing technology

The most common capsule coatings are carbohydrates such as maltodextrins, starch and its modified preparations, gum arabic, trehalose, pectin, and sodium alginate.[43] Extrusion enables encapsulating not only flavors used in the food industry, but also bacteria, yeasts, proteins, bioactive compounds, or pesticides and enzymes. Extrusion itself is considered a green process, which means that it is an energy-saving, efficient and environmentally friendly solution.[45]

3D printing

In contrast to the extrusion method for creating microcapsules, scientists are using the latest technologies available. One of these is 3D printing. In the USA, a method for producing microcapsules has been developed that can potentially release drugs for several weeks, called PULSED (Particles Uniformly Liquified and Sealed to Encapsulate Drugs). Using 3D printing, microcylinders made of biodegradable poly(lactic-co-glycolic) acid (PLGA) assembled into arrays are created. In a study by Graf et al., microcapsules filled with labeled dextran were administered to mice in the form of a subcutaneous injection. The compatibility of the PULSED system with proteins and its low cost enabled its multi-faceted applications, from delivering small-molecule drugs to biological therapies and prophylaxis.[46]

Chemical methods

Polymerization is one of the chemical methods for creating microcapsules. The most popular types are interfacial polymerization and in situ polymerization.

Interfacial polymerization

Interfacial polymerization (formerly referred to as 'interfacial polycondensation') was first discovered by Emerson L. Wittbecker and Paul W. Morgan in 1959 as an alternative to the typical high-temperature, low-pressure polymerization technique. This first interfacial polymerization was carried out using the Schotten–Baumann reaction, a method for synthesizing amides from amines and acid chlorides.[47] This process involves dissolving reactive monomers or prepolymers in 2 immiscible phases. After the formation of droplets through dispersion, polymerization occurs at the phase boundary, leading to the formation of microcapsules

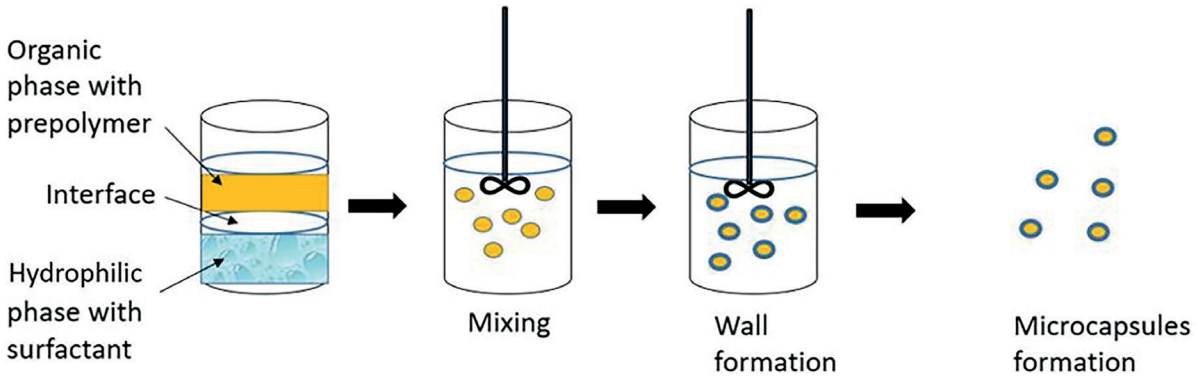

Fig. 5. Scheme for the use of the interfacial polymerization method to produce microcapsules

(Fig. 5).[48] This technique has been employed to produce relatively small capsules (3–6 mm) and has found applications in pharmaceuticals and food products.[49–51] A notable limitation of this approach is that the formation of a thin interfacial polymer layer between the reactants can impede further reaction progress, potentially leading to the formation of microcapsules with compromised mechanical integrity.[52] Moreover, the presence of the reactive monomer within the core phase may pose a risk to the encapsulated substances. Additionally, the diffusion of monomers into the core phase may promote the formation of solid microspheres rather than microcapsules.[53]

In situ polymerization

The in situ polymerization process involves introducing a solution of the monomeric or oligomeric wall material into the core phase, which is then dispersed to the desired size. Polymerization occurs at the phase interface, where controlled deposition and precipitation of the polymer take place. This process can be initiated using precipitants or by altering parameters such as pH, temperature or solvent quality. Depending on the solubility of the monomer and polymer, 3 main types of in situ polymerization are distinguished[53]:

1. Suspension polymerization occurs when the monomer is insoluble in the dispersion medium, resulting in the formation of suspended monomer droplets that polymerize in the solution to form polymer microparticles. In this case, the reactor conditions and stirring rate are critical for maintaining a uniform particle size distribution (Fig. 6);
2. Precipitation polycondensation takes place when the monomer is soluble in the dispersion medium, but the polymer is not. As the reaction progresses, flocculation and aggregation of the polymer (typically of low molecular weight) occur, leading to the formation of particles with a broad size distribution and irregular shape;
3. Dispersion polycondensation is observed when the dispersion medium is a good solvent for the monomer but a poor solvent for the polymer. In this case, polymer swelling occurs, and microcapsule growth takes place through the continuous addition of monomer and oligomer to the particle. This process results in the formation of microparticles with a narrow size distribution.

In situ polymerization can be particularly advantageous when working with volatile[54] or less stable substances in emulsion form.[55] This technique allows the polymerization to occur directly in the dispersed phase, where the volatile or unstable substances are encapsulated within a polymer matrix. By initiating polymerization in situ,

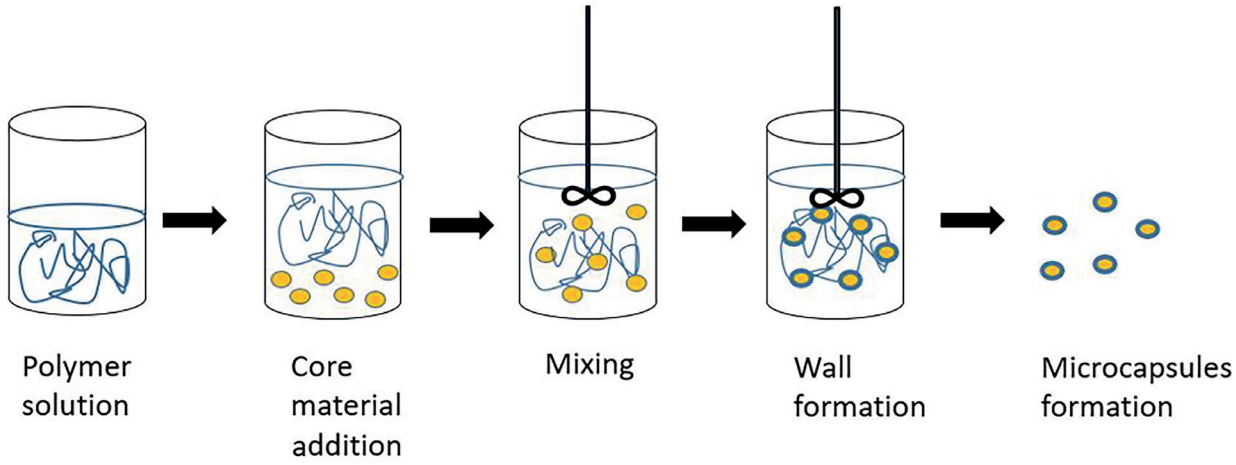

Fig. 6. Scheme for the use of the in situ polymerization method to produce microcapsules

it is possible to stabilize these substances, preventing their degradation or volatilization during processing. Additionally, the controlled polymerization at the phase interface can protect sensitive compounds from environmental factors such as heat, light or oxygen, making it an effective method for handling materials that are difficult to maintain in stable emulsion form. The ability to regulate the in situ polymerization process through variable conditions such as temperature or pH has enabled the use of phase change materials (PCMs) – polymers that alter their conformation in response to changes in physical conditions. Examples of such polymers include poly(N-isopropylacrylamide) (PNIPAM)[56] and poly(NIPAM-co-AA).[57] These materials can undergo reversible phase transitions, making them suitable for applications where the polymer's properties need to change in response to environmental stimuli, such as temperature or pH variations.

Conclusions

Microencapsulation has been a technology in use for nearly 100 years for more and more diverse and complex applications, both in the pharmaceutical and food industries. Substances used as carriers of encapsulated substances range from oil to natural and synthetic polymers. Methods for producing microcapsules are also evolving. Initially, scientists used coacervation between particles of colloidal solutions, but now a 3D printer is employed to produce microcylinders. Despite significant developments in microencapsulation technology, traditional methods are still being researched and used in parallel, especially as we return to using natural substances that are biodegradable and easily assimilated by living organisms.

ORCID iDs

Tomasz Zięba https://orcid.org/0000-0002-2791-342X
Bartosz Raszewski https://orcid.org/0000-0001-6784-9971
Małgorzata Kapelko-Żeberska https://orcid.org/0000-0003-2540-8259
Justyna Hanna Kobryń https://orcid.org/0000-0002-5241-8906

References

1. Lal AK. Origin of life. *Astrophys Space Sci*. 2008;317(3–4):267–278. doi:10.1007/s10509-008-9876-6
2. Fanger GO. Microencapsulation: A brief history and introduction. In: Vandegaer JE, ed. *Microencapsulation*. Boston, USA: Springer US; 1974:1–20. doi:10.1007/978-1-4684-0739-6_1
3. Sussman JI, Baron EJ, Goldberg SM, Kaplan MH, Pizzarello RA. Clinical manifestations and therapy of Lactobacillus endocarditis: Report of a case and review of the literature. *Clin Infect Dis*. 1986;8(5):771–776. doi:10.1093/clinids/8.5.771
4. Korus J, Achremowicz B, Sikora M. Mikrokapsułkowanie substancji spożywczych. *Żywność Nauka Technologia Jakość*. 1997;1:30–40. https://wydawnictwo.pttz.org/wp-content/uploads/2017/12/04_Korus.pdf. Accessed November 21, 2024.
5. Okada J, Kusai A, Ueda S. Factors affecting microencapsulability in simple gelatin coacervation method. *J Microencapsul*. 1985;2(3):163–173. doi:10.3109/02652048509038522
6. Green BK, Lowell S. Oil containing microscopic capsules and method of making them. US Patent 2,800,457. July 23, 1957. https://patents.google.com/patent/US2800457A/en.
7. Smażyński T. *Mikrokapsułkowanie*. Warsaw, Poland: PZWL; 1981. ISBN:978-83-200-0361-1.
8. Balassa LL, Fanger GO, Wurzburg OB. Microencapsulation in the food industry. *Crit Rev Food Technol*. 1971;2(2):245–265. doi:10.1080/10408397109527123
9. Sukhorukov GB, Rogach AL, Garstka M, et al. Multifunctionalized polymer microcapsules: Novel tools for biological and pharmacological applications. *Small*. 2007;3(6):944–955. doi:10.1002/smll.200600622
10. Sukhorukov GB, Rogach AL, Zebli B, et al. Nanoengineered polymer capsules: Tools for detection, controlled delivery, and site-specific manipulation. *Small*. 2005;1(2):194–200. doi:10.1002/smll.200400075
11. O'Hagan DT, Singh M, Ulmer JB. Microparticle-based technologies for vaccines. *Methods*. 2006;40(1):10–19. doi:10.1016/j.ymeth.2006.05.017
12. Garg MA, Chhipa K, Kumar L. Microencapsulation techniques in pharmaceutical formulation. *Eur J Pharm Med Res*. 2018;5(3):199–206. https://storage.googleapis.com/innctech/ejpmr/article_issue/1519801331.pdf. Accessed November 21, 2024.
13. Li SP, Kowarski CR, Feld KM, Grim WM. Recent advances in microencapsulation technology and equipment. *Drug Dev Ind Pharm*. 1988;14(2–3):353–376. doi:10.3109/03639048809151975
14. Rashid A, Khalid SH, Irfan M, et al. In vitro and in vivo evaluation of composite oral fast disintegrating film: An innovative strategy for the codelivery of ranitidine HCl and flurbiprofen. *Pharmaceutics*. 2023;15(7):1987. doi:10.3390/pharmaceutics15071987
15. Hariyadi DM, Hendradi E, Erawati T, Jannah EN, Febrina W. Influence of drug-polymer ratio on physical characteristics and release of metformin hydrochloride from metforminalginate microspheres. *Trop J Pharm Res*. 2018;17(7):1229. doi:10.4314/tjpr.v17i7.1
16. Zuidam NJ, Nedovic V, eds. *Encapsulation Technologies for Active Food Ingredients and Food Processing*. New York, USA: Springer New York; 2010. doi:10.1007/978-1-4419-1008-0
17. Avinash P, Ekta P, Ravindra V, Singh SB, Neelesh KM. Targeted delivery of drugs. In: Jain NK, ed. *Controlled and Novel Drug Delivery*. New Delhi, India: CBS Publishers & Distributors; 2008:107–109. ISBN:978-81-239-0517-4.
18. Lam PL, Gambari R. Advanced progress of microencapsulation technologies: In vivo and in vitro models for studying oral and transdermal drug deliveries. *J Control Release*. 2014;178:25–45. doi:10.1016/j.jconrel.2013.12.028
19. Booij HL, Bungenberg De Jong HG. *Biocolloids and Their Interactions*. Vienna, Austria: Springer Vienna; 1956. doi:10.1007/978-3-7091-5456-4
20. Salaün F. Microencapsulation technology for smart textile coatings. In: Hu J, ed. *Active Coatings for Smart Textiles*. Sawston, UK: Woodhead Publishing; 2016:179–220. doi:10.1016/B978-0-08-100263-6.00009-5
21. Bhatia M, Devi S. Co-crystallization: A green approach for the solubility enhancement of poorly soluble drugs. *CrystEngComm*. 2024;26(3):293–311. doi:10.1039/D3CE01047C
22. Arshady R. Microcapsules for food. *J Microencapsul*. 1993;10(4):413–435. doi:10.3109/02652049309015320
23. Samborska K. Suszenie rozpyłowe w przemyśle spożywczym. *Postępy Techniki Przetwórstwa Spożywczego*. 2008;1:63–69. https://bibliotekanauki.pl/articles/228847. Accessed November 21, 2024.
24. Gharsallaoui A, Roudaut G, Chambin O, Voilley A, Saurel R. Applications of spray-drying in microencapsulation of food ingredients: An overview. *Food Res Int*. 2007;40(9):1107–1121. doi:10.1016/j.foodres.2007.07.004
25. Khaled E, Hassan HNA. Conductometric determination of dextromethorphan hydrobromide. *Analytical Chemistry: An Indian Journal*. 2011;10:134–140. https://www.tsijournals.com/articles/conductometric-determination-of-dextromethorphan-hydrobromide.pdf. Accessed November 21, 2024.
26. Dłużewska E, Florkowska A, Jasiorska E. Wpływ rodzaju nośnika na stabilność β- karotenu mikrokapsułkowanego metodą suszenia rozpyłowego. *Żywność Nauka Technologia Jakość*. 2011;1:140–151. https://wydawnictwo.pttz.org/wp-content/uploads/2015/02/12_Dluzewska.pdf. Accessed November 21, 2024.
27. Sonner C, Maa Y, Lee G. Spray-freeze-drying for protein powder preparation: Particle characterization and a case study with trypsinogen stability. *J Pharm Sci*. 2002;91(10):2122–2139. doi:10.1002/jps.10204
28. Dziezak JD. Microencapsulation and encapsulated ingredients. *Mater Sci Chem*. 1988;2(4):136–151. https://api.semanticscholar.org/CorpusID:222249034. Accessed November 21, 2024.

29. Kim J. Spray cooling heat transfer: The state of the art. *International Journal of Heat and Fluid Flow*. 2007;28(4):753–767. doi:10.1016/j.ijheatfluidflow.2006.09.003
30. Shu B, Yu W, Zhao Y, Liu X. Study on microencapsulation of lycopene by spray-drying. *J Food Eng*. 2006;76(4):664–669. doi:10.1016/j.jfoodeng.2005.05.062
31. Turchiuli C, Fuchs M, Bohin M, et al. Oil encapsulation by spray drying and fluidised bed agglomeration. *Innovative Food Science Emerging Technologies*. 2005;6(1):29–35. doi:10.1016/j.ifset.2004.11.005
32. Dhanalakshmi K, Ghosal S, Bhattacharya S. Agglomeration of food powder and applications. *Crit Rev Food Sci Nutr*. 2011;51(5):432–441. doi:10.1080/10408391003646270
33. Maria Leena M, Gover Antoniraj M, Moses JA, Anandharamakrishnan C. Three fluid nozzle spray drying for co-encapsulation and controlled release of curcumin and resveratrol. *J Drug Deliv Sci Technol*. 2020;57:101678. doi:10.1016/j.jddst.2020.101678
34. Fuchs D, Fuchs LS. Introduction to response to intervention: What, why, and how valid is it? *Reading Research Quarterly*. 2006;41(1):93–99. doi:10.1598/RRQ.41.1.4
35. Arshady R. Microspheres and microcapsules: A survey of manufacturing techniques. Part 1: Suspension cross-linking. *Polym Eng Sci*. 1989;29(24):1746–1758. doi:10.1002/pen.760292404
36. Widder KJ, Senyei AE, Sears B. Experimental methods in cancer therapeutics. *J Pharm Sci*. 1982;71(4):379–387. doi:10.1002/jps.2600710403
37. Jeffery H, Davis SS, O'Hagan DT. The preparation and characterization of poly(lactide-co-glycolide) microparticles. II. The entrapment of a model protein using a (water-in-oil)-in-water emulsion solvent evaporation technique. *Pharm Res*. 1993;10(3):362–368. doi:10.1023/A:1018980020506
38. Juni K, Ogata J, Nakano M, Ichihara T, Mori K, Akagi M. Preparation and evaluation in vitro and in vivo of polylactic acid microspheres containing doxorubicin. *Chem Pharm Bull (Tokyo)*. 1985;33(1):313–318. doi:10.1248/cpb.33.313
39. Bodmeier R, McGinity JW. The preparation and evaluation of drug-containing poly(dl-lactide) microspheres formed by the solvent evaporation method. *Pharm Res*. 1987;04(6):465–471. doi:10.1023/A:1016419303727
40. Yamaguchi Y, Takenaga M, Kitagawa A, Ogawa Y, Mizushima Y, Igarashi R. Insulin-loaded biodegradable PLGA microcapsules: Initial burst release controlled by hydrophilic additives. *J Control Release*. 2002;81(3):235–249. doi:10.1016/S0168-3659(02)00060-3
41. Wójtowicz A. Ekstruzja – wybrane aspekty techniczne i technologiczne. *Zeszyty Problemowe Postępów Nauk Rolniczych*. 2018;(595):131–144. doi:10.22630/ZPPNR.2018.595.42
42. Mościcki L, Mitrus M, Wójtowicz A. *Technika Ekstruzji w Przemyśle Rolno-Spożywczym*. Warsaw, Poland: Państwowe Wydawnictwo Rolnicze i Leśne; 2007. ISBN:978-83-09-01027-2.
43. Fangmeier M, Lehn DN, Maciel MJ, Volken De Souza CF. Encapsulation of bioactive ingredients by extrusion with vibrating technology: Advantages and challenges. *Food Bioprocess Technol*. 2019;12(9):1472–1486. doi:10.1007/s11947-019-02326-7
44. Tackenberg M, Kleinebudde P. Encapsulation of liquids via extrusion: A review. *Curr Pharm Des*. 2015;21(40):5815–5828. doi:10.2174/1381612821666151008150142
45. Gutiérrez TJ, González G. Effects of exposure to pulsed light on surface and structural properties of edible films made from cassava and taro starch. *Food Bioprocess Technol*. 2016;9(11):1812–1824. doi:10.1007/s11947-016-1765-3
46. Graf TP, Qiu SY, Varshney D, et al. A scalable platform for fabricating biodegradable microparticles with pulsatile drug release. *Adv Mater*. 2023;35(22):2300228. doi:10.1002/adma.202300228
47. Wittbecker EL, Morgan PW. Interfacial polycondensation. I. *J Polym Sci*. 1959;40(137):289–297. doi:10.1002/pol.1959.1204013701
48. Zhang Y, Rochefort D. Characterisation and applications of microcapsules obtained by interfacial polycondensation. *J Microencapsul*. 2012;29(7):636–649. doi:10.3109/02652048.2012.676092
49. Perignon C, Ongmayeb G, Neufeld R, Frere Y, Poncelet D. Microencapsulation by interfacial polymerisation: membrane formation and structure. *J Microencapsul*. 2015;32(1):1–15. doi:10.3109/02652048.2014.950711
50. Ravi Kumar MN. Nano and microparticles as controlled drug delivery devices. *J Pharm Pharm Sci*. 2000;3:234–258. https://sites.ualberta.ca/~csps/JPPS3(2)/M.Kumar/Particles-Kumar.pdf. Accessed November 21, 2024.
51. Damgé C, Vranckx H, Balschmidt P, Couvreur P. Poly(alkyl cyanoacrylate) nanospheres for oral administration of insulin. *J Pharm Sci*. 1997;86(12):1403–1409. doi:10.1021/js970124i
52. Hasler DJ, McGhee TA. Microcapsules methods for their preparation, and sheet material carrying microcapsules, US Patent 4,105,823. August 8, 1978. https://patentimages.storage.googleapis.com/97/e7/25/1c1d5d752a5495/US4105823.pdf.
53. Arshady R, George MH. Suspension, dispersion, and interfacial polycondensation: A methodological survey. *Polym Eng Sci*. 1993;33(14):865–876. doi:10.1002/pen.760331402
54. Mustapha AN, Zhang Y, Zhang Z, Ding Y, Li Y. A systematic study on the reaction mechanisms for the microencapsulation of a volatile phase change material (PCM) via one-step in situ polymerisation. *Chem Sci Eng*. 2022;252:117497. doi:10.1016/j.ces.2022.117497
55. Chen Y, Liu H, Zhang Z, Wang S. Preparation of polymeric nanocapsules by radiation induced miniemulsion polymerization. *Eur Polym J*. 2007;43(7):2848–2855. doi:10.1016/j.eurpolymj.2007.04.013
56. Sánchez-Moreno P, De Vicente J, Nardecchia S, Marchal JA, Boulaiz H. Thermo-sensitive nanomaterials: Recent advance in synthesis and biomedical applications. *Nanomaterials*. 2018;8(11):935. doi:10.3390/nano8110935
57. Wang S, Liu H, Wu D, Wang X. Temperature and pH dual-stimuli-responsive phase-change microcapsules for multipurpose applications in smart drug delivery. *J Colloid Interface Sci*. 2021;583:470–486. doi:10.1016/j.jcis.2020.09.073

Applications of bio-printing to promote spinal cord regeneration

Zastosowania biodruku w celu przyspieszenia regeneracji rdzenia kręgowego

Marcin Knefel[1,B,D], Mikołaj Kantor[1,B,D], Karolina Kępka[1,B,D], Aleksandra Owczarzy[2,E,F], Karolina Kulig[2,E,F], Małgorzata Maciążek-Jurczyk[2,E,F]

[1] Student Research Group at the Department of Physical Pharmacy, Faculty of Pharmaceutical Sciences in Sosnowiec, Medical University of Silesia in Katowice, Poland
[2] Department of Physical Pharmacy, Faculty of Pharmaceutical Sciences in Sosnowiec, Medical University of Silesia in Katowice, Poland

A – research concept and design; B – collection and/or assembly of data; C – data analysis and interpretation;
D – writing the article; E – critical revision of the article; F – final approval of the article

Polymers in Medicine, ISSN 0370-0747 (print), ISSN 2451-2699 (online) *Polim Med*. 2024;54(2):127–134

Address for correspondence
Małgorzata Maciążek-Jurczyk
E-mail: mmaciazek@sum.edu.pl

Funding sources
None declared

Conflict of interest
None declared

Received on November 15, 2024
Reviewed on November 27, 2024
Accepted on November 27, 2024

Published online on December 6, 2024

Abstract

The spinal cord is one of the most important part of the human nervous system and great importance is placed on developing the best treatment for its damage. 3D bio-printing technology, and the fabrication of special scaffolds using it, is a potential solution for regenerating damage in spinal cord injuries (SCIs). Bio-printing can be divided into indirect and direct bio-printing, while among the bio-printing methods, inkjet bio-printing, fused deposition modeling (FDM), extrusion bio-printing, or light-assisted bio-printing can be distinguished. The last group can be in turn divided into several separate techniques such as digital light processing (DLP), stereolithography (SLA) and laser-assisted bio-printing (LAB). While bio-printing technology for the treatment of SCI is in the early stages of research, several successful trials have already been performed, where the use of such scaffolds has resulted in at least partial restoration of autonomic nervous system function in patients with chronic and acute SCI.

Key words: central nervous system, spinal cord, bio-printing

Streszczenie

Rdzeń kręgowy jest jedną z najważniejszych części ludzkiego układu nerwowego. Z tego powodu przywiązuje się dużą wagę do opracowania najlepszego leczenia towarzyszących mu uszkodzeń. Technologia biodruku 3D i wytwarzanie specjalnych rusztowań z jego pomocą jest potencjalnym rozwiązaniem w zakresie regeneracji uszkodzeń w urazach rdzenia kręgowego. Głównym podziałem typów biodruku jest podział na biodruk pośredni i bezpośredni, podczas gdy wśród metod biodruku można wyróżnić biodruk atramentowy, modelowanie osadzania topionego materiału (FDM), biodrukowanie ekstruzyjne lub biodrukowanie wspomagane światłem. Ostatnią grupę można z kolei podzielić na kilka odrębnych technik, takich jak cyfrowe przetwarzanie światłem (DLP), stereolitografię (SLA) i biodrukowanie wspomagane laserowo (LAB). Chociaż technologia biodruku w leczeniu urazów rdzenia kręgowego jest na wczesnym etapie badań, przeprowadzono już kilka udanych prób, w których wykorzystanie takich rusztowań doprowadziło do przynajmniej częściowego przywrócenia funkcji autonomicznego układu nerwowego u pacjentów z przewlekłym i ostrym urazem rdzenia kręgowego.

Słowa kluczowe: rdzeń kręgowy, centralny układ nerwowy, biodrukowanie

Cite as
Knefel M, Kantor M, Kępka K, Owczarzy A, Kulig K, Maciążek-Jurczyk M. Applications of bio-printing to promote spinal cord regeneration. *Polim Med*. 2024;54(2):127–134. doi:10.17219/pim/196553

DOI
10.17219/pim/196553

Introduction

The spinal cord consists of externally located white matter and internally located gray matter. These are clusters of nervous tissue, which together with the brain form a system called central nervous system (CNS). The CNS is responsible for the body's basic vital functions. It has low capacity to replace and renew neurons after damage or disease, which is the reason why degeneration in the structure of the CNS caused by disease or physical damage often leads to the loss of nerve cells, axons and glial support.[1–5] Spinal cord injury (SCI) is considered one of the greatest challenges among CNS disorders, and the serious complications and high incidence of paraplegia caused by SCI is a growing concern for both affected individuals and their families. It also poses a significant burden to the whole society.[6] Pathologically, SCI is caused by a primary injury and a series of secondary injuries. Primary injuries are mainly acute injuries caused by mechanical forces, such as spinal disc extrusion and dislocation, including damage to neurons and glial cells in the relevant segments, leading to ruptures in blood vessels.[7,8] Secondary injuries include local edema, disruption of ion homeostasis, ischemia, intense inflammatory response, and excess free radicals.[9]

Currently, clinical treatment can be divided into surgical and non-surgical. One example of non-operative treatment is the use of high doses of methylprednisolone (MP), which is a corticosteroid that inhibits lipid peroxidation and is used to reduce the formation of secondary injuries.[10,11] However, the use of MP is limited due to a number of side effects, including increased risk of urinary tract infections, respiratory tract infections, wounds, sepsis, and pneumonia.[12] In terms of surgical treatment, the most relevant methods are decompression and stiffening of the injured site. The primary goal of SCI treatment is to remove the effect of compression factors and restore spinal stability. The aforementioned methods make a small contribution to the treatment of SCIs; however, all of these methods of clinical treatment can only remove or reduce the action of the factors causing the injury, but do not enable functional regeneration of the damaged nerve. On this basis, it can be concluded that the repair is incomplete.[13] Regeneration of the nervous system involves the repair and re-generation of nerve tissue cells and nerve connections. Tissue engineering involving direct replacement of nerve cells and/or repair of connections through cell transplantation, biochemical molecular signaling and targeting using so-called "scaffolds" is used for this purpose.[14] The ideal scaffold for neural tissue engineering should meet several important criteria, as shown in Fig. 1.[15,16]

Techniques such as melt molding, gas foaming, electrospinning, and phase separation have been used in the production of scaffolds made out of synthetic and natural polymers.[17] The disadvantage of techniques mentioned above is the inability to precisely control and adjust the shape of the scaffolds, the configuration of internal channels and the size of the pores in the scaffold. Additionally, these techniques do not allow for the production of scaffolds using cells due to manufacturing conditions being unfavorable for cells survival. In recent years, 3D bio-printing has emerged as a solution to these problems, attracting

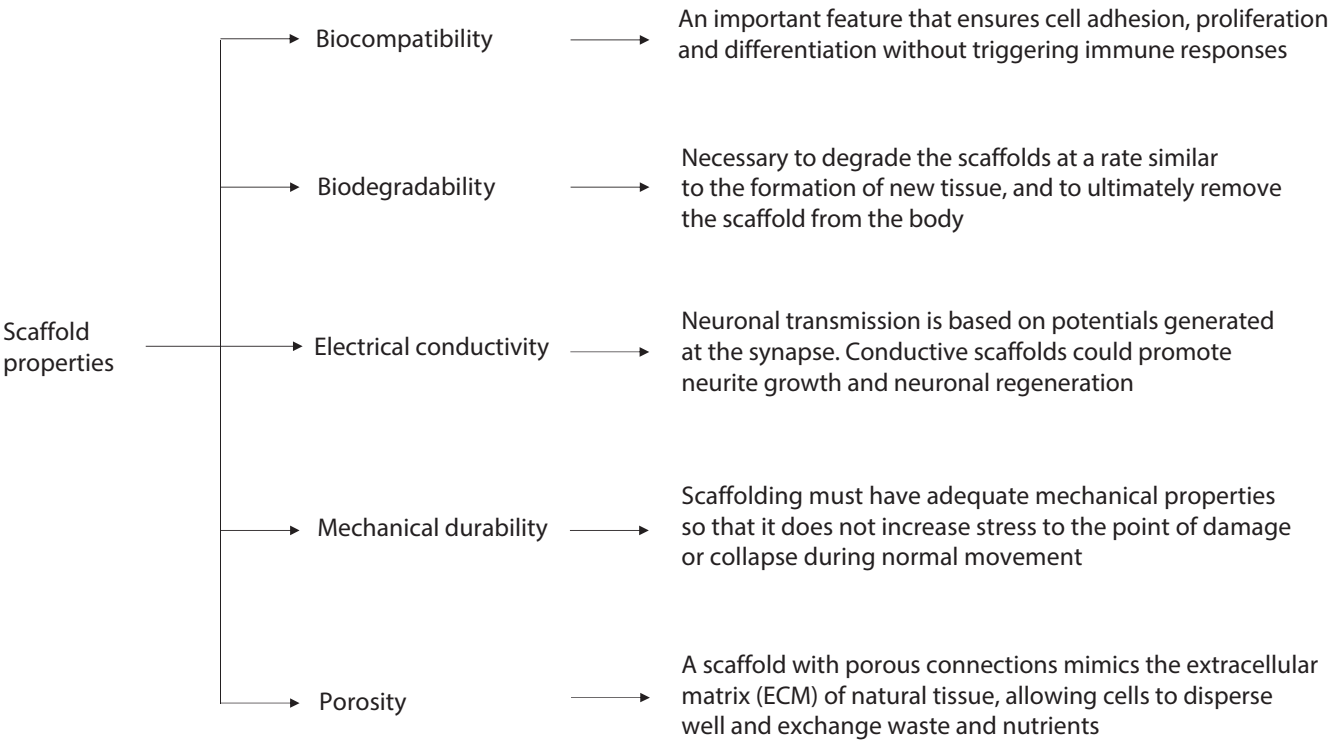

Fig. 1. Characteristics of ideal scaffold

attention due to its ease of controlling shapes and dimensions of scaffolds and creating frameworks for cells.[18]

The method known as additive manufacturing (AM) is used in printing cells, growth factors and biomaterials in layers. Moreover, it allows for the creation of biological structures that exhibit properties similar to organs and mimic natural tissue.[19] For this reason, 3D bio-printing has become a promising and effective strategy for repairing SCI, as AM can easily produce scaffolds for cells while selecting their appropriate dimensions. However, there are also significant challenges associated with 3D bio-printing, such as cumbersome handling, insufficient printability, low cell viability during printing, and minimal cell–material interaction.

In this work, a review and discussion of various available 3D printing methods as well as their theoretical and practical applications in the treatment of various spinal cord injuries was conducted.

3D bio-printing: Theoretical basis and examples of application

Based on the data from scientific literature, one of the basic divisions of 3D bio-printing is that into indirect bio-printing, which aims to produce scaffolds and other types of frameworks that finally can be populated by cells, and direct bio-printing, which allows for the production of structures using biological material with living cells, which in turn ensures greater similarity to naturally formed tissues and increased biocompatibility. This division in bio-printing is presented in Fig. 2.

Among the 3D bio-printing methods, many types can be distinguished; however, in order to facilitate classification

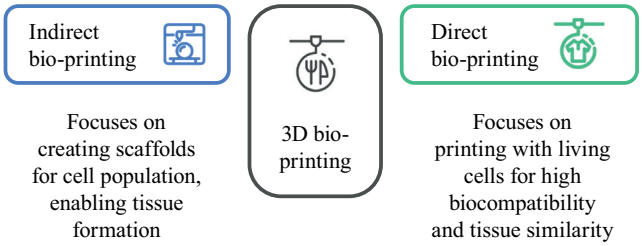

Fig. 2. Basic division of bio-printing

and for better understanding, the following division was applied: inkjet/droplet bio-printing, fused deposition modeling (FDM), light assisted/directed bio-printing, and extrusion-based bio-printing. This division has been illustrated in Fig. 3.

Inkjet/droplet bio-printing

3D inkjet printing technology has been adapted from the 2D printing system, where in this method droplets of the used liquid are deposited on special platform in a "layer by layer" manner, enabling rapid production of a complete structure with micrometer resolution.[20,21] This method can be further differentiated into thermal and piezoelectric.

In thermal printers, the print head is heated to temperatures between 200°C and 300°C, which leads to the formation of pressure pulses that in turn push the droplets out of the nozzle.[20] Furthermore, several studies have shown that local heating to temperatures 200°C and 300°C affects neither the stability of biological molecules nor the viability and function of tissues after printing.[21] This method is characterized by high printing speed and the ability

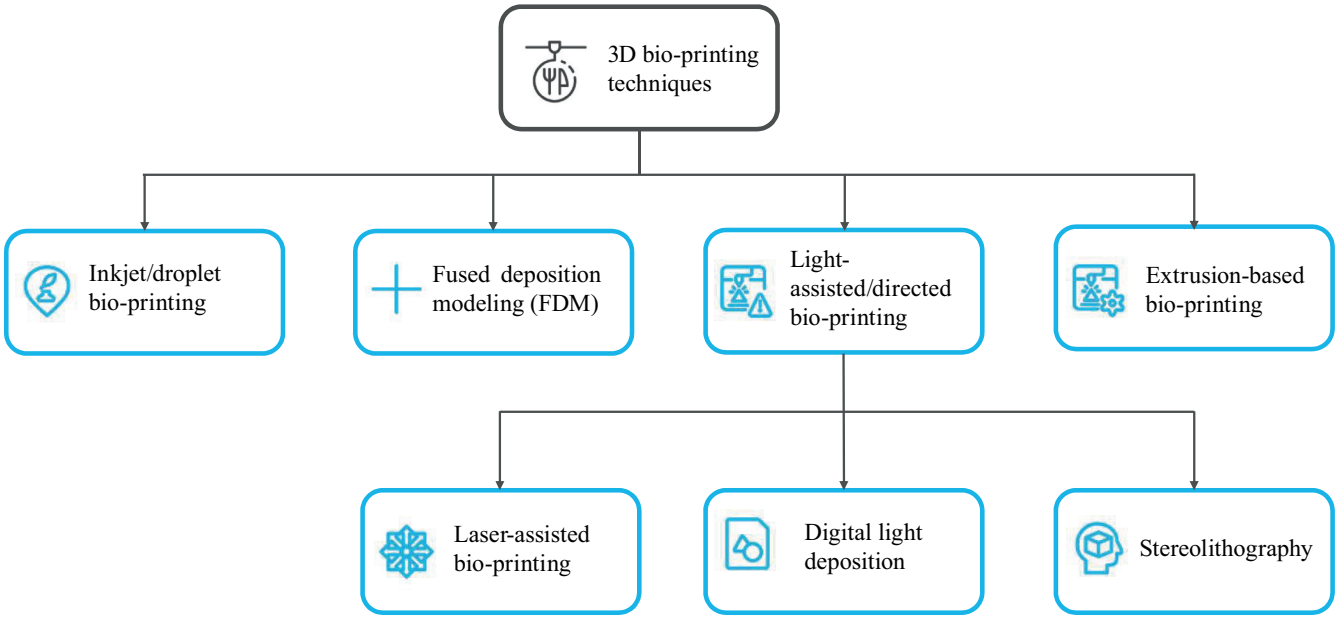

Fig. 3. Classification of bio-printing in this work

to print tissues ranging in size from 20 µm to 100 µm. Additionally, it shows potential for printing in picoliter (pL) volumes to achieve better resolution and accuracy.

In the piezoelectric method, piezoelectric actuators located in the print head are used to generate droplets, which are stimulated by applying voltage. The speed and size of the ejected droplets can be controlled by factors such as timing, pulse frequency and actuator amplitude.[22] Additionally, the piezoelectric method causes less cell damage, resulting in a higher survival rate compared to the thermal method.[23,24]

Common drawbacks of inkjet bio-printing are poor mechanical properties of the printed structures and their low durability. It happens because this technique is only able to distribute bio-ink with a viscosity not exceeding 10 MPa/s.[23,25] Another limitations of 3D inkjet printers are small nozzle size and flow rate, which limit the volume of a single droplet to below 10 pL. To maximize the probability that each droplet will contain a cell, cells must be seeded at a high concentration (above $5{\cdot}10^6$ cells/mL).[25]

Fused deposition modeling

This technique uses thermoplastic polymer filament to produce 3D structures. Depending on the polymer used, the filament is heated in a nozzle to reach semi-liquid state and in this form is extruded onto platform following a computer-designed model.[26] Since this method uses high temperatures, cells are applied and cultured on the structures only after the printing process is completed.[27,28] The types of filaments used in this methods and the required temperatures are presented in Table 1.[29]

The use of thermoplastic polymer fibers in this method is linked to its greatest advantages – low cost and high production speed. Considering the Young's modulus of a given polymeric biomaterial, polyetheretherketone (PEEK) appears to be the most promising. Additionally, since the FDM method does not require any additional solvents or materials, it provides convenience in terms of material handling and allows for continuous production without need to change raw materials.[25] This method also has its drawbacks, such as poor mechanical properties – especially if inter-layer defects occur during printing – and poor surface properties.[30]

Table 1. Filaments and temperatures required in FDM[29]

Type of polymer	Temperature at the nozzle [°C]
PLA (polylactic acid)	160–230
ABS (acrylonitrile butadiene styrene)	215–250
PETG (polyethylene terephthalate glycol)	220–260
TPE (thermoplastic elastomer)	180–230
Nylon	230–250
ASA (acrylonitrile styrene acrylate)	235 255
PVA (polyvinyl alcohol)	160–230
PC (polycarbonate)	200–280
PEEK (polyetheretherketone polymer)	340–440

Light-assisted/directed bio-printing

Light-assisted bio-printing is a group of techniques that include laser-assisted bio-printing (LAB), digital light processing (DLP) and stereolithography (SLA). These are nozzle-free printing methods, so the complexity of the structure does not affect the printing time. Moreover, tissues obtained using this technique exhibit good biocompatibility and cell viability.[31,32]

Laser-assisted bio-printing

Currently, LAB technology is based on 2 techniques – laser direct writing (LDW) and laser-induced transfer (LIFT).[33] It consists of 3 main elements: a pulsed laser, a ribbon and a receiving substrate. After the laser beam is emitted, it is absorbed by the metal containing the ribbon, e.g., gold (Au) or titanium (Ti). Then, the biomaterial suspended on the ribbon evaporates under the influence of the laser, creating high-pressure bubbles that eventually settle on the receiving substrate, creating the appropriate biological pattern/scheme.[34] This method is not as popular as the others described in this paper, but some researchers use it in tissue engineering. It can be attributable to the wide range of viscosities that the bio-ink can have (1–300 MPa/s), the high accuracy of printing scaffolds (accuracy 10 µm) and the possibility of obtaining a resolution of 1 cell per drop of bio-ink.[23,32,35] Among the disadvantages both of this method one can distinguish a very long printing time and a low flow rate, which is caused by the high resolution.[36,37]

Additionally, in this method, it is not possible to print simultaneously using multiple types of cells and materials, which results in a laborious and cumbersome process. A decrease in cell viability in this method below 85% has also been observed, which may be caused by thermal damage of the cells associated with the use of the laser.[36]

Digital light processing

Digital light processing (DLP) relies on the polymerization of light-sensitive polymers using precisely controlled light emitted from a special digital micromirror device (DMD).[32] The 3D structure is obtained by moving the working platform from bottom to top. First, the working platform is immersed in the liquid, after which a 2D image layer is created on the platform. Then, the platform is moved upwards by the distance of the created layer and the process is repeated. As a result of this process,

the 3D structure is created layer by layer.[38] Compared to other methods, this one requires the most preparation; however, the process of creating the structure itself is fast and accurate. An example of the use of DLP is the work of Yu et al.,[39] involving the printing of structures based on decellularized extracellular matrix (dCEM) with a size of only 30 μm. Using this method, complex, hierarchically branched geometries are created in a matter of seconds[39] because, instead of loading the material into the cartridge, the working platform is immersed in a tank with fluid, the printing speed itself is extremely high and the structure is created layer by layer. The resulting product can more effectively simulate the biological structure of the spinal cord compared to other methods. Despite this, DLP is a relatively new technology and the appropriate gels and material used require further research, which can contribute to even greater improvement of this method compared to others.

Stereolithography

Unlike the DLP method, stereolitography (SLA) uses laser reticulation with point or line scanning, while the rest of the procedure is based on the same principle as DLP. This method has no limitations regarding cell viscosity and also allows for printing tissue structures with a resolution of approx. 100 μm.[31,40]

Depending on the photoinitiator used, this method typically requires the use of visible or ultra-visible light to create covalent bonds in the bio-ink. However, in recent years, there has been a shift away from the use of ultra-visible light due to its harmful effects on cell DNA and the risk of skin cancer. Therefore, researchers are focusing primarily on visible light photopolymerization.[41] In a study conducted by Wang et al.[42] involving a stereolithography-based bio-printing system using visible light-crosslinked bio-inks and a commercial projector with a simple water filter, it was proven that the use of visible light as a crosslinking agent enables the printing of hydrogels with a resolution of up to 50 μm and maintains cell viability at 85%.[42]

Sakai et al.,[43] in a similar study also involving the use of stereolithography based on visible light, to create alginate hydrogels with phenolic hydroxyl groups (Alg-Ph), obtained cell viability of about 95%.[43] Despite the advantages of the SLA method, such as no limit on cell viscosity and print resolution, the mechanical limitations of this method result in a significantly slower printing process compared to other methods.[44]

Extrusion-based bio-printing

Of all the described bio-printing methods, extrusion-based printing is the most prevalent and well-developed technique.[45] In this method, a mixture of cells and hydrogels is "extruded" through micro-nozzles or needles onto a substrate to print a 3D structure. The micro-extruder, following instructions from the CAD-CAM system, lays down the material on the substrate in the form of beads. The beads are pre-arranged in the X-Y plane/axes, after which the "extruded" head is moved along the Z axis to create a complex 3D structure.[23]

The most important variations of this method include methods with pneumatic and mechanical (piston and screw) distribution systems. Piston-driven systems provide better control over bio-ink flow, while screw systems allow for more precise spatial control and are useful when using high-viscosity bio-ink. On the other hand, pneumatically driven systems are used regardless of the lightness of the bio-ink due to the possibility of modulating pressure and valve opening time.[46,47]

Hydrogels utilized in this type of printing typically belong to the category of non-Newtonian fluids, whose viscosity depends on shear rate and force.[48] Typical bio-ink viscosity in this technique can range from 30 MPa/s to even 6×10^7 MPa/s, with an average resolution of about 100 μm, and some studies indicate that it can reach even 5 μm.[23,32,49]

The main advantage of extrusion-based bio-printing is the ability to print models with very high cell density. Scaffolds obtained in this procedure provide much stronger and more fundamental support in the recovery process after SCI than scaffolds obtained using methods with lower cell density.[50] Additionally, this method allows for relatively uniform cell distribution in the print. However, there is a difficulty with the formation of shear stress. Increasing bio-ink concentration and viscosity leads to increased shear stress during extrusion, which leads to reduced cell viability.[51] Therefore, optimization of printing parameters is essential for improving cell viability. Recent studies by Smith et al.[52] involving co-extrusion of bovine aortic endothelial cells (BAEC) suspended in soluble type I collagen, using a micro-dispersion pen on the hydrophilic side of polyethylene terephthalate sheets, have shown that with proper optimization of conditions, it is possible to obtain a survival rate exceeding 90%.[52–55] Also, this method has been successfully applied to develop tissue engineering constructs, with aortic valves, tumor models and vascular tissues printed in this manner.[55–58]

As previously discussed, inkjet printing technology faces a significant challenge in treating SCI due to limitations in printing mode; extrusion printing is the most widely used, enables printing of high-resolution scaffolds and is undoubtedly one of the strongest candidates for treating SCI using bio-printing. On the other hand, light-directed methods (DLP, SLA and LAB) are relatively new. However, due to their ability to produce high-resolution and cell-viable scaffolds with very complex geometric features they represent a potential alternative and hope for the application of bio-printing in spinal cord regeneration.

Injuries, diseases and trauma causing spinal cord deficits

Chronic spinal cord injury

Nerve tissue in the damaged mammalian peripheral nervous system shows the ability to guide axons to synaptic targets based on the removal of myelin debris by immune cells and the secretion of cytokines by Schwann cells. However, SCI leads to scarring composed of myelin, cell debris, microglia, astrocytes, oligodendrocytes, fibroblasts, meninges, and extracellular matrix (ECM) molecules, resulting in impaired axonal regeneration in the damaged area. Scarring is thought to be both a physical and chemical barrier preventing nerve regeneration after SCI.[59]

Xiao et al.[59] in 2016 used intraoperative neurophysiological monitoring to identify and excise scar tissue. The next step was to use a NeuroRegen 'scaffold' containing autologous bone marrow mononuclear cells, which were implanted into the resection sites. NeuroRegen bridges the resulting lesion gap and allows the delivery of stem cells or biomolecules to promote neuronal regeneration. In addition to complete loss of motor and sensory function below the injury site, autonomic system dysfunction, including abnormal blood pressure, heart rate control, sweating, and temperature derangement are common clinical consequences of SCI. In the study by Xiao et al., the occurrence of sexual arousal and reduced sweating were observed after application of the NeuroRegen scaffold, indicating partial recovery of autonomic nervous system function. In addition, the return of SSEPs (somatosensory evoked potentials) in the tibia was detected in 2 patients, further evidence of partial nerve regeneration.[59]

Acute spinal cord injury

The American Spinal Injury Association (ASIA) was established in 1973 to facilitate the exchange of research, data and ideas among practitioners involved in the treatment of patients with SCI (Table 2[60]). Its founders sought to create a standardized model of care for the growing number of patients with SCI.

One of the first applications of scaffolding in SCI is the use of this technique in a 2016 clinical trial. A 25-year-old man sustained a T11–12 fracture after a motocross accident, resulting in a T11 ASIA grade A SCI. He underwent surgical decompression with spinal immobilization and was then included in the study using a bioresorbable scaffold that was implanted into the spinal cord parenchyma directly into the traumatic cavity. After 3 months, the patient's neurological condition had improved significantly, and the SCI rating had changed from grade A to grade C. Importantly, there were also no surgical complications or apparent safety-related abnormalities following this procedure.[61]

Table 2. American Spinal Injury Association Impairment (ASIA) Scale[60]

ASIA grade	Description
A	Complete. No sensory or motor function is preserved in the sacral segments S4–S5.
B	Incomplete. Sensory but not motor function is preserved below the neurological level and includes the sacral segments S4–S5.
C	Incomplete. Motor function is preserved below the neurological level, and more than half of key muscles below the neurological level have a muscle grade less that 3 (grades 0–2).
D	Incomplete. Motor function is preserved below the neurological level, and at least half of key muscles below the neurological level have a muscle grade greater than or equal to 3.
E	Normal. Sensory and motor function are normal.

Another case of successful use of the scaffold is its use in a 2018 clinical trial. Two patients with acute SCI at the T11 and C4 levels, respectively, were assessed as ASIA grade A. After magnetic resonance imaging (MRI) and electrophysiology of the nerves, NeuroRegen collagen scaffolds, which contained human mesenchymal stem cells from the umbilical cord, were implanted at the site of injury. During follow-up, no graft-related adverse events were identified. Return of sensory and motor function was observed in both patients. The level of sensation increased below the vertebrae where the injury occurred and, in addition, the patients regained sensation in the bladder and bowel. The patient with the injury at T11 regained the ability to walk, while the patient with the C4 injury regained the ability to move his toes and lift his legs. In both patients, injury status improved from a complete A grade injury on the ASIA scale to an incomplete C grade.[62]

Another study (from 2022) used a collagen scaffold transplant that contained the patients' own bone marrow mononuclear cells or umbilical cord mesenchymal stem cells (UC-MSCs). Fifteen patients with grade A were enrolled in the clinical trial and followed up for 2–5 years. None of the patients experienced serious complications or adverse effects related to the transplantation of the functional scaffold. The study yielded the expected positive results. Five patients with acute SCI achieved an increase in their sensory positions and 6 other patients regained sensation in the bladder. In addition, 4 patients regained their ability to walk.[63]

Amyotrophic lateral sclerosis

Amyotrophic lateral sclerosis (ALS) is a neurodegenerative disease (NDD) that attacks motor neurons, causing weakness, muscle atrophy and spasticity. The only available treatment options for this condition are only symptomatic. However, an innovative approach using 3D bio-printing and induced pluripotent stem cells (iPSCs) is being investigated. The idea behind the 3D bio-printing solution involves providing the cells with an environment as close

to physiological as possible. In a study by Scarian et al.,[64] healthy peripheral blood mononuclear cells and amyotrophic lateral sclerosis cells were induced to change into iPSCs and then differentiated into neural stem cells (NSCs) in 2D. In the next step, these cells were printed in 3D hydrogel-based constructs and later induced to differentiate into motor neuron progenitor cells and, in the next phase, into motor neurons. Using confocal microscopy and reverse transcription quantitative polymerase chain reaction (RT-qPCR), cell viability during 3D differentiation was monitored. The results showed no disruption of normal differentiation or electrophysiological features caused by the hydrogel. Characteristic markers at a given stage of differentiation were also investigated, where the difference compared to the 2D environment was the reduced expression of markers such as SOX1, SOX2 and Nestin. Based on this evidence, it was proven that 3D bio-printing can be considered as a good model to study and treat the pathogenesis of amyotrophic lateral sclerosis.[64]

Summary

To date, treatment of SCI has mainly consisted of surgical bracing of the damaged area, securing it and using drugs to prevent secondary injuries. However, these are not solutions that can permanently restore the functionality of the damaged nerve, and they only reduce the factors causing the injury to a small extent. For this reason, research into 3D bio-printing and scaffolding techniques should be intensively pursued further. Despite their current drawbacks or high costs, in the future, with the advancement of this technique, they may be the main tool capable of fully regenerating a damaged spinal cord.

ORCID iDs

Marcin Knefel https://orcid.org/0009-0005-0228-7708
Mikołaj Kantor https://orcid.org/0009-0005-0781-401X
Karolina Kępka https://orcid.org/0009-0001-1392-8161
Aleksandra Owczarzy https://orcid.org/0000-0003-1571-9643
Karolina Kulig https://orcid.org/0000-0001-9198-2254
Małgorzata Maciążek-Jurczyk https://orcid.org/0000-0003-1054-6309

References

1. Anjum A, Yazid MD, Fauzi Daud M, et al. Spinal cord injury: Pathophysiology, multimolecular interactions, and underlying recovery mechanisms. *Int J Mol Sci*. 2020;21(20):7533. doi:10.3390/ijms21207533
2. Bican O, Minagar A, Pruitt AA. The spinal cord. *Neurol Clin*. 2013;31(1):1–18. doi:10.1016/j.ncl.2012.09.009
3. Purves D, Williams SM, eds. *Neuroscience*. 3rd ed. Sunderland, USA: Sinauer Associates; 2004. ISBN:978-0-87893-725-7 978-0-87893-915-2.
4. Squire L, Berg D, Bloom F, du Lac S, Ghosh A, Spitzer N, eds. *Fundamental Neuroscience*. 3rd ed. Amsterdam, the Netherlands–Paris, France: Academic Press; 2008. ISBN:978-0-12-374019-9.
5. Lindvall O, Kokaia Z. Stem cells for the treatment of neurological disorders. *Nature*. 2006;441(7097):1094–1096. doi:10.1038/nature04960
6. Venugopal C, Chandanala S, Prasad HC, Nayeem D, Bhonde RR, Dhanushkodi A. Regenerative therapy for hippocampal degenerative diseases: Lessons from preclinical studies. *J Tissue Eng Regen Med*. 2017;11(2):321–333. doi:10.1002/term.2052
7. Sobrido-Cameán D, Barreiro-Iglesias A. Role of caspase-8 and Fas in cell death after spinal cord injury. *Front Mol Neurosci*. 2018;11:101. doi:10.3389/fnmol.2018.00101
8. Schwab ME, Bartholdi D. Degeneration and regeneration of axons in the lesioned spinal cord. *Physiol Rev*. 1996;76(2):319–370. doi:10.1152/physrev.1996.76.2.319
9. Orr M, Gensel J. Interactions of primary insult biomechanics and secondary cascades in spinal cord injury: Implications for therapy. *Neural Regen Res*. 2017;12(10):1618. doi:10.4103/1673-5374.217332
10. Cheung V, Hoshide R, Bansal V, Kasper E, Chen C. Methylprednisolone in the management of spinal cord injuries: Lessons from randomized controlled trials. *Surg Neurol Int*. 2015;6(1):142. doi:10.4103/2152-7806.163452
11. Qian T, Guo X, Levi AD, Vanni S, Shebert RT, Sipski ML. High-dose methylprednisolone may cause myopathy in acute spinal cord injury patients. *Spinal Cord*. 2005;43(4):199–203. doi:10.1038/sj.sc.3101681
12. Hurlbert RJ. Methylprednisolone for the treatment of acute spinal cord injury: Point. *Neurosurgery*. 2014;61(Suppl 1):32–35. doi:10.1227/NEU.0000000000000393
13. Silva NA, Sousa N, Reis RL, Salgado AJ. From basics to clinical: A comprehensive review on spinal cord injury. *Prog Neurobiol*. 2014;114:25–57. doi:10.1016/j.pneurobio.2013.11.002
14. Joung D, Lavoie NS, Guo S, Park SH, Parr AM, McAlpine MC. 3D printed neural regeneration devices. *Adv Funct Mater*. 2020;30(1):1906237. doi:10.1002/adfm.201906237
15. Cunha C, Panseri S, Antonini S. Emerging nanotechnology approaches in tissue engineering for peripheral nerve regeneration. *Nanomed Nanotechnol Biol Med*. 2011;7(1):50–59. doi:10.1016/j.nano.2010.07.004
16. Subramanian A, Krishnan UM, Sethuraman S. Development of biomaterial scaffold for nerve tissue engineering: Biomaterial mediated neural regeneration. *J Biomed Sci*. 2009;16(1):108. doi:10.1186/1423-0127-16-108
17. Cheng T, Qu H, Zhang G, Zhang X. Osteogenic and antibacterial properties of vancomycin-laden mesoporous bioglass/PLGA composite scaffolds for bone regeneration in infected bone defects. *Artif Cells Nanomed Biotechnol*. 2017;46(8):1935–1947. doi:10.1080/21691401.2017.1396997
18. Gu BK, Choi DJ, Park SJ, Kim MS, Kang CM, Kim CH. 3-dimensional bioprinting for tissue engineering applications. *Biomater Res*. 2016;20(1):12. doi:10.1186/s40824-016-0058-2
19. Haring AP, Sontheimer H, Johnson BN. Microphysiological human brain and neural systems-on-a-chip: Potential alternatives to small animal models and emerging platforms for drug discovery and personalized medicine. *Stem Cell Rev Rep*. 2017;13(3):381–406. doi:10.1007/s12015-017-9738-0
20. Zheng Q, Lu J, Chen H, Huang L, Cai J, Xu Z. Application of inkjet printing technique for biological material delivery and antimicrobial assays. *Anal Biochem*. 2011;410(2):171–176. doi:10.1016/j.ab.2010.10.024
21. Hendriks J, Willem Visser C, Henke S, et al. Optimizing cell viability in droplet-based cell deposition. *Sci Rep*. 2015;5(1):11304. doi:10.1038/srep11304
22. Murphy SV, Atala A. 3D bioprinting of tissues and organs. *Nat Biotechnol*. 2014;32(8):773–785. doi:10.1038/nbt.2958
23. Xu T, Gregory C, Molnar P, et al. Viability and electrophysiology of neural cell structures generated by the inkjet printing method. *Biomaterials*. 2006;27(19):3580–3588. doi:10.1016/j.biomaterials.2006.01.048
24. Cui X, Dean D, Ruggeri ZM, Boland T. Cell damage evaluation of thermal inkjet-printed Chinese hamster ovary cells. *Biotech Bioenerg*. 2010;106(6):963–969. doi:10.1002/bit.22762
25. O'Brien CM, Holmes B, Faucett S, Zhang LG. Three-dimensional printing of nanomaterial scaffolds for complex tissue regeneration. *Tissue Eng Part B Rev*. 2015;21(1):103–114. doi:10.1089/ten.teb.2014.0168
26. Vyavahare S, Teraiya S, Panghal D, Kumar S. Fused deposition modelling: A review. *Rapid Prototyping Journal*. 2020;26(1):176–201. doi:10.1108/RPJ-04-2019-0106
27. Cui H, Nowicki M, Fisher JP, Zhang LG. 3D bioprinting for organ regeneration. *Adv Healthcare Mater*. 2017;6(1):1601118. doi:10.1002/adhm.201601118
28. Wasti S, Adhikari S. Use of biomaterials for 3D printing by fused deposition modeling technique: A review. *Front Chem*. 2020;8:315. doi:10.3389/fchem.2020.00315

29. Cano-Vicent A, Tambuwala MM, Hassan SkS, et al. Fused deposition modelling: Current status, methodology, applications and future prospects. *Additive Manufacturing*. 2021;47:102378. doi:10.1016/j.addma.2021.102378
30. Warburton A, Girdler SJ, Mikhail CM, Ahn A, Cho SK. Biomaterials in spinal implants: A review. *Neurospine*. 2020;17(1):101–110. doi:10.14245/ns.1938296.148
31. Mandrycky C, Wang Z, Kim K, Kim DH. 3D bioprinting for engineering complex tissues. *Biotechnol Adv*. 2016;34(4):422–434. doi:10.1016/j.biotechadv.2015.12.011
32. Derakhshanfar S, Mbeleck R, Xu K, Zhang X, Zhong W, Xing M. 3D bioprinting for biomedical devices and tissue engineering: A review of recent trends and advances. *Bioact Mater*. 2018;3(2):144–156. doi:10.1016/j.bioactmat.2017.11.008
33. Koch L, Deiwick A, Schlie S, et al. Skin tissue generation by laser cell printing. *Biotech Bioenerg*. 2012;109(7):1855–1863. doi:10.1002/bit.24455
34. Keriquel V, Oliveira H, Rémy M, et al. In situ printing of mesenchymal stromal cells, by laser-assisted bioprinting, for in vivo bone regeneration applications. *Sci Rep*. 2017;7(1):1778. doi:10.1038/s41598-017-01914-x
35. Guillotin B, Souquet A, Catros S, et al. Laser assisted bioprinting of engineered tissue with high cell density and microscale organization. *Biomaterials*. 2010;31(28):7250–7256. doi:10.1016/j.biomaterials.2010.05.055
36. Guillotin B, Guillemot F. Cell patterning technologies for organotypic tissue fabrication. *Trends Biotechnol*. 2011;29(4):183–190. doi:10.1016/j.tibtech.2010.12.008
37. Hopp B. Femtosecond laser printing of living cells using absorbing film-assisted laser-induced forward transfer. *Opt Eng*. 2012;51(1):014302. doi:10.1117/1.OE.51.1.014302
38. Zhang J, Hu Q, Wang S, Tao J, Gou M. Digital light processing based three-dimensional printing for medical applications. *Int J Bioprint*. 2019;6(1):242. doi:10.18063/ijb.v6i1.242
39. Yu C, Ma X, Zhu W, et al. Scanningless and continuous 3D bioprinting of human tissues with decellularized extracellular matrix. *Biomaterials*. 2019;194:1–13. doi:10.1016/j.biomaterials.2018.12.009
40. Gauvin R, Chen YC, Lee JW, et al. Microfabrication of complex porous tissue engineering scaffolds using 3D projection stereolithography. *Biomaterials*. 2012;33(15):3824–3834. doi:10.1016/j.biomaterials.2012.01.048
41. Sinha RP, Häder DP. UV-induced DNA damage and repair: A review. *Photochem Photobiol Sci*. 2002;1(4):225–236. doi:10.1039/b201230h
42. Wang Z, Abdulla R, Parker B, Samanipour R, Ghosh S, Kim K. A simple and high-resolution stereolithography-based 3D bioprinting system using visible light crosslinkable bioinks. *Biofabrication*. 2015;7(4):045009. doi:10.1088/1758-5090/7/4/045009
43. Sakai S, Kamei H, Mori T, et al. Visible light-induced hydrogelation of an alginate derivative and application to stereolithographic bioprinting using a visible light projector and acid red. *Biomacromolecules*. 2018;19(2):672–679. doi:10.1021/acs.biomac.7b01827
44. Daly AC, Prendergast ME, Hughes AJ, Burdick JA. Bioprinting for the biologist. *Cell*. 2021;184(1):18–32. doi:10.1016/j.cell.2020.12.002
45. Shen Y, Tang H, Huang X, et al. DLP printing photocurable chitosan to build bio-constructs for tissue engineering. *Carbohydr Polym*. 2020;235:115970. doi:10.1016/j.carbpol.2020.115970
46. Matai I, Kaur G, Seyedsalehi A, McClinton A, Laurencin CT. Progress in 3D bioprinting technology for tissue/organ regenerative engineering. *Biomaterials*. 2020;226:119536. doi:10.1016/j.biomaterials.2019.119536
47. Pati F, Jang J, Lee JW, Cho DW. Extrusion bioprinting. In: Atala A, Yoo JJ, eds. *Essentials of 3D Biofabrication and Translation*. Amsterdam, the Netherlands–New York, USA: Elsevier; 2015:123–152. doi:10.1016/B978-0-12-800972-7.00007-4
48. Jungst T, Smolan W, Schacht K, Scheibel T, Groll J. Strategies and molecular design criteria for 3D printable hydrogels. *Chem Rev*. 2016;116(3):1496–1539. doi:10.1021/acs.chemrev.5b00303
49. Hölzl K, Lin S, Tytgat L, Van Vlierberghe S, Gu L, Ovsianikov A. Bioink properties before, during and after 3D bioprinting. *Biofabrication*. 2016;8(3):032002. doi:10.1088/1758-5090/8/3/032002
50. Bishop ES, Mostafa S, Pakvasa M, et al. 3-D bioprinting technologies in tissue engineering and regenerative medicine: Current and future trends. *Genes Dis*. 2017;4(4):185–195. doi:10.1016/j.gendis.2017.10.002
51. Nair K, Gandhi M, Khalil S, et al. Characterization of cell viability during bioprinting processes. *Biotechnol J*. 2009;4(8):1168–1177. doi:10.1002/biot.200900004
52. Smith CM, Stone AL, Parkhill RL, et al. Three-dimensional BioAssembly Tool for generating viable tissue-engineered constructs. *Tissue Eng*. 2004;10(9–10):1566–1576. doi:10.1089/ten.2004.10.1566
53. Liu X, Hao M, Chen Z, et al. 3D bioprinted neural tissue constructs for spinal cord injury repair. *Biomaterials*. 2021;272:120771. doi:10.1016/j.biomaterials.2021.120771
54. Seol YJ, Kang HW, Lee SJ, Atala A, Yoo JJ. Bioprinting technology and its applications. *Eur J Cardiothorac Surg*. 2014;46(3):342–348. doi:10.1093/ejcts/ezu148
55. Zhang X, Zhang Y. Tissue engineering applications of three-dimensional bioprinting. *Cell Biochem Biophys*. 2015;72(3):777–782. doi:10.1007/s12013-015-0531-x
56. Hsu S, Chang W, Yen C. Novel flexible nerve conduits made of water-based biodegradable polyurethane for peripheral nerve regeneration. *J Biomed Mater Res A*. 2017;105(5):1383–1392. doi:10.1002/jbm.a.36022
57. Dhariwala B, Hunt E, Boland T. Rapid prototyping of tissue-engineering constructs, using photopolymerizable hydrogels and stereolithography. *Tissue Eng*. 2004;10(9–10):1316–1322. doi:10.1089/ten.2004.10.1316
58. Skardal A, Zhang J, Prestwich GD. Bioprinting vessel-like constructs using hyaluronan hydrogels crosslinked with tetrahedral polyethylene glycol tetracrylates. *Biomaterials*. 2010;31(24):6173–6181. doi:10.1016/j.biomaterials.2010.04.045
59. Xiao Z, Tang F, Tang J, et al. One-year clinical study of NeuroRegen scaffold implantation following scar resection in complete chronic spinal cord injury patients. *Sci China Life Sci*. 2016;59(7):647–655. doi:10.1007/s11427-016-5080-z
60. Schuld C, Wiese J, Hug A, et al. Computer implementation of the international standards for neurological classification of spinal cord injury for consistent and efficient derivation of its subscores including handling of data from not testable segments. *J Neurotrauma*. 2012;29(3):453–461. doi:10.1089/neu.2011.2085
61. Theodore N, Hlubek R, Danielson J, et al. First human implantation of a bioresorbable polymer scaffold for acute traumatic spinal cord injury: A clinical pilot study for safety and feasibility. *Neurosurgery*. 2016;79(2):E305–E312. doi:10.1227/NEU.0000000000001283
62. Xiao Z, Tang F, Zhao Y, et al. Significant improvement of acute complete spinal cord injury patients diagnosed by a combined criteria implanted with NeuroRegen scaffolds and mesenchymal stem cells. *Cell Transplant*. 2018;27(6):907–915. doi:10.1177/0963689718766279
63. Tang F, Tang J, Zhao Y, et al. Long-term clinical observation of patients with acute and chronic complete spinal cord injury after transplantation of NeuroRegen scaffold. *Sci China Life Sci*. 2022;65(5):909–926. doi:10.1007/s11427-021-1985-5
64. Scarian E, Bordoni M, Fantini V, et al. Patients' stem cells differentiation in a 3D environment as a promising experimental tool for the study of amyotrophic lateral sclerosis. *Int J Mol Sci*. 2022;23(10):5344. doi:10.3390/ijms23105344

A review on recent advances in the stability study of anti-mycobacterial drugs

Przegląd najnowszych osiągnięć w badaniu trwałości leków przeciwprątkowych

Marta Karaźniewicz-Łada[A–F]

Department of Physical Pharmacy and Pharmacokinetics, Poznan University of Medical Sciences, Poland

A – research concept and design; B – collection and/or assembly of data; C – data analysis and interpretation;
D – writing the article; E – critical revision of the article; F – final approval of the article

Polymers in Medicine, ISSN 0370-0747 (print), ISSN 2451-2699 (online) *Polim Med*. 2024;54(2):135–142

Address for correspondence
Marta Karaźniewicz-Łada
E-mail: mkaraz@ump.edu.pl

Funding sources
None declared

Conflict of interest
None declared

Received on November 18, 2024
Reviewed on November 27, 2024
Accepted on November 28, 2024

Published online on December 3, 2024

Abstract

Several factors, including characteristic polymer composition of the cell wall, based on peptidoglycans cross-linked with arabinogalactans, together with the lipid layer contribute to the high resistance of *Mycobacterium tuberculosis* to antibiotics and other anti-tuberculosis drugs, leading to the development of new treatment methods. Implementation of therapeutic drug monitoring for anti-mycobacterial drugs in routine clinical practice requires understanding of the limited stability of these drugs. Rifampicin and isoniazid are the main anti-tuberculosis drugs that generate degradation products during sample handling and storage. Therefore, analytical methods used for analysis of clinical samples collected from tuberculosis patients treated with a combination of different drugs should enable the separation of the studied analytes from their metabolites and degradation products. Moreover, the samples require strictly regulated collection and storage conditions to prevent degradation processes.

The purpose of this review was to present recent data on the stability studies of anti-mycobacterial drugs, specifically used as first-line treatment in patients with tuberculosis. Detailed degradation pathway of rifampicin was described, including conditions influencing the formation of specific rifampicin related substances. Moreover, the results of the stability studies of anti-mycobacterial drugs were presented in various matrices in conditions determined by international guidance such as U.S. Food and Drug Administration (FDA) or International Council for Harmonisation (ICH) guidelines. Particular attention was given to analytical methods designed for analysis of anti-mycobacterial drugs in the presence of their degradation products. Finally, recommendations proposed by different authors for collection, processing and storage of clinical samples to increase stability of anti-mycobacterial drugs were summarized.

Key words: tuberculosis, isoniazid, rifampicin, pyrazinamide, ethambutol

Cite as
Karaźniewicz-Łada M. A review on recent advances in the stability study of anti-mycobacterial drugs. *Polim Med*. 2024;54(2):135–142. doi:10.17219/pim/196615

DOI
10.17219/pim/196615

Streszczenie

Zróżnicowane czynniki, w tym charakterystyczny skład polimerowy ściany komórkowej, opartej na peptydoglikanach usieciowanych arabinogalaktanami, wraz z warstwą lipidową, przyczyniają się do wysokiej oporności *Mycobacterium tuberculosis* na antybiotyki i inne leki przeciwgruźlicze, co prowadzi do poszukiwania nowych metod leczenia. Wdrożenie terapeutycznego monitorowania leków przeciwprątkowych w rutynowej praktyce klinicznej wymaga zrozumienia ograniczonej stabilności tych leków. Ryfampicyna i izoniazyd są głównymi lekami przeciwgruźliczymi, które generują produkty degradacji podczas przygotowywania i przechowywania próbek. Z tego względu metody analityczne stosowane do analizy próbek klinicznych pobranych od pacjentów z gruźlicą leczonych kombinacją różnych leków powinny umożliwiać oddzielenie badanych analitów od ich metabolitów i produktów degradacji. Ponadto próbki wymagają ściśle określonych warunków pobierania i przechowywania, aby zapobiec procesom degradacji.

Celem tego przeglądu jest przedstawienie najnowszych danych na temat badań stabilności leków przeciwprątkowych, w szczególności tych stosowanych jako leki pierwszego rzutu u pacjentów z gruźlicą. Szczegółowo opisano proces degradacji ryfampicyny z uwzględnieniem warunków wpływających na powstawanie określonych substancji pochodnych ryfampicyny. Ponadto przedstawiono wyniki badań stabilności leków przeciwprątkowych w różnych matrycach w warunkach określonych przez wytyczne międzynarodowych instytucji takich jak FDA lub ICH. Szczególną uwagę poświęcono metodom analitycznym przeznaczonym do analizy leków przeciwgruźliczych w obecności produktów ich degradacji. Na koniec podsumowano zalecenia zaproponowane przez różnych autorów dotyczące zbierania, przygotowania i przechowywania próbek klinicznych w celu zwiększenia stabilności leków przeciwprątkowych.

Słowa kluczowe: gruźlica, izoniazyd, rifampicyna, pyrazynamid, etambutol

Introduction

Tuberculosis infections pose a serious threat to the human population. One of the factors influencing the drug resistance of the tuberculosis bacillus is the composition of its cell wall, which contains specific polymers and hydrophobic compounds. The characteristic polymer composition of the cell wall, based on peptidoglycans cross-linked with arabinogalactans, together with the lipid layer protects the bacterium against the influence of xenobiotics.[1] The World Health Organization (WHO) reported that tuberculosis remained the 2nd most frequent cause of death from infection in 2022, just behind coronavirus disease (COVID-19). In addition, this disease caused almost twice as many deaths as HIV/AIDS. Approximately 25% of people in the world are infected with *Mycobacterium tuberculosis* and about 5–10% of them will develop an active form of the disease during their lifetime. Every year, 10 million people suffer from tuberculosis. Most cases of the disease occur in the countries of southern Africa and southeast Asia.[2] In Poland, 4,314 new cases of tuberculosis were registered in 2022, which means 17.5% of cases more than in the previous year.[3] According to the WHO recommendations, first-line treatment should include rifampicin (RIF), isoniazid (INH), pyrazinamide (PZA), and ethambutol (ETH). These drugs are given in combination to target different enzymes and minimize bacterial resistance.[4] In cases of treatment resistance, second-line medicines are used, including aminoglycosides, fluoroquinolones (moxifloxacin, levofloxacin), ethionamide, prothionamide, cycloserine, terizidone, and p-aminosalicylic acid.[5]

One of the reasons for the limited effectiveness of tuberculosis treatment are subtherapeutic concentrations of the drugs, which lead to drug resistance and death.[6] Therefore, therapeutic drug monitoring (TDM) is suggested to individualize dosing for a patient. To ensure the effectiveness of bactericidal treatment, therapeutic concentration ranges for anti-tuberculosis drugs in plasma or serum have been established. Due to the limited time and resources in the clinic, typically, only 2 samples are collected post-dose: at 2 h, which corresponds to the peak concentration for most anti-tubercular drugs, and at 6 h, which allows for distinguishing between delayed absorption and malabsorption.[7] High-performance liquid chromatography (HPLC) methods are recommended to analyze concentrations for TDM, and in the case of RIF, chemiluminescence and spectrophotometry can be also applied.[8]

Despite recommendations, TDM is not widely used in countries where tuberculosis is common. The main reasons include high costs, limited availability of analytical instruments including mass spectrometry (MS) or HPLC, difficulties in storing and transporting biological material due to high temperatures, and the need for multiple blood collection, which is problematic, particularly in the case of malnourished children. Therefore, a urine sample was proposed as an alternative to blood for TDM. Among anti-tubercular drugs, RIF is monitored using colorimetry due to the red discoloration of urine in people taking this drug.[8,9] Recently, a colorimetric method using mobile phone application and standardized light box have been proposed to measure RIF in urine samples for personalized treatment of children with tuberculosis based on predicted RIF levels.[10] However, urinary RIF concentrations were poorly correlated with serum C_{max}, which raises doubts regarding the utility of urine as a matrix useful for TDM of RIF.[9]

Difficulties in TDM may be also caused by limited stability of the drugs. Degradation of RIF depends on pH and leads to the formation of rifampicin quinone (RIF-Q), 3-formyl-rifampicin (3-F-RIF) and 25-desacetylrifampicin (25-D-RIF).[11] Moreover, limited stability of INH at ambient temperature was confirmed for whole blood, serum and

plasma. Hence, it is recommended to process collected specimen at low temperatures.[12] All RIF compounds except RIF-Q have similar UV-VIS absorbance spectra with maximum absorbance at 474 nm, while the maximum absorption of RIF-Q shifts to 540 nm.[13] Therefore, when using spectrophotometric methods, the observed absorbance values may not correspond to the actual concentrations of RIF because its products of degradation (3-F-RIF and 25-D-RIF) show absorbance at the same wavelength.

To overcome abovementioned problems with stability, Xing et al.[14] suggested adding ascorbic acid to protect RIF against autooxidation in clinical samples. Pršo et al.[15] suspected that the observed inaccuracy in their assay was caused by RIF degradation and therefore RIF was not included in the measurements. Moreover, liquid chromatography–tandem mass spectrometry (LC–MS/MS) methods are recommended for analysis of several anti-mycobacterial agents due to their higher sensitivity and selectivity compared to other analytical methods. As mentioned by Kuhlin et al.,[16] LC–MS/MS offers adequate separation and fast analysis of multi-analyte samples collected from patients with tuberculosis despite using non-selective procedures for preparation of samples. Nevertheless, among articles focusing on the analysis of anti-mycobacterial agents in various matrices, very few mentioned separation and detection of degradation products.[14,15,17–19]

This article focuses on a review of recent advances in anti-mycobacterial drug stability studies, including stability-indicating techniques, analysis of degradation products, and recommendations for sample storage and handling to enhance stability.

Degradation pathway of RIF

The RIF is a lipophilic substance with a partition coefficient log p-value of 2.77 and a pKa of 1.7 and 7.9 related to the 4-hydroxy and 3-piperazine nitrogen, respectively.[20] The stability of the drug is pH-dependent. In neutral pH, the drug is stable, whereas in acidic and basic pH, its decomposition was observed (Fig. 1). At low pH, RIF undergoes decomposition to 3-F-RIF, which is poorly soluble and contributes to the reduced bioavailability of RIF. The compound possesses high activity against *Mycobacterium tuberculosis* in vitro but not in vivo. At acidic pH of stomach and in the presence of INH, the degradation process of RIF is even more pronounced. Interaction between RIF and INH leads to the formation of the isonicotinyl

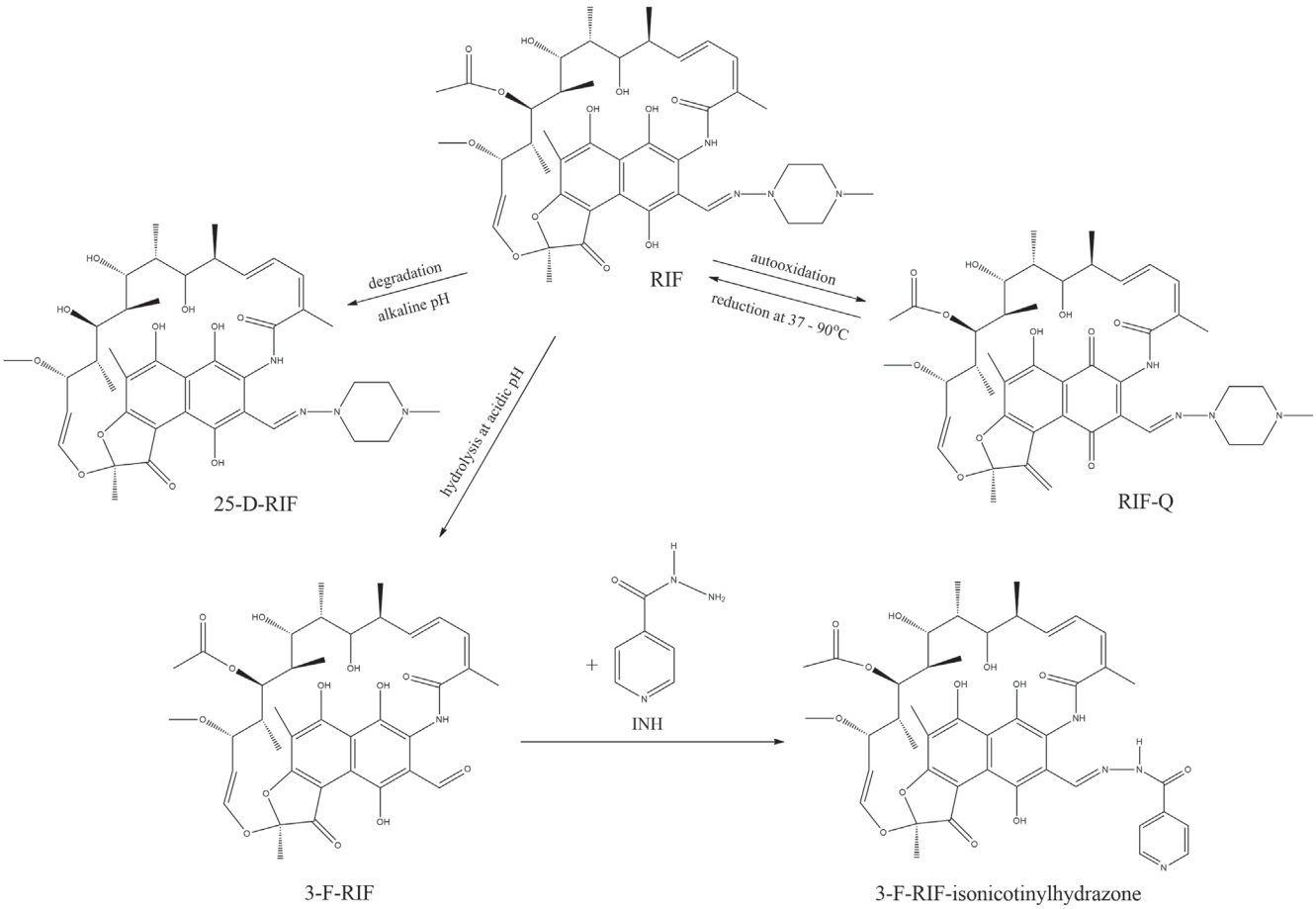

Fig. 1. Degradation pathway of rifampicin (RIF)

RIF-Q – rifampicin quinone; 25-D-RIF – 25-desacetylrifampicin; 3-F-RIF – 3-formylrifampicin; 3-F-RIF-isonicotinylhydrazone – 3-formyl-rifampicin isonicotinylhydrazone; INH – isoniazid.

hydrazone derivative of 3-F-RIF (3-F-RIF-isonicotinylhydrazone; Fig. 1) and subsequent production of hydrazine and 1-amino-4-methyl-piperazine.[11] Sankar et al.[21] showed that degradation of RIF and INH is caused by interaction between the compounds in fasting pH conditions under which combination of both drugs are administered. At pH 2 (the maximum pH in the fasting condition) and in 50 min, RIF decomposed by approx. 34%, while INH by 10%. The extent of decomposition for RIF and INH ranged between 13–35% and 4–11%, respectively, in several marketed formulations.

At higher pH, deacetylation process of RIF to 25-D-RIF is observed.[12] It is worth mentioning that 25-D-RIF is also the main metabolite of RIF in vivo.[22] In addition, at the mild alkaline conditions (pH 8.0), RIF is transformed into RIF-Q.[12] The latter is a main compound formed from RIF in a process of nonenzymatic autooxidation.[13,23,24] The degradation product is regarded as an impurity in RIF samples and an indicator of poor quality of RIF tablets. Sutradhar and Zaman[13] observed that RIF-Q in solution undergoes chemical conversion to RIF in the presence of microorganisms. This process is temperature-dependent, may result in an increase in antimicrobial activity of RIF, and promotes the development of antimicrobial resistance due to incorrect determination of medicine quality.[13] Data on potential interconversion between RIF and RIF-Q in vivo and the analyte stability in human clinical samples are scarce. Only few articles mentioned the appearance of RIF-Q in plasma and urine of patients treated with RIF.[17–19] Kivrane et al.[17] noticed the formation of RIF-Q in real samples but did not measure the concentration of the compound. In another report, plasma concentrations of RIF-Q in patients suffering from tuberculosis and being administered the first-line anti-mycobacterial drugs were in the range of 0.114–0.325 mg/L and comprised 2.30–4.50% of the sum of RIF and RIF-Q. Moreover, presence of 3-F-RIF was confirmed in all samples but its concentrations were below the quantification limit of the analytical method.[19] RIF-Q and 3-F-RIF appeared also in urine, suggesting RIF degradation during sample processing and storage. The concentration of RIF-Q was in the range of 0.71–2.62 mg/L, which constituted 3.6–13.2% of the total RIF concentration (RIF plus RIF-Q) and was twice higher than the concentration found in plasma.[18]

Stability of anti-mycobacterial drugs

Several guidelines on bioanalytical method validation released by U.S. Food and Drug Administration (FDA), European Medicine Agency (EMA) and International Council for Harmonisation (ICH) provide general principles for the stability testing, including recommendations on the acceptance criteria for stability results and the duration of stability tests. The chemical stability of the analyzed compound should be proved in stock solutions and biological fluid, and the effects of sample collection, handling and storage of the analyte should be assessed.[25–27] Hence, most data regarding the stability of anti-mycobacterial drugs were generated during developing and validating methods designed for analysis of these compounds. Several studies confirmed stability of these drugs in stock and working solutions stored for at least 1 month at –80°C[28–30] and –20°C.[18,19] However, significant degradation of INH and RIF was noticed in biological samples. Matrix components were suspected to significantly impact the stability of both compounds. Unsatisfactory benchtop stability was confirmed for INH at room temperature in plasma or serum. Sturkenboom et al.[31] reported significantly better stability of INH in ultrafiltrate than in plasma, and suggested that plasma proteins might be responsible for INH degradation. The INH stability in samples stored at room temperature for 12 h were reported by some authors.[15,32] However, other reports indicated that INH undergoes a significant decay at room temperature and is stable for 4 h[17,33] or as short as for 1 h.[17,19] There is inconsistency of results obtained in the stability study of RIF in plasma and serum samples. Some studies have shown that RIF remains stable in plasma/serum samples at room temperature for up to 24 h,[23,34] while other authors have reported lower stability of the compound. Le Guellec et al.[35] noticed that RIF undergoes rapid decomposition in plasma at room temperature, and its concentration decreases by 54% within 8 h. Karaźniewicz-Łada et al.[19] reported stability of RIF and 3-F-RIF in plasma samples at room temperature for 4 h, while 25-D-RIF was stable for only 1 h. The same results for 25-D-RIF were obtained by Kivrane et al.[17] However, in the study of Sundell et al.,[36] the compound was stable for 4 h of storage. The ambiguous results regarding RIF stability could be partly caused by the fact that RIF is sensitive to light and samples should be protected from light during processing and storage.[37] Poor stability of RIF and its derivatives in urine samples was also reported. The compounds were stable for 1 h if urine samples were kept at room temperature.[18] Other anti-bacterial drugs proved to be stable on a benchtop. Most authors noticed that PZA was stable in plasma or serum in room temperature for up to 4 h,[14,17,19,30,33,36] and in 1 study, the compound was stable for up to 24 h.[31] In urine samples, stability of INH, PZA and ETH was confirmed during 4 h of storage.[18]

There is inconsistency in results of long-term storage of samples containing anti-mycobacterial drugs. In most studies, stability of INH and RIF in plasma or serum samples was confirmed when stored for 1 month[29,30,38] at –80°C. Longer storage stability of 12 weeks at –80°C was reported by Sundell et al.[36] However, Kim et al.[38] noticed substantial degradation of the compounds over 12 weeks of storage and confirmed stability for only 4 weeks. Another report indicated stability of RIF in plasma samples kept for

70 weeks at –85°C.[39] Such long stability of the compound might be connected to the procedure of sample preparation, which included charcoal-stripping, ultracentrifugation and filtration. As a result, many matrix components of the samples were removed, leading to improved RIF stability. It was proved that higher temperature for long-term storage may cause degradation of RIF and INH within few days; INH was stable for 7-day storage at –20°C,[17,19] while RIF stability ranges from <1 week[19,35] to 3 months.[17] Poor stability of RIF-Q (<1 week) was also confirmed.[19] Other anti-mycobacterial drugs exhibit better stability during long-term storage. Samples with PZA were stable at –20°C when stored for up to 3 months.[17]

Freezing and thawing samples is known to affect analyte stability. Both RIF, INH and PZA remained stable after 3 cycles of freezing (at –70°C or –80°C) and thawing at room temperature.[29,30,36,40] According to Gao et al.,[32] INH, PZA and RIF were stable during 3 cycles of freezing at –20°C and thawing at room temperature. In 2 other articles, a significant degradation of INH and RIF was observed under similar conditions.[17,19]

Abouzid et al.[18] performed extended stability study of anti-mycobacterial drugs in urine considering differences in physiological pH of urine samples ranged from 4 to 8. They proved stability of RIF, RIF-Q, 3-F-RIF, 25-D-RIF, INH, and PZA at pH 6 for 24 h of storage at –20°C, and ETH was stable in all sample pH values. However, after 30 days, significant degradation was observed for RIF-Q and 3-F-RIF in all samples, while other analytes were stable in urine of pH 6–8. Moreover, the stability of RIF, INH, PZA, and ETH were studied in conditions mimicking the urine collection process in medical centers and peripheral clinics at room temperature and at 37.5°C. Abouzid et al. noted that RIF was stable at pH 6–7 for up to 8 h, INH was stable at pH 6–7 for up to 24 h, and both PZA and ETH remained stable at pH 4–8 for up to 24 h. During the stability studies, an increase in the RIF-Q was observed, while RIF concentrations decreased, with this process being significantly accelerated at 37.5°C.[18]

Stability-indicating methods

According to the ICH guidance document, a bioanalytical method should be selective and specific enough to detect and differentiate the active substance from other compounds, such as products of degradation found during sample processing.[25] Since RIF and INH are the main anti-tuberculosis drugs that generate degradation products during sample handling and storage, the method used in the stability study should enable the separation of all compounds present in clinical samples collected from tuberculosis patients treated with a combination of different drugs. Therefore, the most suitable technique is HPLC because it enables chromatographic resolution of the analytes from their related substances. This method in combination with MS/MS detection is characterized by high selectivity and specificity, demands low sample volumes and may involve simple preparation techniques such as protein precipitation.[16] There are only few articles on HPLC methods for the determination of RIF and its derivatives in different matrices. Sankar et al.[21] developed and validated an HLPC with UV detection (HLPC-UV) method for measurements of RIF, INH and their degradation products including 3-F-RIF, RIF-Q and isonicotinyl hydrazone in solutions. After determining validation parameters including linearity, precision and accuracy, this method was applied for the decomposition study of RIF in samples containing INH, in the pH range of 1–3. Sutradhar and Zaman[13] used HPLC-UV and LC–MS methods to identify RIF as the product of the chemical change of RIF-Q observed upon heating. Both compounds were chromatographically separated and changes in RIF-Q absorbance were measured to track the conversion of the compound for 2 h. However, no validation parameters of the methods were presented. Prasad et al.[24] reported an liquid chromatography–diode array detector–mass spectrometry/time-of-flight (LC–DAD–MS/TOF) technique to identify 21 RIF related substances using modern LC–MS tools such as multiple stage MS, high resolution MS and hydrogen/deuterium exchange MS. The method was applied for the detection of the compounds in rat liver microsomes and in rat blood, urine and feces after administration of 50 mg/kg of RIF. The samples were processed prior to the analysis using protein precipitation with acetonitrile, liquid-freeze separation and solid phase extraction. The authors detected 6 known metabolites and degradation products (25-D-RIF, RIF glucuronide, N-demethyl-RIF, 3-F-RIF, RIF-Q, and desacetyl-3-F-RIF) and 15 new RIF related substances. However, their concentrations in biological fluids were not measured. Kivrane te al.[17] reported the development and validation of the LC–MS/MS method for simultaneous quantification of first-line antituberculosis drugs (ETH, INH, PZA, and RIF) along with their 6 primary metabolites (25-D-RIF, isonicotinic acid, acetylisoniazid, 5-hydroxypyrazine-2-carboxylic acid, pyrazine-2-carboxylic acid, and 5-hydroxypyrazinamide). They reported 2 RIF peaks as the result of the formation of RIF-Q in plasma samples and used 2 ion-transitions (from 821.4 to 789.3 specific for RIF-Q and from 823.4 to 791.3 specific for RIF) for accurate RIF quantification. Only 2 articles are available on the development and validation of sensitive and selective UPLC–MS/MS methods for the simultaneous analysis of RIF and its metabolite and degradation products – 25-D-RIF, 3-F-RIF and RIF-Q – in the presence of other anti-mycobacterial drugs INH, ETH and PZA in clinical samples.[18,19] For the measurements, small plasma (20 µL) and urine (10 µL) volumes were required, which were processed using protein precipitation with methanol and

Table 1. Methods for analysis of degradation products of anti-mycobacterial drugs

Analytical method	Conditions	Analyzed compounds	Application	Reference
HPLC-UV	column: Supelcosil LC-18-DB (250 × 4.6 mm, 5 µm); mobile phase: 65% methanol and 35% 0.01 M phosphate buffer at pH 7.00; detection: 254 nm	RIF, RIF-Q, 3-F-RIF, INH, isonicotinyl hydrazone	decomposition of RIF in the presence of INH at pH 1–3	21
LC-UV, LC–MS	column: C18 (parameters not provided); mobile phase: 80% acetonitrile, 20% water detection: 470 nm	RIF, RIF-Q	evaluation of the effect of temperature on the stability and antimicrobial activity of RIF-Q	13
LC-UV/DAD-MS/TOF	column: Zorbax C18 (250 × 4.6 mm, 5 µm); mobile phase: acetonitrile, 10 mM ammonium acetate, gradient elution; detection: 254 nm, MS/TOF	RIF, RIF-Q, 3-F-RIF, 25-D-RIF, RIF N-oxide	identification of 21 RIF metabolites and degradation products formed in vitro and in vivo	24
LC–MS/MS	column: Waters Acquity UPLC BEH C8 (75 mm × 2.1 mm, 1.7 µm); mobile phase: methanol, 0.1% formic acid in water, gradient elution; detection: TQ	RIF, RIF-Q, 25-D-RIF, INH, PZA, ETH and their metabolites	analysis of anti-mycobacterial drugs and their metabolites in plasma	17
LC–MS/MS	column: Kinetex Polar C18 column (15 x 3 mm, 2.6 µm); mobile phase: 0.1% formic acid in 5 mM ammonium formate and acetonitrile, gradient elution detection: TQ	RIF, RIF-Q, 3-F-RIF, 25-D-RIF, INH, PZA	pharmacokinetic and stability study of RIF, INH, and PZA in plasma samples	19
LC–MS/MS	column: Kinetex Polar C18 column (15 x 3 mm, 2.6 µm); mobile phase: 0.1% formic acid in 5 mM ammonium formate and acetonitrile, gradient elution detection: TQ	RIF, RIF-Q, 3-F-RIF, 25-D-RIF, INH, PZA, ETH	pharmacokinetic and stability study of RIF, INH, PZA and ETH in urine samples	18
MLC	column: SPHER-100 C18 (250 × 4.6 mm, 5 µm); mobile phase: 0.15 M SDS-6% 1-pentanol-0.01 M phosphate buffer at pH 7; detection: 337 nm	RIF, RIF-Q	stability study of RIF in solutions and spiked biological fluids	23

MLC – micellar liquid chromatography; RIF – rifampicin, RIF-Q – rifampicin quinone; 3-F-RIF – 3-formyl-rifampicin; 25-D-RIF – 25-desacetylrifampicin; INH – isoniazid; PZA – pyrazinamide; ETH – ethambutol;TQ – triple quadrupole tandem mass spectrometer; HPLC-UV – high-performance liquid chromatography with UV detection; LC–MS – liquid chromatography–mass spectrometry; LC–MS/MS – liquid chromatography–tandem mass spectrometry; LC-UV/DAD–MS/TOF – liquid chromatography with UV detection/diode array detector–mass spectrometry/time-of-flight.

further diluted with acetonitrile. For optimal separation of the compounds significantly different in polarity (logP from –0.7 for INH to 2.7 for RIF), Kinetex Polar C18 column and gradient elution were applied, allowing for the total analysis time of 12 min. Both methods were successfully validated in terms of selectivity, linearity and lower limit od quantification, precision and accuracy, matrix effect, carry-over, and stability. The applicability of the methods for analysis of INH, PZA, ETH, and RIF was verified in plasma and urine samples collected from patients with tuberculosis and in the extensive stability study of RIF under various conditions of sample collection and storage.[18,19]

Another useful analytical technique for studying the conversion of RIF to RIF-Q in plasma and urine is micellar liquid chromatography (MCL), as proved by Mishra et al.[23] The advantage of the method was simple sample preparation consisting of dilution in a micellar sodium dodecyl sulfate (SDS) solution. The method validation was carried out according to the EMA recommendations and tested employing the analysis of RIF in samples collected from tuberculosis patients. Moreover, the authors applied the method for the degradation study of RIF to RIF-Q in solutions and biological fluids spiked with RIF.

The summary of the methods for analysis of degradation products of anti-mycobacterial drugs are presented in Table 1.

Recommendations to increase stability

Limited stability of anti-mycobacterial drugs may impact TDM results. Therefore, results of numerous stability studies of the analytes at various storage conditions were utilized to prepare recommendations for handling the clinical samples. Some articles suggested that antioxidants, e.g., ascorbic acid, should be added after sample collection to protect RIF from autooxidation occurring when the samples are processed or stored.[14] Le Guellec et al.[35] indicated better stability of RIF in solutions when stored in higher concentrations and when ascorbic acid was added as a protecting agent. However, Peloquin[39] reported no benefits from such stabilization. The author suggested using a specific sample preparation procedure before adding RIF, including charcoal stripping, ultracentrifugation and filtration to remove matrix components that may increase RIF degradation. Mishra et al.[23] indicated that oxidation of RIF to RIF-Q is accelerated

in higher temperatures; thus, storage conditions for samples containing RIF should be strictly controlled. Similarly, INH and ethionamide are not stable in human serum and whole blood at room temperature. Therefore, Peloquin[41] suggested that the blood samples should be promptly centrifuged, the serum harvested and frozen immediately after collection. According to the latest recommendations,[19] centrifugation should be performed at low temperatures (preferably 4°C); samples can be left on the bench at ambient temperature for no longer than 1 h; protection from light is recommended by using amber and non-transparent glass tubes for sample storage and processing. In addition, storage at –80°C for no longer than 1 month, shipment of frozen samples with dry ice and limited sample thawing-freezing cycle number were suggested. Abouzid et al.[18] presented recommendations specifically for urine samples based on the observation that pH of urine and temperature affect the analyte stability. The authors suggested that stability of RIF during TDM can be prolonged to 8 h if the pH of collected urine is maintained in the range of 6–7.

Conclusions

Implementation of TDM for anti-tuberculosis drugs to individualize dosing for a patient requires determination of stability of these drugs in different conditions mimicking the sample collection, processing and storage in clinics. Numerous studies have confirmed the limited stability of RIF and INH in biological fluids, which is probably due to the presence of proteins and other matrix components. Factors that accelerate the decomposition process include higher temperatures during long-term storage, multiple freeze-thaw cycles or acidic and alkaline pH of the sample. Therefore, to increase analyte stability, strictly regulated handling conditions for samples containing anti-mycobacterial drugs have been established. It is increasingly apparent that methods used for determination of anti-tuberculosis agents in real samples should separate the analytes from their degradation products. These conditions are met by LC–MS/MS, which is the most suitable technique for stability studies and pharmacokinetic applications due to its selectivity and specificity.

ORCID iDs

Marta Karaźniewicz-Łada https://orcid.org/0000-0003-4091-7035

References

1. Brennan PJ. Structure, function, and biogenesis of the cell wall of *Mycobacterium tuberculosis*. *Tuberculosis*. 2003;83(1–3):91–97. doi:10.1016/S1472-9792(02)00089-6
2. World Health Organization (WHO). *Global Tuberculosis Report 2023*. Geneva, Switzerland: World Health Organization (WHO); 2023. https://www.who.int/teams/global-tuberculosis-programme/tb-reports/global-tuberculosis-report-2023. Accessed November 13, 2024.
3. European Centre for Disease Prevention and Control (ECDC). Tuberculosis surveillance and monitoring in Europe: 2024–2022 data. Stockholm, Sweden: European Centre for Disease Prevention and Control (ECDC); 2024. https://www.ecdc.europa.eu/en/publications-data/tuberculosis-surveillance-and-monitoring-europe-2024-2022-data. Accessed November 13, 2024.
4. Sachan RSK, Mistry V, Dholaria M, et al. Overcoming *Mycobacterium tuberculosis* drug resistance: Novel medications and repositioning strategies. *ACS Omega*. 2023;8(36):32244–32257. doi:10.1021/acsomega.3c02563
5. Patil K, Bagade S, Bonde S, Sharma S, Saraogi G. Recent therapeutic approaches for the management of tuberculosis: Challenges and opportunities. *Biomed Pharmacother*. 2018;99:735–745. doi:10.1016/j.biopha.2018.01.115
6. Hiruy H, Rogers Z, Mbowane C, et al. Subtherapeutic concentrations of first-line anti-TB drugs in South African children treated according to current guidelines: The PHATISA study. *J Antimicrob Chemother*. 2015;70(4):1115–1123. doi:10.1093/jac/dku478
7. Peloquin C. The role of therapeutic drug monitoring in mycobacterial infections. *Microbiol Spectr*. 2017;5(1):5.1.03. doi:10.1128/microbiolspec.TNMI7-0029-2016
8. Xie YL, Modi N, Handler D, et al. Simplified urine-based method to detect rifampin underexposure in adults with tuberculosis: A prospective diagnostic accuracy study. *Antimicrob Agents Chemother*. 2023;67(11):e00932-23. doi:10.1128/aac.00932-23
9. Zentner I, Schlecht HP, Khensouvann L, et al. Urine colorimetry to detect low rifampin exposure during tuberculosis therapy: A proof-of-concept study. *BMC Infect Dis*. 2016;16(1):242. doi:10.1186/s12879-016-1576-1
10. Szipszky C, Van Aartsen D, Criddle S, et al. Determination of rifampin concentrations by urine colorimetry and mobile phone readout for personalized dosing in tuberculosis treatment. *J Pediatric Infect Dis Soc*. 2021;10(2):104–111. doi:10.1093/jpids/piaa024
11. Shishoo CJ, Shah SA, Rathod IS, Savale SS, Kotecha JS, Shah PB. Stability of rifampicin in dissolution medium in presence of isoniazid. *Int J Pharm*. 1999;190(1):109–123. doi:10.1016/S0378-5173(99)00286-0
12. Singh S, Mariappan TT, Shankar R, Sarda N, Singh B. A critical review of the probable reasons for the poor variable bioavailability of rifampicin from anti-tubercular fixed-dose combination (FDC) products, and the likely solutions to the problem. *Int J Pharm*. 2001;228(1–2):5–17. doi:10.1016/S0378-5173(01)00754-2
13. Sutradhar I, Zaman MH. Evaluation of the effect of temperature on the stability and antimicrobial activity of rifampicin quinone. *J Pharm Biomed Anal*. 2021;197:113941. doi:10.1016/j.jpba.2021.113941
14. Xing Y, Yin L, Le X, et al. Simultaneous determination of first-line anti-tuberculosis drugs and one metabolite of isoniazid by liquid chromatography/tandem mass spectrometry in patients with human immunodeficiency virus-tuberculosis coinfection. *Heliyon*. 2021;7(7):e07532. doi:10.1016/j.heliyon.2021.e07532
15. Pršo K, Žideková N, Porvazník I, Solovič I, Mokrý J, Kertys M. A high-throughput LC–MS/MS method for simultaneous determination of isoniazid, ethambutol and pyrazinamide in human plasma. *Rapid Commun Mass Spectrom*. 2023;37(2):e9425. doi:10.1002/rcm.9425
16. Kuhlin J, Sturkenboom MGG, Ghimire S, et al. Mass spectrometry for therapeutic drug monitoring of anti-tuberculosis drugs. *Clin Mass Spectrom*. 2019;14:34–45. doi:10.1016/j.clinms.2018.10.002
17. Kivrane A, Grinberga S, Sevostjanovs E, et al. LC-MS/MS method for simultaneous quantification of the first-line anti-tuberculosis drugs and six primary metabolites in patient plasma: Implications for therapeutic drug monitoring. *J Chromatogr B Analyt Technol Biomed Life Sci*. 2021;1185:122986. doi:10.1016/j.jchromb.2021.122986
18. Abouzid M, Kosicka-Noworzyń K, Karaźniewicz-Łada M, et al. Development and validation of a UPLC-MS/MS method for therapeutic drug monitoring, pharmacokinetic and stability studies of first-line antituberculosis drugs in urine. *Molecules*. 2024;29(2):337. doi:10.3390/molecules29020337
19. Karaźniewicz-Łada M, Kosicka-Noworzyń K, Rao P, et al. New approach to rifampicin stability and first-line anti-tubercular drug pharmacokinetics by UPLC-MS/MS. *J Pharm Biomed Anal*. 2023;235:115650. doi:10.1016/j.jpba.2023.115650

20. Khan MF, Rita SA, Kayser MdS, et al. Theoretically guided analytical method development and validation for the estimation of rifampicin in a mixture of isoniazid and pyrazinamide by UV spectrophotometer. *Front Chem*. 2017;5:27. doi:10.3389/fchem.2017.00027
21. Sankar R, Sharda N, Singh S. Behavior of decomposition of rifampicin in the presence of isoniazid in the pH range 1–3. *Drug Dev Ind Pharm*. 2003;29(7):733–738. doi:10.1081/DDC-120021772
22. Seng KY, Hee KH, Soon GH, Chew N, Khoo SH, Lee LSU. Population pharmacokinetics of rifampicin and 25-deacetyl-rifampicin in healthy Asian adults. *J Antimicrob Chemother*. 2015;70(12):3298–3306. doi:10.1093/jac/dkv268
23. Mishra P, Pawar RP, Bose D, et al. Stability studies of rifampicin in plasma and urine of tuberculosis patients according to the European Medicines Agency guidelines. *Bioanalysis*. 2019;11(8):713–726. doi:10.4155/bio-2018-0174
24. Prasad B, Singh S. In vitro and in vivo investigation of metabolic fate of rifampicin using an optimized sample preparation approach and modern tools of liquid chromatography–mass spectrometry. *J Pharm Biomed Anal*. 2009;50(3):475–490. doi:10.1016/j.jpba.2009.05.009
25. European Medicines Agency (EMA). ICH M10 on bioanalytical method validation: Scientific guideline. Amsterdam, the Netherlands: European Medicines Agency (EMA); 2023. https://www.ema.europa.eu/en/ich-m10-bioanalytical-method-validation-scientific-guideline. Accessed November 17, 2024.
26. European Medicines Agency (EMA). Bioanalytical method validation: Scientific guideline. Amsterdam, the Netherlands: European Medicines Agency (EMA); 2012. https://www.ema.europa.eu/en/bioanalytical-method-validation-scientific-guideline. Accessed November 17, 2024.
27. U.S. Food and Drug Administration (FDA). Bioanalytical method validation Guidance for industry. Rockville, USA: U.S. Food and Drug Administration (FDA); 2018. https://www.fda.gov/files/drugs/published/Bioanalytical-Method-Validation-Guidance-for-Industry.pdf. Accessed November 17, 2024.
28. Notari S, Mancone C, Sergi M, et al. Determination of antituberculosis drug concentration in human plasma by MALDI-TOF/TOF. *IUBMB Life*. 2010;62(5):387–393. doi:10.1002/iub.321
29. Baietto L, Calcagno A, Motta I, et al. A UPLC–MS-MS method for the simultaneous quantification of first-line antituberculars in plasma and in PBMCs. *J Antimicrob Chemother*. 2015;70(9):2572–2575. doi:10.1093/jac/dkv148
30. Zhou Z, Wu X, Wei Q, et al. Development and validation of a hydrophilic interaction liquid chromatography–tandem mass spectrometry method for the simultaneous determination of five first-line antituberculosis drugs in plasma. *Anal Bioanal Chem*. 2013;405(19):6323–6335. doi:10.1007/s00216-013-7049-0
31. Sturkenboom MGG, Van Der Lijke H, Jongedijk EM, et al. Quantification of isoniazid, pyrazinamide and ethambutol in serum using liquid chromatography–tandem mass spectrometry. *J Appl Bioanal*. 2015;1(3):89–98. doi:10.17145/jab.15.015
32. Gao S, Wang Z, Xie X, et al. Rapid and sensitive method for simultaneous determination of first-line anti-tuberculosis drugs in human plasma by HPLC–MS/MS: Application to therapeutic drug monitoring. *Tuberculosis*. 2018;109:28–34. doi:10.1016/j.tube.2017.11.012
33. Luyen LT, Hung TM, Huyen LT, et al. Simultaneous determination of pyrazinamide, rifampicin, ethambutol, isoniazid and acetyl isoniazid in human plasma by LC–MS/MS method. *J Appl Pharm Sci*. 2018;8(9):61–73. doi:10.7324/JAPS.2018.8910
34. De Velde F, Alffenaar JWC, Wessels AMA, Greijdanus B, Uges DRA. Simultaneous determination of clarithromycin, rifampicin and their main metabolites in human plasma by liquid chromatography–tandem mass spectrometry. *J Chromatogr B Analyt Technol Biomed Life Sci*. 2009;877(18–19):1771–1777. doi:10.1016/j.jchromb.2009.04.038
35. Le Guellec C, Gaudet ML, Lamanetre S, Breteau M. Stability of rifampin in plasma: Consequences for therapeutic monitoring and pharmacokinetic studies. *Ther Drug Monit*. 1997;19(6):669–674. doi:10.1097/00007691-199712000-00011
36. Sundell J, Bienvenu E, Birgersson S, Äbelö A, Ashton M, Hoffmann KJ. Simultaneous quantification of four first line antitubercular drugs and metabolites in human plasma by hydrophilic interaction chromatography and tandem mass spectrometry. *J Chromatogr B Analyt Technol Biomed Life Sci*. 2019;1105:129–135. doi:10.1016/j.jchromb.2018.10.027
37. Hartkoorn R, Khoo S, Back D, et al. A rapid and sensitive HPLC–MS method for the detection of plasma and cellular rifampicin. *J Chromatogr B Analyt Technol Biomed Life Sci*. 2007;857(1):76–82. doi:10.1016/j.jchromb.2007.07.005
38. Kim HJ, Seo KA, Kim HM, et al. Simple and accurate quantitative analysis of 20 anti-tuberculosis drugs in human plasma using liquid chromatography–electrospray ionization–tandem mass spectrometry. *J Pharm Biomed Anal*. 2015;102:9–16. doi:10.1016/j.jpba.2014.08.026
39. Peloquin CA. Rifampin stability. *Ther Drug Monit*. 1998;20(4):450–451. doi:10.1097/00007691-199808000-00017
40. Wu L, Ye Z, Liu H, et al. Rapid and highly sensitive quantification of the anti-tuberculosis agents isoniazid, ethambutol, pyrazinamide, rifampicin and rifabutin in human plasma by UPLC–MS/MS. *J Pharm Biomed Anal*. 2020;180:113076. doi:10.1016/j.jpba.2019.113076
41. Peloquin CA. Therapeutic drug monitoring in the treatment of tuberculosis. *Drugs*. 2002;62(15):2169–2183. doi:10.2165/00003495-200262150-00001

Research letter

Rheological properties of pharmaceutical substrates produced with Celugel

Właściwości reologiczne podłoży farmaceutycznych wytwarzanych na bazie Celugelu

Monika Gasztych[A–F], Natalia Jurczak[B,C]

Department of Physical Chemistry and Biophysics, Faculty of Pharmacy, Wroclaw Medical University, Poland

A – research concept and design; B – collection and/or assembly of data; C – data analysis and interpretation;
D – writing the article; E – critical revision of the article; F – final approval of the article

Polymers in Medicine, ISSN 0370-0747 (print), ISSN 2451-2699 (online) *Polim Med*. 2024;54(2):143–147

Address for correspondence
Monika Gasztych
E-mail: monika.gasztych@umw.edu.pl

Funding sources
None declared

Conflict of interest
None declared

Acknowledgements
We would like to express our sincere gratitude to Professor Witold Musiał for his guidance, which have been instrumental of this study. His expertise and support were essential at every stage of our research. The research was carried out in collaboration with the Student Research Club #K130 at the Department of Physical Chemistry, Faculty of Pharmacy, Wroclaw Medical University, Poland.

Received on November 14, 2024
Reviewed on November 18, 2024
Accepted on November 20, 2024

Published online on November 28, 2024

Cite as
Gasztych M, Jurczak N. Rheological properties of pharmaceutical substrates produced with Celugel. *Polim Med*. 2024;54(2):143–147. doi:10.17219/pim/196210

DOI
10.17219/pim/196210

Abstract

Background. Hydrogels, containing a large amount of water and exhibiting high biocompatibility, can improve the rheological properties of formulations and adhere well to the application site. In Poland, only 1 hydrogel substrate is currently approved for pharmaceutical compounding: Celugel, based on hydroxyethyl cellulose (HEC).

Objectives. The aim of this study was to investigate how the variation in the raw material composition of Celugel-based hydrogels affects their osmotic pressure values and selected rheological properties.

Materials and methods. Ten gel formulations were prepared using a commercial Celugel as the base, with varying percentages of added water, alongside a consistent 5 wt% addition of sucrose. The research methods employed include osmotic pressure, dynamic viscosity, pH measurement, and surface tension using the du Noüy ring tensiometer.

Results. The composition of the formulation has a significant impact on the osmotic pressure. Nearly all of the hydrogels exhibited hyperosmotic characteristics relative to living tissues, with measured osmotic pressure values ranging from 160 mOsm/kg H_2O to 1,480 mOsm/kg H_2O. As anticipated, the viscosity of the formulations increased proportionally with the growing concentration of Celugel ranging from 2.19 mPa·s to 562.87 mPa·s.

Conclusions. The composition of Celugel significantly influences its rheological properties and osmotic pressure values, with the concentration of the gelling agent being the most impactful factor. The results suggest that Celugel is suitable for use in formulations intended for nasal administration.

Keywords: osmotic pressure, hydrogel, Celugel, hydroxyethylcellulose

Streszczenie

Wprowadzenie. Hydrożele, zawierające dużą ilość wody i charakteryzujące się wysoką biokompatybilnością, mogą poprawiać właściwości reologiczne formulacji i dobrze przylegać do miejsca aplikacji. W Polsce obecnie tylko jedno podłoże hydrożelowe jest zatwierdzone do receptury aptecznej: Celugel, oparty na hydroksyetylocelulozie.

Cel pracy. Celem badań było zbadanie, jak zmiana składu surowcowego hydrożeli na bazie Celugelu wpływa na wartości ciśnienia osmotycznego oraz wybrane właściwości reologiczne.

Materiał i metody. Przygotowano dziesięć formulacji żelowych, używając komercyjnego Celugelu jako bazy, z różnymi procentowymi dodatkami wody oraz stałym dodatkiem 5 wt.% sacharozy. W zastosowanych metodach badawczych uwzględniono pomiary ciśnienia osmotycznego, lepkości dynamicznej, pH oraz napięcia powierzchniowego za pomocą tensjometru pierścieniowego du Noüy.

Wyniki. Skład formulacji ma istotny wpływ na ciśnienie osmotyczne. Niemal wszystkie hydrożele wykazywały właściwości hipertoniczne w odniesieniu do tkanek żywych, a wartości ciśnienia osmotycznego wynosiły od 160 mOsm/kg H_2O do 1480 mOsm/kg H_2O. Zgodnie z oczekiwaniami, lepkość formulacji wzrastała proporcjonalnie do rosnącego stężenia Celugelu, w zakresie od 2,19 mPa·s do 562,87 mPa·s.

Wnioski. Skład Celugelu znacząco wpływa na jego właściwości reologiczne i wartości ciśnienia osmotycznego, przy czym największy wpływ ma stężenie substancji żelującej. Uzyskane wyniki sugerują, że Celugel nadaje się do stosowania w formulacjach przeznaczonych do podania donosowego.

Słowa kluczowe: hydroksyetyloceluloza, hydrożel, ciśnienie osmotyczne, Celugel

Background

Ointments are semi-solid pharmaceutical formulations intended for application on the skin or mucous membranes, functioning as emollients, protective agents or, when combined with active ingredients, as therapeutic agents. These preparations also contain excipients that provide essential organoleptic properties, rheological behavior and stability.[1]

According to the 12th edition of the Polish Pharmacopoeia,[2] ointment bases are classified into 5 main categories, including gels. A significant subgroup within gels is hydrogels, distinguished by a 3-dimensional network structure that retains large amounts of water within a swollen polymer matrix.[3] This structure closely resembles that of living tissues, providing hydrogels with superior biocompatibility. As a result, hydrogels are extensively used in medical and pharmaceutical applications such as drug delivery systems, wound dressings, tissue-engineering scaffolds, and contact lenses.[4]

In Poland, Celugel is an authorized hydrogel base composed of hydroxyethyl cellulose (HEC) and glycerol, preserved with sorbic acid and its potassium salt. Due to its beneficial characteristics, such as easy rinsability and high mucoadhesive capacity, Celugel is widely applied in formulations for the skin and mucous membranes, including nasal preparations. It offers a practical alternative to traditional glycerol-based formulations, which often have the disadvantage of flowing away from the application site.[5]

Osmotic pressure is a crucial factor influencing the local effects and effectiveness of various formulations, including those applied nasally.[6] While isotonic formulations are generally preferred, especially for prolonged use, non-isotonic formulations may be acceptable in specific cases. Furthermore, osmotic pressure can drive the release of active ingredients from certain drug delivery systems, enhancing their therapeutic impact.[7,8]

Objectives

The aim of this study was to investigate how variations in the composition of Celugel-based hydrogels affect osmotic pressure values and selected rheological properties.

Materials and methods

Celugel (Actifarm, Poland), hydroxyethyl cellulose with high viscosity and a molecular weight of approximately 300,000 Da (Pol-Aura, Poland) and sucrose (Pol-Aura, Poland) were used in the studies. Deionized water, used in all experiments, was obtained through an ion-exchange column in accordance with the requirements for purified water described in Polish Pharmacopoeia.[9]

Preparation of gels was based on Celugel with variable water content and a 5 wt% sucrose addition. A measured amount of Celugel base and water was combined in a vessel, followed by the addition of micronized sucrose, prepared in advance using a mortar. The mixture was stirred until a homogeneous gel was obtained. The specific compositions of these formulations are shown in Table 1, with all gels stored at 2–8°C.

Osmotic pressure measurements were performed, and subsequent rheological analyses included assessments of dynamic viscosity, surface tension and pH. Osmotic pressure measurements of the gels were conducted using the Marcel OS 3000 osmometer (Marcel S.A., Zielonka,

Table 1. The composition of tested hydrogels

No.	Acronym	Celugel [g]	Sucrose [g]	H_2O [g]
1	CL1	100.00	–	–
2	S1	95.00	5.00	–
3	S2	85.00	5.00	10.00
4	S3	75.00	5.00	20.00
5	S4	65.00	5.00	30.00
6	S5	55.00	5.00	40.00
7	S6	45.00	5.00	50.00
8	S7	35.00	5.00	60.00
9	S8	25.00	5.00	70.00
10	S9	15.00	5.00	80.00
11	S10	–	5.00	95.00

Poland), an automated device enabling precise, rapid osmotic analysis based on freezing-point depression. The pH was determined conductometrically using the Elmetron CPC-505 (Elmetron, Zabrze, Poland) in conjunction with the Elmetron ERH-11S pH electrode.

Dynamic viscosity was measured with the Brookfield RVDV 3+ rotational rheometer (Ametek, Middleborough, USA), which operates by detecting the torque required to overcome the resistance exerted by the sample's viscosity. Measurements employed 2 cone-and-plate setups: cone CP40 (0.8° angle and 4.8 cm diameter) operated at 5 rpm to generate a shear rate of 37.5 s^{-1}, while cone CP51 (1.565° angle, 2.3–2.4 cm diameter) operated at 100 rpm with shear rates of 384 s^{-1}, 750 s^{-1} and 1500 s^{-1}, measured for 10 s at a controlled temperature of 24°C.

Surface tension was assessed using the ring method on the D-MT1A tensiometer (SITA Messtechnik GmbH, Dresden, Germany), supported by D-MT1A.exe software (Polon-Izot Sp. z o.o., Warsaw, Poland) for precise analysis.

These methods provided comprehensive data on the physicochemical properties of the gels, contributing valuable insight into their suitability for various pharmaceutical and therapeutic applications.

Results

The osmotic pressure measurements for the CL1 and S1–S10 hydrogels ranged from 160 mOsm/kg H_2O to 1,480 mOsm/kg H_2O. Virtually all hydrogels were found to be hyperosmotic relative to living tissues, with the exception of formulation S10, which exhibited osmotic pressure values below physiological levels. The exact results of the osmotic pressure measurements are shown in Table 2. Values of pH were determined for examined (CL1 and S1–S10), The pH of gels S1–S9 ranged from 4.4 to 4.5, while a value of 6.4 was obtained for the 5 wt% aqueous sucrose solution (S10). The pH for CL1 was measured at 4.4. All results are presented in Fig. 1.

Table 2. The results of osmotic pressure measurements of the tested hydrogels

Acronym	Osmotic pressure [mOsm/kg H_2O]	SD
CL1	1,183	7
S1	1,480	13
S2	1,321	8
S3	1,063	10
S4	931.7	7
S5	844.3	8
S6	708.3	6
S7	601.0	10
S8	452.0	10
S9	317.3	8
S10	160.0	8

SD – standard deviation.

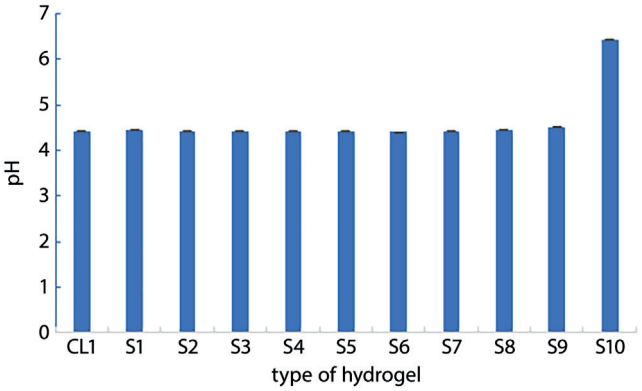

Fig. 1. The pH results obtained for all the preparations examined (CL1 and S1–S10), with standard deviation (SD)

Viscosity measurements were conducted for Celugel and samples S1–S10. The mean viscosity value for Celugel was recorded at 548.57 mPa·s. For formulation S1, a slightly higher viscosity of 562.44 mPa·s was observed. Subsequent samples exhibited a decreasing trend in viscosity with a reduction in the percentage of the finished substrate within the formulation. Notably, hydrogel S8 displayed a viscosity value that exceeded those of hydrogels S7 and S9.

Surface tension values were also measured for Celugel and the S1–S10 formulations derived from it. The surface tension for Celugel alone was determined to be 60.71 mN/m, while for formulation S1, it was 62.73 mN/m. Surface tension values for hydrogels S2–S9 demonstrated a decreasing trend, ranging from 66.47 mN/m to 62.83 mN/m. Conversely, formulation S10 exhibited a surface tension value of 71.68 mN/m.

Discussion

We demonstrated the varied impacts of hydrogel formulation composition, specifically those based on Celugel, on osmotic pressure and selected rheological properties.

Hydrogels were prepared with commercial Celugel, differing in water content and supplemented with a 5 wt% sucrose concentration.

Results reveal a marked influence of formulation composition on osmotic pressure. Nearly all hydrogels showed hyperosmotic values compared to physiological levels, which are typically in the range of range 275–295 mOsm/kg H_2O; however, formulation S10 exhibited osmotic pressure below physiological thresholds.[10–12] Commercial nasal preparations vary widely in osmotic pressure, from approx. 300 mOsm/kg H_2O to as high as 700 mOsm/kg H_2O. Hyperosmotic solutions may induce nasal mucosal irritation, triggering an increase in watery secretion, thereby reducing congestion and swelling of nasal tissue. Nonetheless, prolonged exposure to hypertonic formulations may damage the mucosal membrane, leading to discomfort, burning sensation or irritation, indicating limited suitability for long-term use.[7,13]

In formulations S1–S10, an incremental rise in osmotic pressure was observed in correlation with increased Celugel concentration. Sucrose, given its water solubility, also contributes osmotic activity, thereby elevating the osmotic pressure within the gel matrix.[14]

The pH values for formulations S1–S9 demonstrated notable stability, with a maximum variance of 0.9 units. Formulation S10, a 5 wt% sucrose solution, had a slightly acidic pH of 6.4, likely due to microbial degradation of sucrose into acidic byproducts, as this formulation lacked a preservative.

The pH level of a formulation significantly affects the absorption of active ingredients through the nasal mucosa. For nasal applications, a pH range of 4.5–6.5 is generally optimal, enhancing the stability of light-sensitive compounds, supporting lysozyme activity for microbial control, and inhibiting viral replication. Although most studied formulations displayed pH values slightly above the recommended range, their potential application remains viable.[15]

Viscosity measurements confirmed an expected increase in viscosity with higher Celugel content, supporting the suitability of Celugel as a viscosity-enhancing agent in formulations, including nasal drops. Results also affirm the low viscosity of the base itself, which declines further upon dilution.

Surface tension in the hydrogels was measured to be lower than that of water. Hydroxyethyl cellulose, classified as a non-ionic amphiphilic molecule, decreases surface tension by disrupting the hydrogen bonding within water molecules that are bound within the hydrogel matrix.[16]

Analysis of viscosity and surface tension values revealed a shift in trends beginning with formulation S7, as depicted in Fig. 2. This is likely due to reaching or nearing the critical micelle concentration (CMC) of HEC, which exhibits surfactant properties. At the CMC, the surface tension reaches a minimum, after which further concentration increases lead to a rise in surface tension, likely due to greater cohesion among polymer chains. The observed micelle formation suggests that beyond CMC, intermolecular forces within the polymer network intensify, impacting both viscosity and surface properties.[17,18]

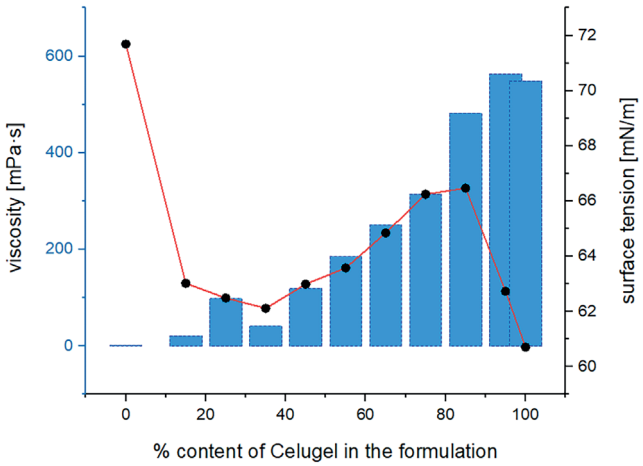

Fig. 2. Summary of the values obtained for the viscosity and the surface tension of the hydrogels tested

Conclusions

These findings provide insight into the physicochemical properties and potential therapeutic applications of Celugel-based hydrogels, informing their formulation for targeted biomedical applications. Based on them, several key conclusions can be drawn regarding Celugel-based hydrogel formulations. The formulation's composition plays a crucial role in determining its rheological properties, which directly impacts its behavior and stability. Among the various components, the concentration of the gelling agent stands out as the primary factor affecting these properties, indicating its central role in defining the overall characteristics of the hydrogel. Furthermore, the results confirm that Celugel is a suitable candidate for formulations intended for nasal administration, suggesting its potential for effective use in targeted delivery systems through this route.

ORCID iDs

Monika Gasztych https://orcid.org/0000-0002-4868-8727
Natalia Jurczak https://orcid.org/0009-0007-6943-5781

References

1. Garg T, Rath G, Goyal AK. Comprehensive review on additives of topical dosage forms for drug delivery. *Drug Deliv*. 2015;22(8):969–987. doi:10.3109/10717544.2013.879355
2. Urząd Rejestracji Produktów Leczniczych, Wyrobów Medycznych i Produktów Biobójczych. *Farmakopea Polska. T. 1*. 12th ed. Warsaw, Poland: Wydawnictwo Dragon; 2020. ISBN:978-83-8172-541-5.
3. Buwalda SJ, Boere KWM, Dijkstra PJ, Feijen J, Vermonden T, Hennink WE. Hydrogels in a historical perspective: From simple networks to smart materials. *J Control Release*. 2014;190:254–273. doi:10.1016/j.jconrel.2014.03.052
4. Peppas N, Bures P, Leobandung W, Ichikawa H. Hydrogels in pharmaceutical formulations. *Eur J Pharm Biopharm*. 2000;50(1):27–46. doi:10.1016/S0939-6411(00)00090-4

5. Von Zuben EDS, Eloy JO, Inácio MD, et al. Hydroxyethylcellulose-based hydrogels containing liposomes functionalized with cell-penetrating peptides for nasal delivery of insulin in the treatment of diabetes. *Pharmaceutics*. 2022;14(11):2492. doi:10.3390/pharmaceutics14112492
6. Jucha W, Pandyra-Kowalska B. The use of the new base gel in Hospital Recipe's practice [in Polish]. *Farm Pol*. 2020;76(7):407–412. doi:10.32383/farmpol/126991
7. Banyś K, Kańka P. Wpływ właściwości fizykochemicznych aerozoli do nosa na ich skuteczność i bezpieczeństwo. *Medycyna po Dyplomie*. 2019;11:[no pages given]. https://podyplomie.pl/medycyna/33544,wplyw-wlasciwosci-fizykochemicznych-aerozoli-do-nosa-na-ich-skutecznosc-i-bezpieczenstwo?srsltid=AfmBOoqUzmqnYwlgGfcitnXnjQUUT1UjuGjSpu5MfSPr0RTLRVfE9teP. Accessed August 15, 2024.
8. Laffleur F, Keckeis V. Advances in drug delivery systems: Work in progress still needed? *Int J Pharm*. 2020;590:119912. doi:10.1016/j.ijpharm.2020.119912
9. Urząd Rejestracji Produktów Leczniczych, Wyrobów Medycznych i Produktów Biobójczych. *Farmakopea Polska. T. 3*. 12th ed. Warsaw, Poland: Wydawnictwo Dragon; 2020. ISBN:978-83-8172-543-9.
10. Lord RCC. Osmosis, osmometry, and osmoregulation. *Postgrad Med J*. 1999;75(880):67–73. doi:10.1136/pgmj.75.880.67
11. Vujovic P, Chirillo M, Silverthorn DU. Learning (by) osmosis: An approach to teaching osmolarity and tonicity. *Adv Physiol Educ*. 2018;42(4):626–635. doi:10.1152/advan.00094.2018
12. Nakajima T, Hoshino K ichi, Guo H, Kurokawa T, Gong JP. Experimental verification of the balance between elastic pressure and ionic osmotic pressure of highly swollen charged gels. *Gels*. 2021;7(2):39. doi:10.3390/gels7020039
13. Bergmann C, Müller K, Thieme U, et al. Real-world data on the use of hypertonic saline nasal spray in ENT practice. *SN Compr Clin Med*. 2019;1(5):354–361. doi:10.1007/s42399-019-0050-y
14. Almoshari Y. Osmotic pump drug delivery systems: A comprehensive review. *Pharmaceuticals (Basel)*. 2022;15(11):1430. doi:10.3390/ph15111430
15. Kulkarni V, Shaw C. Formulation and characterization of nasal sprays. *Inhalation*. 2012;6:10–15. https://www.inhalationmag.com/wp-content/uploads/pdf/inh_20120601_0010.pdf. Accessed August 15, 2024.
16. Noreen A, Zia KM, Tabasum S, Khalid S, Shareef R. A review on grafting of hydroxyethylcellulose for versatile applications. *Int J Biol Macromol*. 2020;150:289–303. doi:10.1016/j.ijbiomac.2020.01.265
17. Wang T, Zhao X, Yang H, Qi Y. On the roles of HEC in Pechini sol-gel method: Enhancement of stability, wettability of the sol and surface roughness of Bi2212 film. *Ceram Int*. 2018;44(11):12144–12148. doi:10.1016/j.ceramint.2018.03.258
18. Esmaeili H, Mousavi SM, Hashemi SA, Lai CW, Chiang WH, Bahrani S. Application of biosurfactants in the removal of oil from emulsion. In: *Green Sustainable Process for Chemical and Environmental Engineering and Science*. Amsterdam, the Netherlands–New York, USA: Elsevier; 2021:107–127. doi:10.1016/B978-0-12-822696-4.00008-5

Interaction of meloxicam derivatives with phosphatidylcholine bilayers: A calorimetric study

Oddziaływanie pochodnych meloksykamu z dwuwarstwami fosfatydylocholiny: badania kalorymetryczne

Jadwiga Maniewska[A–F], Berenika Marta Szczęśniak-Sięga[C,E]

Department of Medicinal Chemistry, Wroclaw Medical University, Poland

A – research concept and design; B – collection and/or assembly of data; C – data analysis and interpretation;
D – writing the article; E – critical revision of the article; F – final approval of the article

Polymers in Medicine, ISSN 0370-0747 (print), ISSN 2451-2699 (online) *Polim Med*. 2024;54(2):149–153

Address for correspondence
Jadwiga Maniewska
E-mail: jadwiga.maniewska@umw.edu.pl

Funding sources
This research was funded by the Ministry of Health subvention according to the number SUBK.D070.24.067 from the IT Simple System of Wroclaw Medical University, Poland.

Conflict of interest
None declared

Received on November 15, 2024
Reviewed on November 20, 2024
Accepted on November 20, 2024

Published online on November 28, 2024

Abstract

Background. The drug interactions with the lipid membranes are crucial in many biochemical processes. Phospholipid model membranes are often used to assess such interactions. Our team has been researching new compounds with anti-inflammatory and analgesic effects for many years. Such compounds are derivatives of the well-known non-steroidal anti-inflammatory drug (NSAID) – meloxicam (MLX). Their biological target is cyclooxygenase (COX) – a membrane protein. The NSAIDs are mainly taken orally; therefore, drug–membrane interaction is a preliminary stage in the body.

Objectives. The purpose of the present work was to investigate the ability of 2 new MLX derivatives (compound PR51 and PR52) to interact with model membranes, in comparison to known NSAIDs medicine – MLX. The differential scanning calorimetry (DSC) method was used to study those interactions. As a model membrane, bilayers obtained from a phospholipid (1,2-dipalmitoyl-sn-glycero-3-phosphatidylcholine (DPPC)) were used.

Materials and methods. Calorimetric measurements were performed using a differential scanning calorimeter DSC 214 Polyma equipped with an intracooler IC70.

Results. All examined compounds decreased the main transition temperature of DPPC in a concentration-dependent manner. The addition of studied compounds to DPPC also resulted in broadening of the transition peaks. Moreover, all examined compounds decreased the enthalpy of the DPPC main phase transition. For all DPPC gel–liquid crystalline phase transition parameters, the most pronounced effects were found for PR51 compound.

Conclusions. We have shown that the above interactions depend on the chemical structure of individual compound. All studied compounds alter biophysical properties of phospholipid bilayer.

Key words: meloxicam, DSC, model membranes, drug–membrane interaction, benzothiazine derivatives

Cite as
Maniewska J, Szczęśniak-Sięga BM. Interaction of meloxicam derivatives with phosphatidylcholine bilayers: A calorimetric study. *Polim Med*. 2024;54(2):149–153. doi:10.17219/pim/196220

DOI
10.17219/pim/196220

Streszczenie

Wprowadzenie. Interakcje leków z błonami lipidowymi mają kluczowe znaczenie w wielu procesach biochemicznych. Błony modelowe fosfolipidów są często wykorzystywane do badania takich oddziaływań. Nasz zespół od wielu lat prowadzi badania nad nowymi związkami o działaniu przeciwzapalnym i przeciwbólowym; są to pochodne znanego niesteroidowego leku przeciwzapalnego (NLPZ) – meloksykamu. Ich celem biologicznym jest cyklooksygenaza (COX) – białko błonowe. NLPZ są przyjmowane głównie doustnie, dlatego interakcja lek–błona jest wstępnym etapem losu leku w organizmie.

Cel pracy. Celem niniejszej pracy było zbadanie zdolności dwóch nowych pochodnych meloksykamu (związku PR51 i PR52) w porównaniu ze znanym lekiem z grupy NLPZ – meloksykamem, do interakcji z błonami modelowymi. Do zbadania tych oddziaływań wykorzystano metodę różnicowej kalorymetrii skaningowej (DSC). Jako błonę modelową wykorzystano dwuwarstwy, otrzymane z fosfolipidu – 1,2-dipalmitoilo-sn-glicero-3-fosfatydylocholiny (DPPC).

Materiały i metody. W niniejszej pracy opisano wyniki badań kalorymetrycznych 2 nowych analogów meloksykamu (jak również samego meloksykamu) na przemiany fazowe dwuwarstw fosfolipidowych otrzymanych z DPPC. Pomiary kalorymetryczne wykonano przy użyciu różnicowego kalorymetru skaningowego DSC 214 Polyma wyposażonego w chłodnicę wewnętrzną IC70.

Wyniki. Wszystkie badane związki obniżały temperaturę głównej przemiany fazowej DPPC w sposób zależny od stężenia. Dodanie badanych związków do DPPC skutkowało również poszerzeniem pików przemiany. Ponadto wszystkie badane związki obniżyły entalpię głównej przemiany fazowej DPPC. W przypadku wszystkich parametrów przemiany fazowej ze struktury żelu w strukturę ciekło-krystaliczną DPPC najwyraźniejsze efekty stwierdzono dla związku PR51.

Wnioski. W niniejszej pracy wykorzystano metodę DSC do zbadania oddziaływań meloksykamu i jego dwóch pochodnych z dwuwarstwami fosfolipidowymi DPPC. Wykazaliśmy, że oddziaływania te zależą od budowy chemicznej poszczególnych związków. Można stwierdzić, że wszystkie badane związki zmieniają właściwości biofizyczne dwuwarstw fosfolipidowych.

Słowa kluczowe: DSC, meloksykam, pochodne benzotiazyny, oddziaływania lek–błona, modelowe błony

Background

The drug interactions with the lipid membranes is an important issue in numerous biochemical processes.[1] Phospholipid model membranes are often applied as barriers which enable assessment of selected interactions.[2] The polymer science focuses on the molecular structures which are developed from repeating monomer elements. A similar scheme may be observed in the phospholipids molecules, although the carbon chains in their structure are classified as hydrocarbon molecules.[3]

Drug interactions with natural membranes are important factors for revealing molecular mechanism of action of active pharmaceutical ingredients (APIs), as well as their pharmacokinetics.[4] Some of the most commonly used drugs are painkillers, which also have anti-inflammatory effects. The typical pharmacological activity of nonsteroidal anti-inflammatory and analgesic drugs (NSAIDs) is a result of blocked activity of cyclooxygenase (COX). This enzyme is anchored in the endoplasmic reticulum (ER) and microsome membrane. It affects and enables the biosynthesis of molecules engaged in inflammatory state: prostanoids – i.a., thromboxane, as well as prostaglandins, including prostacyclin (i.e., derivatives of arachidonic acid).[5] Because of the very frequent use of painkillers in many patients globally, their side effects such as gastro- and nephrotoxicity or allergic reactions are very well known; therefore, there is an urgent need to search for new, safer drugs with such effects.

Our team has been researching new compounds with anti-inflammatory and analgesic effects for many years. In chemical terms, they are derivatives of the well-known NSAID – meloxicam (MLX). In addition to the study of mechanism, toxicity and pharmacokinetics, new compounds are also tested for interactions with model membranes.

Lichtenberger et al. conducted experiments using a membrane made of mixture of phospholipid (1,2-dipalmitoyl-sn-glycero-3-phosphatidylcholine (DPPC)) and NSAIDs – diclofenac, indomethacin, naproxen, and salicylic acid derivatives were embedded into lipid matrix. The obtained results indicated that these drugs interact with non-charged phospholipids contained in the mucosa of stomach and intestines by forming complexes with them. Such an interaction promotes the gastrotoxic effects due to the reduction of the lipophilic nature of the protective mucosa and an increase of its susceptibility to damage.[6]

Chakraborty and Sarkar investigated the interactions of 2 oxicams with liposomes obtained from DMPC (dimyristoylphosphatidylcholine) and DMPG (dimyristoyl-L-α-phosphatidyl-DL-glycerol). The DMPC is classified as a lipid with zwitterionic properties – the polar group is relatively large, whereas DMPG with its anionic phosphoryl group has a smaller headgroup size.[7] They demonstrated that partitioning of drug molecules of different dipole moment may be directed by specific properties of the membrane, including lipid spatial layout, which all may influence hydrophobicity of the lipid bilayer, even when the direct electrostatic interactions are negligible.[7] Their research confirms that the interactions between drugs and the lipid bilayer need to be studied experimentally, and in silico predictions resulting from knowledge of partition coefficient value of compounds are not sufficient.

Lucio et al. showed that the NSAIDs they tested (acemetacin, indomethacin and nimesulide) influenced the phase transition temperature. Both the main phase transition and the initial phase transition temperature as well as the enthalpy value of the process in the lipid membrane were affected in this study. The strongest effect was observed for acemetacin and indomethacin, which was probably related to their good penetration of the bilayer. Moreover, it was concluded that this effect may have a negative impact to the gastrointestinal mucosa, which is associated with the occurrence of side effects of these medicines.[8]

The thermal effects of selected oxicam derivatives with anti-inflammatory activity, i.e., lornoxicam, MLX, piroxicam, and tenoxicam, were evaluated by Kyrikou et al. using the differential scanning calorimetry (DSC) method. The examined derivatives were immersed in the membrane bilayer based on DPPC.[9] The perturbing effect of the drugs exerted on DPPC bilayers resulted in a decrease of the major phase transition temperature and in widened peak of the temperature of phase transition temperature, whereas the initial phase transition temperature vanished.

Results of all the above studies show that understanding the interaction of NSAIDs with model membranes may reveal more detailed view of mechanisms of biological activity, as well as of possible adverse effects, including the common gastrotoxicity.

Objectives

In this paper, we present the interactions of 2 new MLX derivatives with model biological membranes prepared in our laboratory (Fig. 1). The aim was to investigate the ability of 2 new MLX derivatives (PR51 and PR52) to interact with artificial membranes compared to a known NSAID – MLX, using thermal analysis (namely – the DSC). As a model membrane, bilayers obtained from DPPC were used.

Materials and methods

The DPPC and Tris-EDTA buffer solution (pH 7.4) were purchased from Merck Life Science (Darmstadt, Germany), and applied as non-purified marketed components. Meloxicam was obtained from Thermo Fisher Scientific (Haverhill, USA).

PR51 and PR52 (MLX derivatives) were synthesized at our laboratory. Their purity was confirmed with elemental analysis (C, H, N) together with ^{1}H NMR, ^{13}C NMR, FT-IR, and high-resolution mass spectrometry (HRMS). The synthesis and analysis results of PR51 and PR52 was described elsewhere.[10] The chemical structure of the tested oxicam derivatives is presented in Table 1.

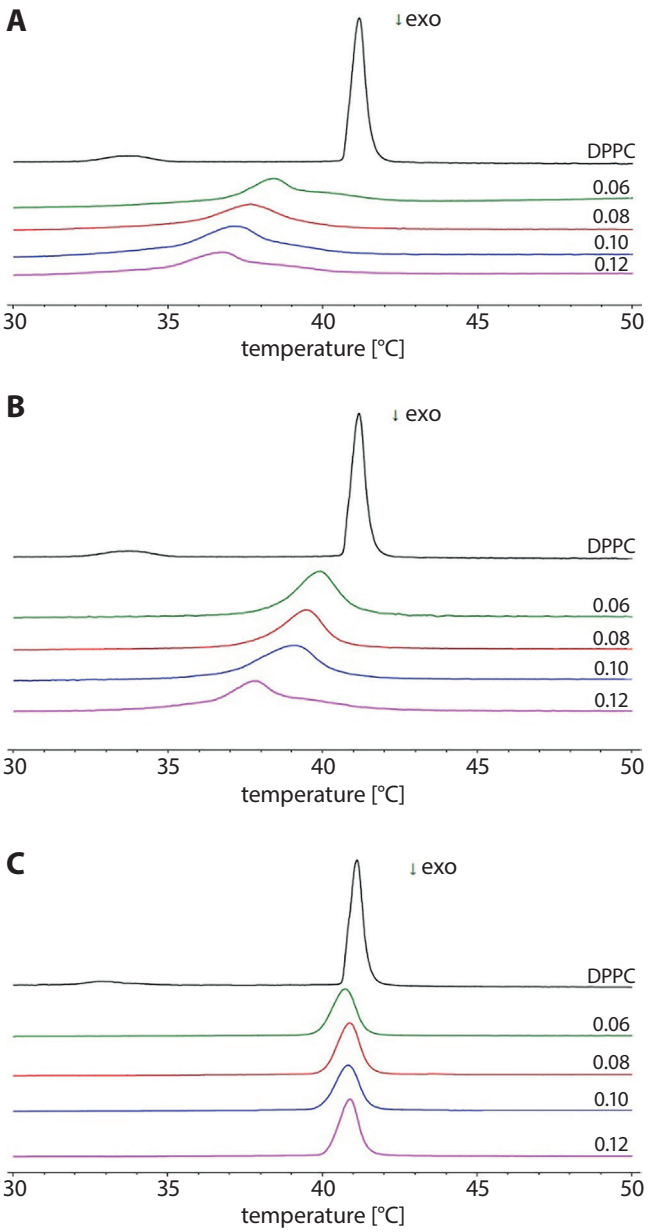

Fig. 1. The exemplary thermograms obtained for DPPC (1,2-dipalmitoyl-sn-glycero-3-phosphatidylcholine) mixed with compounds: (A) PR51, (B) PR52 and (C) meloxicam (MLX), and for pure lipid (the 1st curve from the top); curves represent the thermograms obtained for different compound–lipid molar ratios (from the top to the bottom: 0, 0.06, 0.08, 0.1, 0.12); the exothermic direction in this graph is downward

The differential scanning calorimeter DSC 214 Polyma (Netzsch GmbH & Co., Selb, Germany) equipped with an Intracooler IC70 was used to perform the calorimetric measurements. They were carried out in the Laboratory of Elemental Analysis and Structural Research at the Faculty of Pharmacy of Wroclaw Medical University (Poland). The method of samples preparation for calorimetric measurements has been described previously.[11] The DSC measurements were performed using the heat-flow measurement method, in a nitrogen dynamic atmosphere (25 mL/min), at a heating rate of 1°C/min (over a temperature range of 30–50°C). Measurement data were analyzed

Table 1. Chemical structure of the studied compounds

symbol	compound
PR51	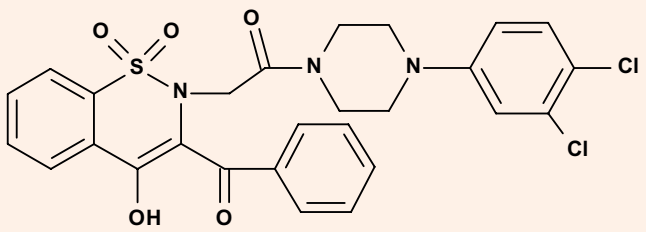
PR52	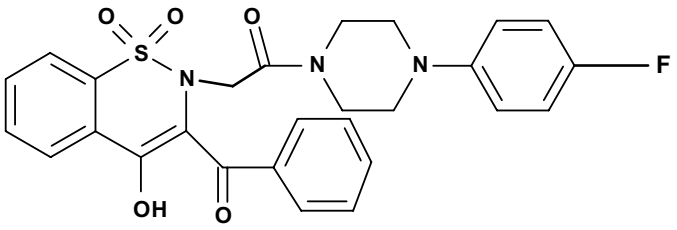
MLX	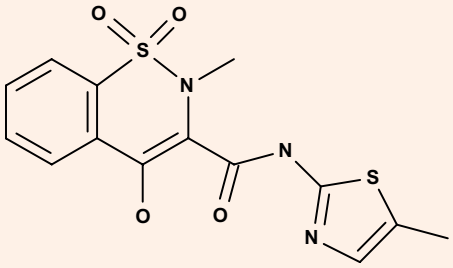

offline (Netzsch Proteus® 7.1.0 analysis software; Netzsch GmbH & Co.). The measured heat was normalized per gram of DPPC. The enthalpies of phospholipid main phase transition were stated in [J/g].

Results and Discussion

Our team used DSC method, which show how the studied compounds perturb the phospholipid thermal behavior.[12,13]

The impact of the studied additives on the phase transition profile of DPPC is presented in Fig. 1. It shows the exemplary thermograms of lipid in the presence of increasing amounts of PR51, PR52 and a well-known drug from the group of NSAIDs – MLX. The perturbing effect of the studied compounds exerted on phospholipid bilayers resulted in concentration-dependent decrease of the main phase transition temperature and in widening of the peak of the phase transition temperature, whereas the pre-transition vanished (Fig. 1A–C, respectively). Compounds PR51 and PR52 had a greater perturbing impact on the phase transition profile of the DPPC than MLX (Fig. 1C). In DPPC membranes doped with PR51, the asymmetry of the calorimetric peaks was also observed (Fig. 1A), which may suggest phase separation within a phospholipid bilayer.

The influence of PR51, PR52 and MLX on phospholipid gel-liquid crystalline phase transition parameters – temperature (T_m), the transition peak half-height width ($\Delta T_{½}$) and enthalpy (ΔH) – are shown in Fig. 2. The addition of studied compounds to the DPPC multi-lamellar structures increased the main transition peak half-height width (Fig. 2B). It also caused concentration dependent lowering of the T_m values (Fig. 2B). The addition of compound PR51 perturbed the DPPC phase transition profiles most effectively.

Our results are consistent with those of other teams that investigated the effects of NSAIDs on model phospholipid membranes.[9] However, our studies showed that compounds PR51 and PR52 have a more pronounced effect on altering the phospholipid bilayer obtained from DPPC than MLX.

Limitations

In biological systems, interactions of medicines with biological membranes (which are very complex systems) may be complicated processes. For this reason, simplified models of cell membranes (e.g., phospholipid mono- and bilayers and liposomes) are used to study such processes.[14] However, the use of a membrane model, which is a phospholipid bilayer made of the model phospholipid (DPPC) in a buffer solution, is a limitation of this study, because it is a simplification of the biological membrane.

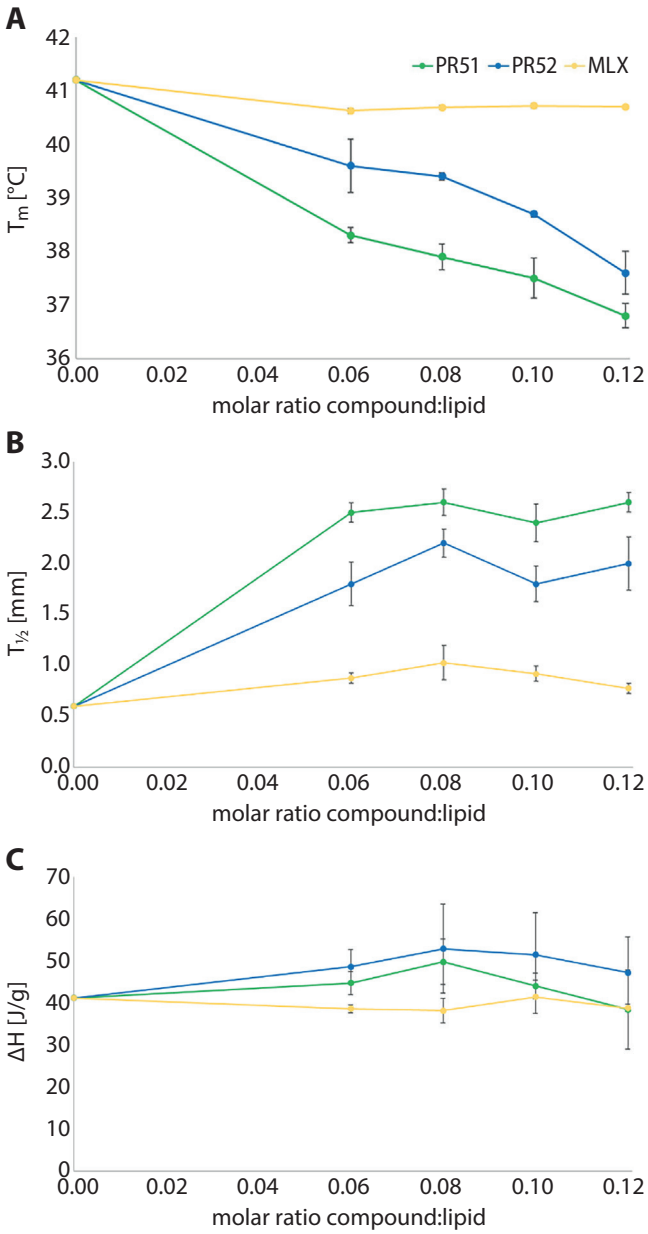

Fig. 2. Influence of studied compounds on the parameters of DPPC (1,2-dipalmitoyl-sn-glycero-3-phosphatidylcholine) main phase transition: temperature T_m (A), peak half-width $\Delta T_{½}$ (B) and phase transition enthalpy ΔH (C) (mean ± standard deviation (SD), n = 8)

Conclusions

In present work, DSC method was applied to investigate the interactions of MLX derivatives with phospholipid bilayers. The results revealed that oxicam analogues interact with model membranes obtained from DPPC. Compounds PR51 and PR52 influenced phospholipid gel–liquid crystalline phase transition parameters to a greater extent than MLX, and the effect was more pronounced for PR51, (the green curve in Fig. 2), lowered the temperature of the main phase transition of DPPC the most and increased the half-width of the transition peaks (so broadened them) the most, so it also perturbed the main phase transition of the model membrane the most. That is why we may conclude that the presence of 2 chlorine substituents in MLX derivative benzene ring of side chain of the compound (PR51) seems to enhance the interaction with phospholipid bilayers, compared to the presence of only 1 fluorine substituent in the compound benzene ring of its side chain (PR52). Compound PR51 may also induce lateral DPPC phase separation in studied model membranes, probably due to the appearance of compound-rich or -poor microdomains in the lipid bilayer.

ORCID iDs

Jadwiga Maniewska https://orcid.org/0000-0003-3201-4661
Berenika Marta Szczęśniak-Sięga https://orcid.org/0000-0003-3770-5760

References

1. Seddon AM, Casey D, Law RV, Gee A, Templer RH, Ces O. Drug interactions with lipid membranes. *Chem Soc Rev*. 2009;38(9):2509. doi:10.1039/b813853m
2. Sharma B, Moghimianavval H, Hwang SW, Liu AP. Synthetic cell as a platform for understanding membrane-membrane interactions. *Membranes (Basel)*. 2021;11(12):912. doi:10.3390/membranes11120912
3. Smith BC. The infrared spectra of polymers III: Hydrocarbon polymers. *Spectroscopy*. 2021;11:22–25. doi:10.56530/spectroscopy.mh7872q7
4. Lucio M, Lima JLFC, Reis S. Drug–membrane interactions: Significance for medicinal chemistry. *Curr Med Chem*. 2010;17(17):1795–1809. doi:10.2174/092986710791111233
5. Mbonye UR, Wada M, Rieke CJ, Tang HY, DeWitt DL, Smith WL. The 19-amino acid cassette of cyclooxygenase-2 mediates entry of the protein into the endoplasmic reticulum-associated degradation system. *J Biol Chem*. 2006;281(47):35770–35778. doi:10.1074/jbc.M608281200
6. Lichtenberger LM, Wang ZM, Romero JJ, et al. Non-steroidal anti-inflammatory drugs (NSAIDs) associate with zwitterionic phospholipids: Insight into the mechanism and reversal of NSAID-induced gastrointestinal injury. *Nat Med*. 1995;1(2):154–158. doi:10.1038/nm0295-154
7. Chakraborty H, Sarkar M. Interaction of piroxicam and meloxicam with DMPG/DMPC mixed vesicles: Anomalous partitioning behavior. *Biophys Chem*. 2007;125(2–3):306–313. doi:10.1016/j.bpc.2006.09.002
8. Lúcio M, Bringezu F, Reis S, Lima JLFC, Brezesinski G. Binding of non-steroidal anti-inflammatory drugs to DPPC: Structure and thermodynamic aspects. *Langmuir*. 2008;24(8):4132–4139. doi:10.1021/la703584s
9. Kyrikou I, Hadjikakou SK, Kovala-Demertzi D, Viras K, Mavromoustakos T. Effects of non-steroid anti-inflammatory drugs in membrane bilayers. *Chem Phys Lipids*. 2004;132(2):157–169. doi:10.1016/j.chemphyslip.2004.06.005
10. Szczęśniak-Sięga BM, Zaręba N, Czyżnikowska Ż, Janek T, Kepinska M. Rational design, synthesis, molecular docking, and biological evaluations of new phenylpiperazine derivatives of 1,2-benzothiazine as potential anticancer agents. *Molecules*. 2024;29(18):4282. doi:10.3390/molecules29184282
11. Maniewska J, Gąsiorowska J, Czyżnikowska Ż, Michalak K, Szczęśniak-Sięga BM. New meloxicam derivatives: Synthesis and interaction with phospholipid bilayers measured by differential scanning calorimetry and fluorescence spectroscopy. *Membranes (Basel)*. 2023;13(4):416. doi:10.3390/membranes13040416
12. Jain MK, Wu NM. Effect of small molecules on the dipalmitoyl lecithin liposomal bilayer: III. Phase transition in lipid bilayer. *J Membrain Biol*. 1977;34(1):157–201. doi:10.1007/BF01870299
13. Zambrano P, Manrique-Moreno M, Petit K, et al. Differential scanning calorimetry in drug–membrane interactions. *Biochem Biophys Res Commun*. 2024;709:149806. doi:10.1016/j.bbrc.2024.149806
14. Knobloch J, Suhendro DK, Zieleniecki JL, Shapter JG, Köper I. Membrane–drug interactions studied using model membrane systems. *Saudi J Biol Sci*. 2015;22(6):714–718. doi:10.1016/j.sjbs.2015.03.007

Anti-acne preparations containing tetracycline, azelaic acid and azeloglycine: Optimization of stability and physicochemical properties

Preparaty przeciwtrądzikowe zawierające tetracyklinę, kwas azelainowy i azeloglicynę: optymalizacja stabilności i właściwości fizykochemicznych

Agnieszka Kostrzębska[A–F], Gabriela Szczepaniak[B–D]

Department of Physical Chemistry and Biophysics, Faculty of Pharmacy, Wroclaw Medical University, Poland

A – research concept and design; B – collection and/or assembly of data; C – data analysis and interpretation;
D – writing the article; E – critical revision of the article; F – final approval of the article

Polymers in Medicine, ISSN 0370-0747 (print), ISSN 2451-2699 (online) *Polim Med*. 2024;54(2):155–159

Address for correspondence
Agnieszka Kostrzębska
E-mail: agnieszka.kostrzebska@umw.edu.pl

Funding sources
None declared

Conflict of interest
None declared

Acknowledgements
The research was done in collaboration with the K130 Student Scientific Association in the Department of Physical Chemistry and Biophysics. We would like to express our sincere gratitude to Professor Witold Musiał for his invaluable help and substantial support.

Received on November 15, 2024
Reviewed on November 19, 2024
Accepted on November 20, 2024

Published online on December 3, 2024

Cite as
Kostrzębska A, Szczepaniak G. Anti-acne preparations containing tetracycline, azelaic acid and azeloglycine: Optimization of stability and physicochemical properties. *Polim Med*. 2024;54(2):155–159. doi:10.17219/pim/196256

DOI
10.17219/pim/196256

Abstract

Background. Acne vulgaris is a common inflammatory skin condition affecting almost 85% of the adolescent and young adult population. The etiopathogenesis of this dermatosis involves an imbalance in the skin microbiome, leading to inflammation of both the skin and hair follicles.

Objectives. The aim of this study was to develop topical anti-acne formulations with increased therapeutic efficacy and reduced risk of developing antibiotic resistance. Six hydrogel formulations containing azelaic acid or its derivative, azeloglycine, in combination with tetracycline hydrochloride were prepared as part of the study.

Materials and methods. The investigated formulations were prepared using an Eprus U500 pharmaceutical mixer and the pH was determined using an ERH-11S electrode designed for dense substances and a CPC-505 Elmetron pH-meter. The formulations were analyzed for tetracycline stability in the presence of additional active ingredients and varying pH over a period of 35 days using high-performance liquid chromatography (HPLC). In addition, the effects of azeloglycine and azelaic acid on the viscosity of the prepared formulations were evaluated using a Brookfield DV2T rotational viscometer.

Results. Chromatographic analysis showed significant stability of tetracycline in most formulations, with azeloglycine-containing formulations showing less degradation of the antibiotic than azelaic acid-containing preparations. In addition, azeloglycine-containing gels exhibited more favorable rheological properties, which may facilitate better application and be more beneficial to patients.

Conclusions. The results suggest that formulations containing azeloglycine and tetracycline may be a promising strategy for acne therapy, offering increased tetracycline stability and an optimal rheological profile, which may result in prolonged therapeutic effect and more effective drug delivery to the skin.

Key words: stability, azelaic acid, tetracycline, potassium azeloyl diglycinate, azeloglycine

Streszczenie

Wprowadzenie. Trądzik pospolity to powszechna zapalna choroba skóry, dotykająca blisko 85% populacji nastoletniej i młodych dorosłych. Etiopatogeneza tej dermatozy obejmuje zaburzenie równowagi mikrobiomu skóry, prowadzące do stanów zapalnych zarówno w obrębie skóry, jak i mieszków włosowych.

Cel pracy. Celem niniejszego badania było opracowanie miejscowych preparatów przeciwtrądzikowych o udoskonalonej efektywności terapeutycznej oraz zredukowanym ryzyku rozwoju oporności na antybiotyki. W ramach badań przygotowano sześć hydrożelowych formulacji, zawierających kwas azelainowy lub jego pochodną — azeloglicynę, w połączeniu z chlorowodorkiem tetracykliny.

Materiały i metody. Badane preparaty otrzymano przy użyciu miksera farmaceutycznego Eprus U500, wartość pH wyznaczono przy użyciu elektrody ERH-11S przeznaczonej do substancji gęstych oraz pH-metru CPC-505 firmy Elmetron. Formulacje analizowano pod kątem stabilności tetracykliny w obecności dodatkowych składników aktywnych oraz zmiennego pH przez okres 35 dni przy użyciu wysokosprawnej chromatografii cieczowej HPLC. Ponadto, oceniano wpływ azeloglicyny oraz kwasu azelainowego na lepkość przygotowanych preparatów przy użyciu wiskozymetru rotacyjnego Brookfield DV2T.

Wyniki. Analiza chromatograficzna wykazała znaczną stabilność tetracykliny w większości formulacji, przy czym preparaty zawierające azeloglicynę cechowały się mniejszą degradacją antybiotyku w porównaniu do formulacji z kwasem azelainowym. Ponadto, żele z azeloglicyną wykazały korzystniejsze właściwości reologiczne, co może sprzyjać lepszej aplikacji i być korzystniejsze w użyciu dla pacjentów.

Wnioski. Uzyskane wyniki sugerują, że preparaty zawierające azeloglicynę i tetracyklinę mogą stanowić obiecującą strategię w terapii trądziku, oferując zwiększoną stabilność tetracykliny oraz optymalny profil reologiczny, co może przekładać się na przedłużone działanie terapeutyczne i efektywniejsze dostarczanie substancji aktywnych do skóry.

Słowa kluczowe: kwas azelainowy, stabilność, azeloglicyna, diglicynian azeloilu potasu, tetracyklina

Background

Acne vulgaris, a common inflammatory skin condition, affects nearly 85% of the adolescent and young adult population.[1,2] This dermatosis is associated with an overgrowth of the skin microbiome, including *Cutibacterium acnes*, as well as increased skin sebum secretion, increased keratinization of the sebaceous gland orifices and the development of local inflammation.[3–5] Topical therapy is used for mild to moderate forms of acne, with satisfactory results in more than half of patients.[6,7] In the present study, an attempt was made to develop anti-acne formulations with multidirectional topical activity. The key formulation ingredients to inhibit pathogenic microorganisms are tetracycline hydrochloride and azelaic acid or potassium azeloyl diglycinate, called azeloglycine. This combination aims to increase the efficacy of topical therapy while reducing the risk of developing antibiotic resistance.[8–11]

Materials and methods

Tetracycline hydrochloride (Merck Life Science Sp. z o.o., Poznań, Poland), 2-amino-2-methyl-1,3-propanediol (AMPD; Merck Life Science Sp. z o.o.), Carbopol 980 NF – polyacrylic acid crosslinked with allyl pentaerythritol (Lubrizol, Wickliffe, USA), ethanol (Stanlab, Lublin, Poland), potassium azeloyl diglycinate (azeloglycine), sol (Zrób Sobie Krem, Prochowice, Poland), azelaic acid (PolAura, Morąg, Poland), and demineralized, bi-distilled water were used to prepare the formulations. Acetonitrile (Merck Life Science Sp. z o.o.), formic acid (Merck Life Science Sp. z o.o.) and demineralized, bi-distilled water were used in the high-performance liquid chromatography (HPLC) analysis.

Six hydrogels were prepared, differing in the type of active ingredient. Three hydrogels (designated 1KA, 2KA and 3KA) contained azelaic acid at concentrations of 1%, 2% and 3%, while the other 3 (1A, 2A and 3A) contained azeloglycine at analogous concentrations. All hydrogels contained the same tetracycline content of 0.2%. The Carbopol content of the formulations was constant and homogeneous for all gels. The concentration of AMPD was uniform in all groups of formulations, but was higher in gels containing azelaic acid than in gels containing azeloglycine due to the acidic nature of this ingredient. All formulations also contained the same amount of ethanol, which acted as a co-solvent. The detailed composition is summarized in Table 1.

The formulations were obtained by homogenization for 16 min using an Eprus U500 pharmaceutical mixer (Eprus, Bielsko-Biała, Poland) at 630 rpm to obtain optimal dispersion of the active ingredient. The developed gels were stored at 3°C in opaque containers protected from light throughout the study.

The pH of all hydrogels was measured using an ERH-11S pH electrode (Elmetron, Zabrze, Poland), designed for the analysis of highly viscous materials, and a CPC-505 pH meter (Elmetron). Five pH measurements were made for each of the hydrogels tested.

Viscosity measurements of all formulations were performed using a Brookfield DV2T rotational viscometer (Ametek, Middleborough, USA) with spindle number 6. The viscosity of each formulation was measured

Table 1. Compositions of the analyzed formulations

Formulation	TC [g]	Azelaic acid [g]	Azeloglycine [g]	Ethanol [g]	AMPD [g]	Carbopol 980NF [g]	Water [g]
1KA	0.2	1.0	0.0	14.0	3.4	1.5	79.9
2KA	0.2	2.0	0.0	14.0	3.4	1.5	78.9
3KA	0.2	3.0	0.0	14.0	3.4	1.5	77.9
1A	0.2	0.0	1.0	14.0	2.1	1.5	81.2
2A	0.2	0.0	2.0	14.0	2.1	1.5	80.2
3A	0.2	0.0	3.0	14.0	2.1	1.5	79.2

at a constant spindle speed of 120 rpm for 1 min. To ensure repeatability of results, identical measurement conditions were maintained for all samples. Six measurements were performed for each hydrogel.

Each hydrogel tested was subjected to HPLC analysis at equal intervals every 7 days for a period of 35 days. For sample preparation, 0.5 g of hydrogel was taken from each formulation and dissolved in 99.5 g of water. The dissolution process was carried out on an Arex Digital Pro magnetic stirrer (Velp Scientifica, Usmate, Italy) at a constant speed of 900 rpm for 20 min. Six 1 mL samples were taken from each preparation.

The HPLC analysis was performed on a Thermo Scientific Dionex UltiMate 3000 liquid chromatograph (Dionex Corporation, Sunnyvale, USA) using an TCC-3000SD column oven, LPG-3400SD pump, WPS-3000TSL autosampler and DAD-3000 detector. A RP-18 LiChroCART column (125 mm × 4 mm, 5 µm) was used for the chromatographic separation. Separation was performed at 40°C using a mixture of 0.1% formic acid in water (phase A) and 0.1% formic acid in acetonitrile (phase B) as mobile phase. The phase flow rate was 1.0 mL/min. The elution gradient started at 7% of phase B for 0.5 min, reached 50% at 4th min and increased to 95% at 5th min, which was maintained for 2 min. From the 7th to the 9th min, the gradient returned to 7% phase B. The retention time was 4.14 min and detection was performed at 280 nm. A series of market dilutions of tetracycline were prepared and a standard curve was obtained with a correlation coefficient (R) of 0.9993 (y = 0.2517x – 0.0428).

Results

The highest pH value, with an average of 7.89, was recorded for hydrogel 1KA, while the lowest pH value for formulation 3KA was 5.38. Hydrogels containing azeloglycine had similar pH values of around 7.78. The results of all pH measurements are summarized in Table 2.

Hydrogels containing azelaic acid had significantly lower viscosity values compared to azeloglycine formulations. There were also more significant differences in viscosity between the azelaic acid gels. Hydrogel 1KA had the highest viscosity, with an average value of approx. 8,314 cP. The viscosity of formulation 2KA was around 4,336 cP and gel 3KA had the lowest viscosity of around 3,133 cP. The azeloglycine hydrogels showed significantly higher viscosity values, with smaller differences between the values. Hydrogel 1A had the highest viscosity close to 12,460 cP. The viscosity value for gel 2A was around 10 127 cP and gel 3A was 9,222 cP. The viscosity values of all formulations are shown in Fig. 1.

Chromatographic analysis showed tetracycline stability for most formulations over a period of 35 days. The greatest decrease in antibiotic concentration was observed in the hydrogel, 1KA, in which tetracycline concentration decreased from 10.86 µg/mL on the 1st day to 5.45 µg/mL on the last day of measurements. Tetracycline in the 2KA and 3KA hydrogels remained more stable. In the 2KA formulation, it decreased from 11.77 µg/mL on 1st day to 10.5 µg/mL on 35th day. In the 3KA hydrogel, the initial concentration was 10.2 µg/mL and reached 9.27 µg/mL on the last day. In the formulations with azeloglycine, small decreases in drug concentration were observed over the 35 days of analysis. In hydrogel 1A, the concentration

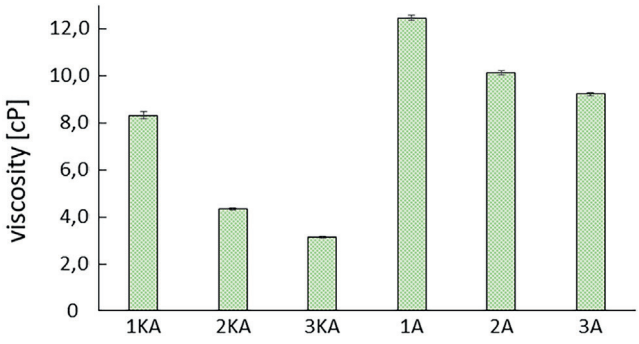

Fig. 1. The viscosity values of formulations containing azelaic acid – 1KA, 2KA and 3KA, and azeloglycine – 1A, 2A and 3A

Table 2. The pH values of evaluated formulations containing azelaic acid – 1KA, 2KA, 3KA and azeloglycine – 1A, 2A and 3A

Formulation	1KA	2KA	3KA	1A	2A	3A
pH value	7.89 ±0.01	5.90 ±0.01	5.38 ±0.01	7.82 ±0.01	7.81 ±0.01	7.71 ±0.01

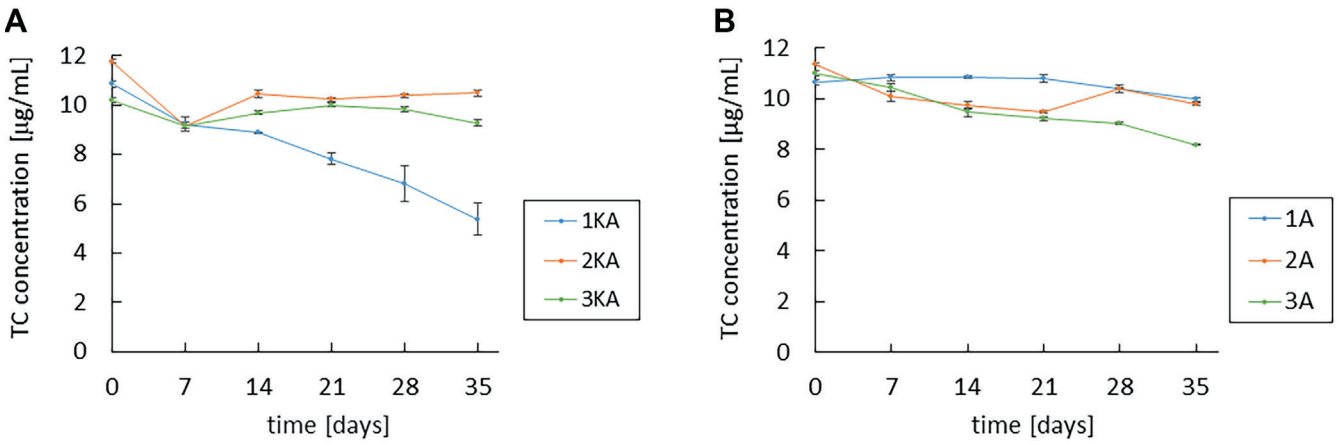

Fig. 2. Changes in tetracycline concentration values in formulations containing azelaic acid – 1KA, 2KA and 3KA (A), and azeloglycine – 1A, 2A and 3A (B) during 35-day observation

of tetracycline decreased from 10.65 µg/mL to 9.98 µg/mL and in hydrogel 2A from 11.35 µg/mL to 9.8 µg/mL. Only formulation 3A showed a greater decrease, from 11.0 µg/mL to 8.18 µg/mL. The course of drug concentration changes is shown in Fig. 2.

Discussion

The formulations presented in this paper constitute a new proposal for the treatment of acne vulgaris. The choice of tetracycline allows the use of its antipathogenic and anti-inflammatory properties, which are crucial in the context of anti-acne therapies.[11,12] Additional ingredients incorporated into the formulation, such as azelaic acid or azeloglycine, have a proven use in the topical treatment of acne lesions. They have comedolytic and keratolytic properties and lighten acne hyperpigmentation Fig. 3.[8–10]

The pH of the formulations is critical to the stability of tetracycline, which is most stable at pH conditions ranging from weakly acidic to neutral. Either an excessively acidic or an excessively alkaline environment will result in rapid degradation of the antibiotic. At a pH above 8, maroon quinones can be formed in the presence of oxygen and light.[13,14] At a pH close to 2, the tetracycline molecule is dehydrated and nephrotoxic compounds such as 4-epianhydrotetracycline are formed.[15–17] In the pH range of 2–6, a reversible epimerization process can also take place, leading to the formation of 4-epitetracycline, which has no antimicrobial activity.[18,19] Therefore, all the preparations tested were characterized by a weakly acidic or neutral pH, which favors their stability.[20]

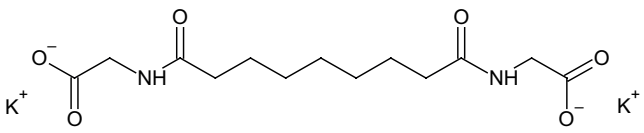

Fig. 3. The chemical structure of azeloglycine

Formulations containing azeloglycine presented higher viscosity values compared to hydrogels containing azelaic acid. Azelaic acid was found to cause a significant reduction in hydrogel viscosity, which should be taken into account when designing formulations containing this substance.

The HPLC analysis showed high stability of the antibiotic in most of the formulations analyzed. In formulations 2KA, 3KA, 1A, and 2A the degradation process was very slight. A modestly higher loss of drug concentration was observed in hydrogel 3A, but the process was also found to be slow. The greatest degradation was observed in hydrogel 1KA, where disintegration was faster than in the other formulations and the tetracycline concentration at day 35 was only 50% of the initial value.

Azeloglycine has more effective therapeutic activity at lower concentrations than azelaic acid. It is also more widely used than azelaic acid in skin care formulations due to its near-neutral pH, low number of interactions and high compatibility with various ingredients in cosmetic preparations.

The proposed formulations can have multidirectional efficacy based on the antibacterial activity of the antibiotic used. In addition, azeloglycine is an excellent ingredient for anti-acne formulations due to its ability to lighten hyperpigmentation, reduce redness and regulate excess sebum. The alcoholamine AMPD contained in the preparations can support the cleansing process of the hair follicles from sebum deposits thanks to its activity against free fatty acids.[20]

Conclusions

The present study focuses on new anti-acne preparations that combine the bacteriostatic and anti-inflammatory properties of tetracycline with the anti-acne effects of azelaic acid and azeloglycine. The use of these substances aims to treat acne vulgaris more effectively while reducing the risk of antibiotic resistance.

A comparison of the rheological properties showed that azeloglycine provided a formulation viscosity averaging approx. 10,500 cP, which may contribute to more favorable skin application compared to azelaic acid gels with lower viscosity values averaging approx. 5,200 cP. Chromatographic results showed high tetracycline stability in most of the formulations tested, and formulations with azeloglycine showed less loss of drug. The developed azeloglycine-containing formulations could be an interesting and effective proposal for a topical anti-acne preparation due to the high persistence of the antibiotic and the favorable rheological parameters.

ORCID iDs

Agnieszka Kostrzębska https://orcid.org/0000-0002-6902-919X
Gabriela Szczepaniak https://orcid.org/0009-0007-5692-501X

References

1. Lee YB, Byun EJ, Kim HS. Potential role of the microbiome in acne: A comprehensive review. *J Clin Med*. 2019;8(7):987. doi:10.3390/jcm8070987
2. Lynn D, Umari T, Dellavalle R, Dunnick C. The epidemiology of acne vulgaris in late adolescence. *Adolesc Health Med Ther*. 2016;7:13–25. doi:10.2147/AHMT.S55832
3. Dessinioti C, Katsambas AD. The role of *Propionibacterium acnes* in acne pathogenesis: Facts and controversies. *Clin Dermatol*. 2010;28(1):2–7. doi:10.1016/j.clindermatol.2009.03.012
4. Farrar MD, Ingham E. Acne: Inflammation. *Clin Dermatol*. 2004;22(5):380–384. doi:10.1016/j.clindermatol.2004.03.006
5. Rozas M, Hart De Ruijter A, Fabrega MJ, et al. From dysbiosis to healthy skin: Major contributions of *Cutibacterium acnes* to skin homeostasis. *Microorganisms*. 2021;9(3):628. doi:10.3390/microorganisms9030628
6. Krautheim A, Gollnick HPM. Acne: Topical treatment. *Clin Dermatol*. 2004;22(5):398–407. doi:10.1016/j.clindermatol.2004.03.009
7. Gollnick H, Schramm M. Topical therapy in acne. *Acad Dermatol Venereol*. 1998;11(Suppl 1):S8–S12. doi:10.1111/j.1468-3083.1998.tb00901.x
8. Webster G. Combination azelaic acid therapy for acne vulgaris. *J Am Acad Dermatol*. 2000;43(2 Pt 3):S47–S50. doi:10.1067/mjd.2000.108318
9. Maramaldi G, Esposito MA. Potassium azeloyl diglycinate: A multifunctional skin lightener. *Cosmetics & Toiletries*. 2008;117:43–72. https://img.cosmeticsandtoiletries.com/files/base/allured/all/image/2021/06/ct.CT_117_03_043_05.pdf. Accessed August 15, 2024.
10. Sieber MA, Hegel JKE. Azelaic acid: Properties and mode of action. *Skin Pharmacol Physiol*. 2014;27(Suppl 1):9–17. doi:10.1159/000354888
11. Burton J; The Dermatology Research Group. A placebo-controlled study to evaluate the efficacy of topical tetracycline and oral tetracycline in the treatment of mild to moderate acne. *J Int Med Res*. 1990;18(2):94–103. doi:10.1177/030006059001800204
12. Sapadin AN, Fleischmajer R. Tetracyclines: Nonantibiotic properties and their clinical implications. *J Am Acad Dermatol*. 2006;54(2):258–265. doi:10.1016/j.jaad.2005.10.004
13. Oka H, Ikai Y, Kawamura N, et al. Photodecomposition products of tetracycline in aqueous solution. *J Agric Food Chem*. 1989;37(1):226–231. doi:10.1021/jf00085a052
14. Davies AK, McKellar JF, Phillips GO, Reid AG. Photochemical oxidation of tetracycline in aqueous solution. *J Chem Soc Perkin Trans 2*. 1979;3:369. doi:10.1039/p29790000369
15. Hasan T, Allen M, Cooperman BS. Anhydrotetracycline is a major product of tetracycline photolysis. *J Org Chem*. 1985;50(10):1755–1757. doi:10.1021/jo00210a038
16. Schlecht KD, Frank CW. Dehydration of tetracycline. *J Pharm Sci*. 1975;64(2):352–354. doi:10.1002/jps.2600640241
17. Kelly RG. Determination of anhydrotetracycline and 4-epianhydrotetracycline in a tetracycline mixture. *J Pharm Sci*. 1964;53(12):1551–1552. doi:10.1002/jps.2600531234
18. Grobben-Verpoorten A, Dihuidi K, Roets E, Hoogmartens J, Vanderhaeghe H. Determination of the stability of tetracycline suspensions by high performance liquid chromatography. *Pharm Weekbl Sci*. 1985;7(3):104–108. doi:10.1007/BF01968711
19. Khan NH, Wera P, Roets E, Hoogmartens J. Quantitative analysis of tetracycline by high performance liquid chromatography on polystyrene-divinylbenzene packing materials. *J Liquid Chromatogr*. 1990;13(7):1351–1374. doi:10.1080/01483919008049254
20. Kostrzębska A, Pączek K, Weselak A, Musiał W. Effect of hydrogel substrate components on the stability of tetracycline hydrochloride and swelling activity against model skin sebum. *Int J Mol Sci*. 2023;24(3):2678. doi:10.3390/ijms24032678

High-filler content electrospun fibers from biodegradable polymers and hydroxyapatite: Toward improved scaffolds for tissue engineering

Elektroprzędzone włókna o wysokiej zawartości napełniacza otrzymane z biodegradowalnych polimerów i hydroksyapatytu: w kierunku ulepszonych rusztowań dla inżynierii tkankowej

Aleksandra Korbut[A–F]

Department of Polymer Engineering and Technology, Faculty of Chemistry, Wroclaw University of Science and Technology, Poland

A – research concept and design; B – collection and/or assembly of data; C – data analysis and interpretation;
D – writing the article; E – critical revision of the article; F – final approval of the article

Polymers in Medicine, ISSN 0370-0747 (print), ISSN 2451-2699 (online) *Polim Med*. 2024;54(2):161–166

Address for correspondence
Aleksandra Korbut
E-mail: aleksandra.korbut@pwr.edu.pl

Funding sources
This research was funded by the Foundation for Polish Science through the European Union under the European Regional Development Fund, within the TEAM-NET program entitled "Multifunctional biologically active composite for application in bone regenerative medicine" (grant POIR.04.04.00-00-16D7/18-00).

Conflict of interest
None declared

Received on November 19, 2024
Reviewed on November 22, 2024
Accepted on November 22, 2024

Published online on November 28, 2024

Abstract

Background. One of the key challenges in tissue engineering area is the creation of biocompatible scaffolds that support cell growth and mimic the structural and mechanical properties of native tissues. Among various materials used for scaffold fabrication, composite materials based on biodegradable polymers reinforced with bioactive inorganic fillers have attracted significant attention due to their properties. One of the important problems with the preparation of composite electrospun fibers is the low filler content in the fiber.

Objectives. This study aims to select the best composition for electrospun polymer fibers in terms of potential application in tissue engineering. The effect of the viscosity of polymer solution/dispersion and filler content on the structure and properties of the fibers was determined. Morphology and filler content were compared.

Materials and methods. Series of electrospun composite fibers were fabricated from poly(ε-caprolactone) (PCL), poly(L-lactic acid) (PLLA) and hydroxyapatite (HAP), containing from 10 wt% to 40 wt% HAP. The properties of the resulting composites were studied using scanning electron microscopy (SEM), differential scanning calorimetry (DSC) and viscosimetry measurements.

Results. The addition of HAP to the polymer solution caused a significant increase in viscosity, but the results showed that it is possible to obtain composite electrospun fibers even with 40 wt% filler content. Scanning electron microscopy analysis shows randomly oriented electrospun fibers with an average diameter in the range of 3.8–8.5 µm for solution and dispersion with high viscosity (1,210–2,000 mPa·s) and significantly larger diameters (approx. 12 µm) for the PCL solution (326 mPa·s).

Conclusions. It is possible to transform the composite dispersion from biopolymers and HAP into nonwoven fabrics at up to 40 wt% filler content. Due to their unique properties, such materials are promising for application in tissue engineering.

Key words: electrospun fibers, bio-based materials, hydroxyapatite, bone regeneration

Cite as
Korbut A. High-filler content electrospun fibers from biodegradable polymers and hydroxyapatite: Toward improved scaffolds for tissue engineering. *Polim Med*. 2024;54(2):161–166. doi:10.17219/pim/196351

DOI
10.17219/pim/196351

Streszczenie

Wprowadzenie. Jednym z kluczowych wyzwań w dziedzinie inżynierii tkankowej jest wytworzenie biokompatybilnych rusztowań, które wspierają wzrost komórek i naśladują strukturalne i mechaniczne właściwości natywnych tkanek. Spośród różnych materiałów wykorzystywanych do produkcji rusztowań, ze względu na swoje właściwości materiały kompozytowe oparte na biodegradowalnych polimerach wzmocnionych bioaktywnymi napełniaczami nieorganicznymi zyskały znaczną uwagę. Jednym z istotnych problemów związanych z przygotowaniem kompozytowych elektroprzędzonych włókien jest niska zawartość napełniacza we włóknie.

Cel pracy. Niniejsza praca miała na celu określenie najlepszego składu elektroprzędzonych włókien polimerowych pod względem potencjalnego zastosowania w inżynierii tkankowej. Zbadano wpływ lepkości roztworu/dyspersji polimeru i zawartości napełniacza na morfologię oraz właściwości włókien.

Materiały i metody. Wytworzono serię mat kompozytowych z polikaprolaktonu (poly(ε-caprolactone) (PCL)), kwasu polimlekowego (poly(L-lactic acid) (PLLA)) i hydroksyapatytu (HAP), zawierających od 10% do 40% wag. HAP. Właściwości otrzymanych materiałów zbadano za pomocą skaningowej mikroskopii elektronowej (scanning electron microscopy (SEM)) i skaningowej kalorymetrii różnicowej (differntial scanning calorimetry (DSC)) oraz wykonano pomiary lepkości.

Wyniki. Dodatek HAP do roztworu polimeru spowodował znaczny wzrost lepkości, ale uzyskane wyniki pokazały, że możliwe jest wytworzenie kompozytowych włókien dobrej jakości nawet przy zawartości 40% wag. napełniacza. Zdjęcia SEM przedstawiają losowo zorientowane włókna o średnicach w zakresie 3,8–8,5 µm dla roztworu i dyspersji o wysokiej lepkości (1210–2000 mPa·s) i znacznie większych średnicach (ok. 12 µm) dla roztworu PCL (326 mPa·s).

Wnioski. Możliwe jest przekształcenie dyspersji kompozytowej na bazie biopolimerów z dodatkiem HAP w włókniny o zawartości napełniacza do 40% wag. Ze względu na swoje unikalne właściwości, takie materiały są obiecujące do zastosowania w inżynierii tkankowej.

Słowa kluczowe: włókna elektroprzędzone, biomateriały, hydroksyapatyt, regeneracja tkanek kostnych

Background

Electrospinning of biodegradable polymers is a modern technique for producing fibrous structures widely used in regenerative medicine that involves forming fibers from a polymer solution using electrostatic forces generated by high-voltage electric fields. Those forces stretch liquid to the form of thin fibers, which are deposited on a collector to form matrices that may resemble the structure of natural tissues.[1,2]

Among the popular polymers used in this process are polylactide,[3,4] polycaprolactone,[5–7] and lactic and glycolic acid copolymers[8,9] characterized by biocompatibility and biodegradability, which allows them to be used safely in the body.[10,11] It is possible to easily modify their mechanical and surface properties, allowing them to be tailored to the specific needs of different therapies.[12]

Various fillers are added to polymers to enhance fiber properties and create composites with improved performance.[6,13,14] One of the most popular fillers used in composite fibers is hydroxyapatite (HAP), naturally found in bones and teeth. Its addition increases bioactivity, stimulating osteogenesis and accelerating bone tissue regenerative processes.[15] Hydroxyapatite also helps to integrate the implant into the tissue, reducing the risk of rejection and promoting the formation of new bone structures.[16,17]

Nonwoven fabrics prepared with electrospinning can be used as scaffolds for tissue engineering. Because of their high surface-to-volume ratio and porous structure, these scaffolds allow efficient exchange of nutrients and metabolites, which promotes the regeneration process.[18,19] Using biopolymers reduces the risk of long-term inflammatory reactions after implantation, as the material gradually decomposes and is resorbed in a controlled way.

Objectives

The study aimed to obtain composite nonwoven fabrics made of biocompatible polymers, containing the highest possible amount of bioactive filler (HAP), which support cell growth, differentiation and new tissue formation.[20–22] The unique structure of nonwoven fabrics obtained with electrospinning mimics very well the structure of real tissues, which, combined with the bioactivity of HAP, offers the possibility of their potential use in regenerative medicine.

Materials and methods

The following reagents were used: poly(ε-caprolactone) (PCL; CAPA 6800, Mw ~80,000 g/mol; Perstorp Specialty Chemicals AB, Perstorp, Sweden), Resomer L210s (Mw ~600,000 g/mol; Evonik, Essen, Germany), HAP (synthetic, 99.8%, Sigma-Aldrich, St. Louis, USA), and solvents (POCH S.A., Gliwice, Poland).

Solution/dispersion preparation

In the first step, 3 wt% solution of poly(L-lactic acid) (PLLA) in a mixture of chloroform/N,N-dimethylformamide (9/1v/v) and 15 wt% PCL solution in a mixture of chloroform/methanol (3/1v/v) were prepared. Next, the required amounts of HAP were suspended in the polymer solutions and sonicated for 30 min to obtain a homogeneous dispersion.

Electrospinning process

The electrospinning process was carried out under constant environmental parameters, at 25°C, 40% humidity and constant speed of the rotating drum collector at 300 rpm. The other process parameters were set individually for every mixture: voltage on the needle and collector (from –30.0 kV to 30.0 kV), needle-to-collector distance (100–180 mm) and the solution flow rate (1.0–6.0 mL/h; DOXA Microfluidics, Málaga, Spain).

Characterization of the polymer solutions/dispersions and electrospun mats

For viscosity measurements, a Brookfield DV1 rotational viscometer (AMETEK Brookfield, Middlesborough, USA) was used. The morphology and size of fibers were determined with scanning electron microscopy (SEM) images (Nova NanoSEM 200; FEI, Eindhoven, the Netherlands). The differential scanning calorimetry (DSC) measurements were performed with a Mettler-Toledo DSC1 system (Mettler-Toledo, Columbus, USA) under the following conditions: ~5.5 mg; N_2: 60 mL/min; 10°C/min; from –80°C to 120°C (PCL samples) or 0–200°C (PLLA-based samples); thermal equilibrium: 120°C or 200°C for 5 min; then, the solutions were cooled down to –80°C or 0°C, respectively. The crystallinity degree (X_c) was calculated as (Equation 1):

$$X_c = \frac{\Delta H_m - \Delta H_{cc}}{w \cdot \Delta H_m^{100\%}} \cdot 100\%, \quad (1)$$

where: ΔHm – measured enthalpies of melting of PCL or PLLA samples, $\Delta Hm^{100\%}$ – the enthalpy of melting of fully crystalline PCL ($\Delta Hm^{100\%}$ = 139 J/g))[23] or PLLA ($\Delta Hm^{100\%}$ = 93.7 J/g)),[24] ΔHCC – measured enthalpies of cold crystallization of PLLA samples, and w – mass fraction of polymer.

Results and discussion

The effect of solution properties and process parameters on polymer and composite fiber morphology obtained with electrospinning was investigated. Especially, the viscosity of the solution has an important role in determining the range of concentrations from which continuous fibers can be obtained. The addition of dimethylformamide (DMF) to the other solvent (9/1v/v) enabled the production of defect-free and uniform fibers. A binary solvent system containing the 2nd solvent (DMF) with a higher boiling point evaporates slower from the ejected charged jet, causing the jet's viscoelastic properties to change and therefore improving the jet's stretching.

However, obtaining composite fibers with mineral filler is a challenge. One of the key parameters determining the success of the electrospinning process is the proper viscosity of the solution/suspension. Even a small addition of filler significantly increases the viscosity of the electrospun dispersion, resulting in difficulties with obtaining homogeneous fibers associated with needle plugging. For this reason, it was necessary to select new, optimal electrospinning process parameters for generating PLLA-HAP or PCL-HAP composite fibers. Each time, the voltage set at the needle is less than at the collector. However, for a pure polymer solution, this value is significantly lower. The flow rate of the electrospun solution/suspension had to be increased with increasing viscosity (from 1.0 mL/h for the pure polymer solution to 6.0 mL/h for the highest viscosity samples).

The morphologies of all electrospun fibers are shown in Fig. 1. Scanning electron microscopy analysis shows randomly oriented electrospun fibers with an average diameter presented in Table 1. For most samples, uniform fibers were obtained over the entire electrospun mats. Spindle-shaped deformations were observed on some fibers formed from a solution of pure PLLA (Fig. 1E). The reason for their formation may be incomplete evaporation of the solvent during the electrospinning process. The images also confirmed the incorporation of HAP particles into polymer fibers. The highest degree of fiber filling was obtained for the polylactide dispersion PLLA_HAP_60/40 at the process parameters: 15 kV, 6.0 mL/h and 180 mm. In this case, it was possible to fill the fibers with 40 wt% HAP due to the lower impact of mineral filler on the overall suspension viscosity. Up to now, it has been possible to obtain fibers with a maximum HAP content of 30 wt% relative to the polymer.[14,15,25] Moreover, nonwoven fabricated from this dispersion was the best oriented, and HAP particles were better distributed (Fig. 1H) than in other combinations. The same polymer/filler ratio was tested for the 2nd polymer (PCL); however, the viscosity increase made it impossible to carry out the electrospinning process and thus form fibers.

Despite slight differences in viscosity values for the 2 polymers, the process was substantially more efficient for electrospinning from the PLLA solution. This may be due to the difference in polymer solution concentrations. In the case of PLLA, it is already possible to have a polymer concentration 5 times lower (3 wt%) in order to obtain a solution with the viscosity necessary for the electrospinning process and produce mats of good quality, while the minimum concentration for PCL is 15 wt%.

In the case of PCL, a significant effect of HAP addition on solution viscosity was observed (addition of 10 wt% HAP increased the viscosity of 15 wt% PCL solution more than 5 times; Fig. 2). For PCL with increasing HAP content, and at the same time viscosity of the system, the average fiber diameter decreases. In the case of PLLA, the effect of the presence of mineral filler on viscosity is significantly smaller. This is also reflected in the diameters of fibers obtained in the electrospinning process, which in the case of PLLA have similar diameters regardless of HAP content. From the solution with the lowest viscosity and highest polymer concentration (PCL 15 wt%, 326 mPa·s), fibers

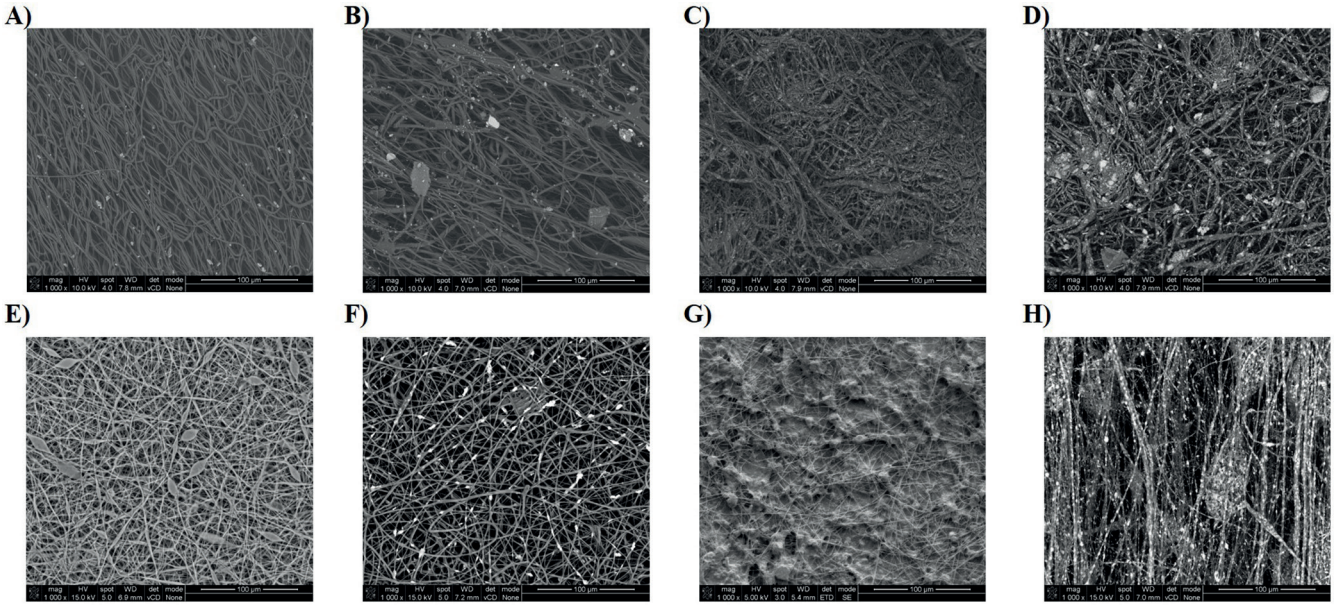

Fig. 1. Scanning electron microscopy (SEM) images of electrospun fibrous scaffolds. A. pure PCL; B. PCL_HAP_90/10; C. PCL_HAP_80/20; D. PCL_HAP_70/30; E. pure PLLA; F. PLLA_HAP_85/15; G. PLLA_HAP_75/25; H. PLLA_HAP_60/40

PCL – poly(ε-caprolactone); PLLA – poly(L-lactic acid); HAP – hydroxyapatite.

Table 1. List of parameters of the samples investigated in the study

Sample	Polymer concentration [wt%]	Viscosity [mPa·s]	Average fiber diameter [μm]	Apatite content [wt%]
PCL	15	326	12.2	–
PCL_HAP_90/10		1,765	8.5	10
PCL_HAP_80/20		1,842	6.0	20
PCL_HAP_70/30		1,887	4.4	30
PLLA	3	1,210	3.8	–
PLLA_HAP_85/15		1,520	4.6	15
PLLA_HAP_75/25		1,750	6.2	25
PLLA_HAP_60/40		2,200	3.9	40

PCL – poly(ε-caprolactone); PLLA – poly(L-lactic acid); HAP – hydroxyapatite.
PCL_HAP_X/Y – where X is the polymer content (wt%) and Y is the hydroxyapatite content (wt%), e.g., PCL_HAP_90/10 – sample containing 90 wt.% of poly(ε-caprolactone) and 10 wt.% of hydroxyapatite, etc.

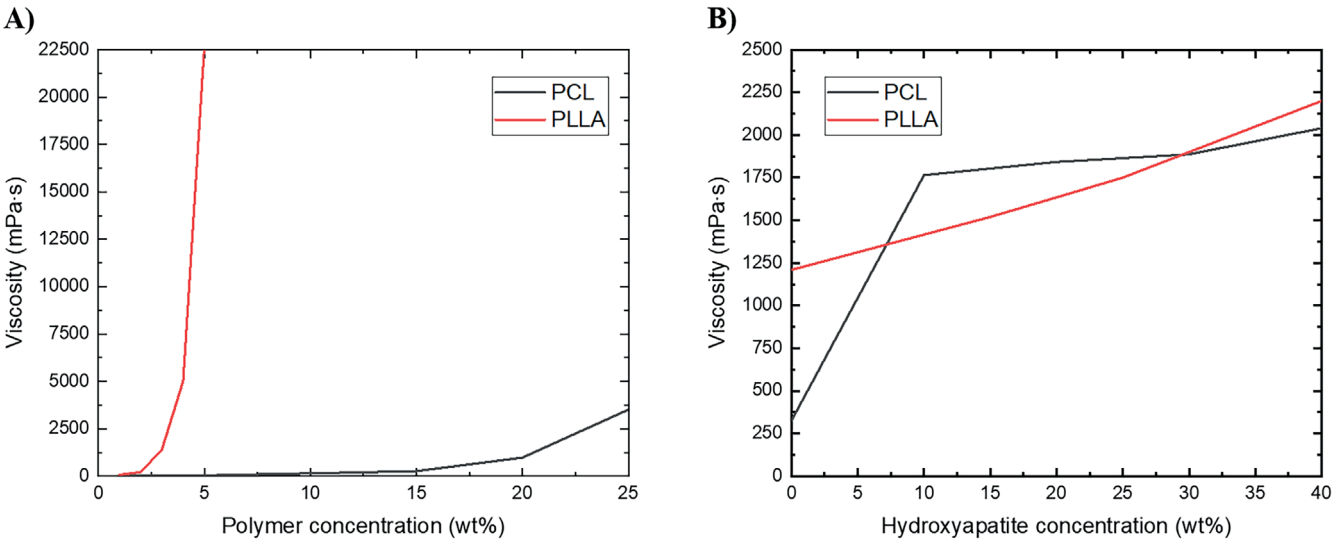

Fig. 2. The effect of polymer concentration and filler content on viscosity

Table 2. Selected parameters determined from the differential scanning calorimetry (DSC) curves

Sample	1st heating scan			2nd heating scan			Cooling scan		
	T_g [°C]	T_{cc} [°C]	ΔH_{cc} [J/g]	T_g [°C]	T_m [°C]	ΔH_m [J/g]	X_c (%)	T_c [°C]	ΔH_c [J/g]
PCL	–59.5	–	–	–68.8	58.7	74.9	53.9	30.2	–64.3
PCL_HAP_90/10	–59.7	–	–	–71.5	58.0	63.1	50.5	31.9	–56.9
PCL_HAP_80/20	–60.2	–	–	–71.3	58.6	69.1	62.2	31.9	–56.1
PCL_HAP_70/30	–59.5	–	–	–71.5	57.5	51.7	53.2	32.4	–47.8
PLLA	67.1	78.3	28.9	72.7	170.6	45.4	17.5	115.9	5.1
PLLA_HAP_85/15	67.2	81.4	21.6	72.0	170.9	40.5	23.7	116.8	30.4
PLLA_HAP_75/25	66.3	76.1	20.1	73.9	172.6	33.3	18.7	117.7	33.4
PLLA_HAP_60/40	67.6	84.4	6.1	72.6	171.5	35.9	79.5	117.4	35.9

PCL – poly(ε-caprolactone); PLLA – poly(L-lactic acid); HAP – hydroxyapatite.
PCL_HAP_X/Y – where X is the polymer content (wt%) and Y is the hydroxyapatite content (wt%), e.g., PCL_HAP_90/10 – sample containing 90 wt% of poly(ε-caprolactone) and 10 wt% of hydroxyapatite, etc.
T_g – glass transition temperature; T_{cc} – cold crystallization temperature; ΔH_{cc} – the cold crystallization enthalpy; T_m – melting temperature; ΔH_m – the melting enthalpy; X_c – degree of crystallization; T_c – crystallization temperature; ΔH_c – the crystallization enthalpy.

with significantly larger diameters (approx. 12 μm) were obtained. Viscosity of the remaining solutions and dispersions is in the range of 1,210–2,000 mPa·s and fibers obtained from them have average diameter in the range of 3.8–8.5 μm.

The melting and crystallization behavior of electrospun mats was investigated using DSC. As shown in Table 2, the crystallization temperature appears at approx. 116°C for pure PLLA and 30°C for pure PCL, and increases to 118°C and 32°C for PLLA and PCL composite samples, respectively. The subsequent heating curves of PLLA samples show a baseline shift and an endothermic peak located at approx. 72°C and approx. 170°C, respectively, corresponding to glass transition and melting of α/α' crystals. Besides, an exothermic peak present in the 1st heating curve at 76–84°C can be assigned to cold crystallization. For PCL composite samples T_g is approx. –71°C and –69°C for pure polymer, while T_m is approx. 58°C.

Conclusions

This paper presents the possibility of creating bioactive polymeric composite scaffold based on 2 types of biopolymer (PCL and PLLA) and micro-sized HAP particles in varying ratios, using the electrospinning technique. It was shown that the solvent properties, especially polymer concentration and viscosity, have a significant effect on process productivity, morphology and diameter of the fibers.

Incorporation of a large amount of HAP particles into polymer fibers made them more hydrophilic, which can be useful for tissue engineering applications. These results highlight the potential of using electrospun polymer nonwovens combined with HAP in tissue engineering as materials for bone regeneration. Hydroxyapatite excellently supports bone cell growth and matrix formation. Moreover, the electrospun fiber structure can mimic the natural extracellular matrix (ECM). However, fabrication of stable and durable fibers with HAP requires precise and high control over the electrospinning process, which can be challenging.

ORCID iDs

Aleksandra Korbut https://orcid.org/0000-0001-7982-9038

References

1. Liu J, Lin DY, Wei B, Martin DC. Single electrospun PLLA and PCL polymer nanofibers: Increased molecular orientation with decreased fiber diameter. *Polymer (Guildf)*. 2017;118:143–149. doi:10.1016/j.polymer.2017.04.070
2. Khalili S, Khorasani SN, Razavi SM, Hashemibeni B, Tamayol A. Nanofibrous scaffolds with biomimetic composition for skin regeneration. *Appl Biochem Biotechnol*. 2019;187(4):1193–1203. doi:10.1007/s12010-018-2871-7
3. Wu JH, Hu TG, Wang H, Zong MH, Wu H, Wen P. Electrospinning of PLA nanofibers: Recent advances and Its potential application for food packaging. *J Agric Food Chem*. 2022;70(27):8207–8221. doi:10.1021/acs.jafc.2c02611
4. Lu Z, Zhang B, Gong H, Li J. Fabrication of hierarchical porous poly (l-lactide) (PLLA) fibrous membrane by electrospinning. *Polymer (Guildf)*. 2021;226:123797. doi:10.1016/j.polymer.2021.123797
5. Vogt L, Rivera LR, Liverani L, Piegat A, El Fray M, Boccaccini AR. Poly(ε-caprolactone)/poly(glycerol sebacate) electrospun scaffolds for cardiac tissue engineering using benign solvents. *Mater Sci Eng C Mater Biol Appl*. 2019;103:109712. doi:10.1016/j.msec.2019.04.091
6. Luginina M, Schuhladen K, Orrú R, Cao G, Boccaccini AR, Liverani L. Electrospun PCL/PGS composite fibers incorporating bioactive glass particles for soft tissue engineering applications. *Nanomaterials*. 2020;10(5):978. doi:10.3390/nano10050978
7. Cao Y, Han W, Pu Z, et al. Fabrication of hierarchically porous superhydrophilic polycaprolactone monolith based on nonsolvent-thermally induced phase separation. *RSC Adv*. 2020;10(44):26319–26325. doi:10.1039/D0RA04687F
8. Behtaj S, Karamali F, Masaeli E, Anissimov Y, Rybachuk M. Electrospun PGS/PCL, PLLA/PCL, PLGA/PCL and pure PCL scaffolds for retinal progenitor cell cultivation. *Biochem Eng J*. 2021;166:107846. doi:10.1016/j.bej.2020.107846
9. Li X, Zhang S, Zhang X, Xie S, Zhao G, Zhang L. Biocompatibility and physicochemical characteristics of poly(ε-caprolactone)/poly(lactide-co-glycolide)/nano-hydroxyapatite composite scaffolds for bone tissue engineering. *Mater Des*. 2017;114:149–160. doi:10.1016/j.matdes.2016.10.054
10. Deng L, Taxipalati M, Zhang A, et al. Electrospun chitosan/poly(ethylene oxide)/lauric arginate nanofibrous film with enhanced antimicrobial activity. *J Agric Food Chem*. 2018;66(24):6219–6226. doi:10.1021/acs.jafc.8b01493

11. Sheng D, Li J, Ai C, et al. Electrospun PCL/Gel-aligned scaffolds enhance the biomechanical strength in tendon repair. *J Mater Chem B*. 2019; 7(31):4801–4810. doi:10.1039/C9TB00837C
12. Fakhrali A, Semnani D, Salehi H, Ghane M. Electrospun PGS/PCLnanofibers: From straight to sponge and spring-like morphology. *Polym Adv Technol*. 2020;31(12):3134–3149. doi:10.1002/pat.5038
13. Segala K, Nista SVG, Cordi L, et al. Silver nanoparticles incorporated into nanostructured biopolymer membranes produced by electrospinning: A study of antimicrobial activity. *Braz J Pharm Sci*. 2015;51(4): 911–921. doi:10.1590/S1984-82502015000400017
14. Shitole AA, Raut PW, Sharma N, Giram P, Khandwekar AP, Garnaik B. Electrospun polycaprolactone/hydroxyapatite/ZnO nanofibers as potential biomaterials for bone tissue regeneration. *J Mater Sci Mater Med*. 2019;30(5):51. doi:10.1007/s10856-019-6255-5
15. Tetteh G, Khan AS, Delaine-Smith RM, Reilly GC, Rehman IU. Electrospun polyurethane/hydroxyapatite bioactive scaffolds for bone tissue engineering: The role of solvent and hydroxyapatite particles. *J Mech Behav Biomed Mater*. 2014;39:95–110. doi:10.1016/j.jmbbm.2014.06.019
16. Rajzer I. Fabrication of bioactive polycaprolactone/hydroxyapatite scaffolds with final bilayer nano-/micro-fibrous structures for tissue engineering application. *J Mater Sci*. 2014;49(16):5799–5807. doi:10.1007/s10853-014-8311-3
17. Doyle SE, Henry L, McGennisken E, et al. Characterization of polycaprolactone nanohydroxyapatite composites with tunable degradability suitable for indirect printing. *Polymers (Basel)*. 2021;13(2):295. doi:10.3390/polym13020295
18. Venugopal J, Low S, Choon AT, Kumar AB, Ramakrishna S. Electrospun-modified nanofibrous scaffolds for the mineralization of osteoblast cells. *J Biomed Mater Res A*. 2008;85A(2):408–417. doi:10.1002/jbm.a.31538
19. Palamà IE, Arcadio V, D'Amone S, Biasiucci M, Gigli G, Cortese B. Therapeutic PCL scaffold for reparation of resected osteosarcoma defect. *Sci Rep*. 2017;7(1):12672. doi:10.1038/s41598-017-12824-3
20. Zhang J, Li J, Jia G, et al. Improving osteogenesis of PLGA/HA porous scaffolds based on dual delivery of BMP-2 and IGF-1 via a polydopamine coating. *RSC Adv*. 2017;7(89):56732–56742. doi:10.1039/C7RA12062A
21. Szustakiewicz K, Gazińska M, Kryszak B, et al. The influence of hydroxyapatite content on properties of poly(L-lactide)/hydroxyapatite porous scaffolds obtained using thermal induced phase separation technique. *Eur Polym J*. 2019;113:313–320. doi:10.1016/j.eurpolymj.2019.01.073
22. Korbut A, Włodarczyk M, Rudnicka K, et al. Three component composite scaffolds based on PCL, hydroxyapatite and L-lysine obtained in TIPS-SL: Bioactive material for bone tissue engineering. *Int J Mol Sci*. 2021;22(24):13589. doi:10.3390/ijms222413589
23. Patrício T, Bártolo P. Thermal stability of PCL/PLA blends produced by physical blending process. *Procedia Eng*. 2013;59:292–297. doi:10.1016/j.proeng.2013.05.124
24. Chen J, Deng C, Hong R, Fu Q, Zhang J. Effect of thermal annealing on crystal structure and properties of PLLA/PCL blend. *J Polym Res*. 2020;27(8):221. doi:10.1007/s10965-020-02206-1
25. Lee JB, Kim SE, Heo DN, Kwon IK, Choi BJ. In vitro characterization of nanofibrous PLGA/gelatin/hydroxyapatite composite for bone tissue engineering. *Macromol Res*. 2010;18(12):1195–1202. doi:10.1007/s13233-010-1206-5